

7 201

**STUDIES ON HEAT DIFFUSION IN SELECTED CONDUCTING
POLYMERS USING PROBE BEAM DEFLECTION AND
PHOTOACOUSTIC TECHNIQUES**

Thesis submitted to

The Cochin University of Science and Technology

in partial fulfilment of the requirements for the award of the Degree of

Doctor of Philosophy

Thomas P Zachariah



**Department of Physics
Cochin University of Science and Technology
Kochi-682 022, India**

March 2008

**Studies on Heat Diffusion in Selected Conducting Polymers using Probe
Beam Deflection and Photoacoustic Techniques**

*Ph.D Thesis in the field of material characterization using photothermal
techniques*

Author:

**Thomas P Zachariah
Research Fellow, Department of Physics
Cochin University of Science and Technology
Kochi-682 022, India.**



Supervising Guide:

**Dr. T. M. Abdul Rasheed,
Reader, Department of Physics
Cochin University of Science and Technology
Kochi-682 022, India.**

**Laser and Spectroscopy Lab
Department of Physics
Cochin University of Science and Technology
Kochi-682 022, India.**

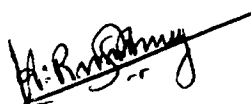
March 2008.

**Department of Physics
Cochin University of Science and Technology
Kochi - 682022**

CERTIFICATE

Certified that the work presented in this thesis entitled “STUDIES ON HEAT DIFFUSION IN SELECTED CONDUCTING POLYMERS USING PROBE BEAM DEFLECTION AND PHOTOACOUSTIC TECHNIQUES” is based on the bonafide research work done by Mr. Thomas P Zachariah under my guidance in the Department of Physics, Cochin University of Science and Technology, Cochin 682022, and has not been included in any other thesis submitted previously for the award of any degree.

Dammam,
14. 03. 2008.



Dr. T.M Abdul Rasheed
(Supervising Guide)
Reader, Department of Physics
CUSAT, Kochi-22.

Present Affiliation:
Assistant Professor
Department of Physics
King Faisal University
Dammam, Saudi Arabia.

DECLARATION

I hereby declare that work presented in the thesis entitled "STUDIES ON HEAT DIFFUSION IN SELECTED CONDUCTING POLYMERS USING PROBE BEAM DEFLECTION AND PHOTOACOUSTIC TECHNIQUES", is based on the original research work done by me under the guidance and supervision of Dr. T. M. Abdul Rasheed, Reader, Department of Physics, Cochin University of Science and Technology, Kochi-22 and has not been included in any other thesis submitted previously for the award of any degree.



Thomas P Zachariah.

Kochi-22,
17. 03. 08.

Acknowledgement

The work presented in this thesis has been carried out in the Department of Physics, Cochin University of Science and Technology under the guidance and supervision of Dr. T M Abdul Rasheed. I am deeply indebted to him for the patient interest he has shown in this work and his timely suggestions and directions. His competent advice and constant encouragement has been a source of strength throughout this work.

I express my sincere gratitude to Prof. K P Rajappan Nair, Former Dean, Faculty of Science, Cochin University of Science and Technology for his support and encouragement during the course of this work.

I remain thankful to Prof L Godfrey, Head of the Department and Prof V C Kuriakose, former Head for providing necessary facilities for this study. I extend my sincere thanks to Dr. M R Anantharaman, Dr Jayalakshmi and Dr M K Jayaraj for their valuable suggestions and advice. I express my sincere gratitude to the entire Physics faculty for their support.

I remain thankful to Dr. Jyotsna Ravi, Dr. S Shaji and Dr. Shibu M Eapen for their constant support and assistance. The services of Dr. Alex Mathew, Dr. Saji Augustine, Dr. Sajeev and Mr. Sanoj are gratefully acknowledged. I express my sincere gratitude to Dr. Honey John for her support and suggestions. I extend my sincere thanks to Dr. Sunny Kuriakose, Dr. K K Vijayan, Dr. Usha John, Dr. B Shyamalakumari and Dr T Nandini for their support and cooperation. I remain thankful to Mrs. Anila E I and Dr. Rachel Reena Philip for the timely help rendered to me.

I remain thankful to the administrative staff and library staff of the Physics Department for their cooperation.

Thomas P Zachariah.

CONTENTS

Preface

Chapter 1	Photothermal Effects – An Overview	1 - 30
1.1	Introduction	1
1.2	Photothermal effects and detection	3
1.2.1	Temperature rise	5
1.2.2	Pressure change	5
1.2.3	Refractive index gradient	6
1.2.4	Surface deformation	9
1.2.5	Infrared emission	9
1.3	Transverse probe beam deflection methods	11
1.3.1	Zero crossing method	13
1.3.2	Thermal wave coupling method	13
1.3.3	Phase method	13
1.3.4	Amplitude method	15
1.4	Probe beam deflection – A theoretical approach	15
1.5	Photoacoustic effect – Rosencwaig-Gersho theory	20
1.6	Open photoacoustic cell method	24
1.6.1	OPC configuration theory	25
	References	27

Chapter 2 **Conducting polymers** **31 - 76**

2.1	Introduction	31
2.1.1	π -conjugated polymers	32
2.1.2	Electrically conducting polymers	34

2.1.3	Conduction mechanisms	36
2.1.4	Applications of conducting polymers	38
▪	Polymer rechargeable batteries	38
▪	Sensors	38
▪	Electroluminescent devices	39
▪	Antistatic coatings	39
▪	Printed circuit boards	39
▪	Molecular electronics	39
▪	Microwave engineering	40
2.2	Polymerization techniques	40
2.2.1	Step growth polymerization	40
2.2.2	Chain growth polymerization	41
2.2.3	Radiation polymerization	42
2.2.4	Plasma polymerization	42
▪	Mechanisms of plasma polymerization	43
▪	Basic reactions in a glow discharge	43
▪	Merits of plasma polymerization technique	45
▪	Applications of plasma polymerized films	45
▪	Experimental setup for plasma polymerization	46
▪	RF plasma polymerization system	47
2.3	Synthesis of conducting polymers	48
2.3.1	Chemical synthesis	49
▪	Polyaniline	49
▪	Polypyrrole	49
2.3.2	Preparation of plasma polymerized films	50
▪	Preparation of polyaniline films	50
▪	Preparation of polypyrrole films	51

▪ Preparation of poly N-methyl pyrrole films	52
▪ Preparation of polythiophene films	52
▪ FTIR spectra of plasma polymerized films	52
2.4 Electrical conductivity measurements	57
▪ Chemically prepared PANI	57
▪ Chemically prepared PPy	57
▪ Plasma polymerized aniline film	57
▪ Plasma polymerized pyrrole film	58
▪ Plasma polymerized N-methyl pyrrole film	58
▪ Plasma polymerized thiophene film	58
2.4.1 Results and discussion	58
2.5 Band gap measurements	65
Conclusions	76
References	76

Chapter 3 Thermal diffusivity measurements of RF Plasma polymerized films by probe beam deflection method 81 - 110

3.1 Introduction	81
3.1.1 Thermal diffusivity	82
3.2 Transverse probe beam deflection configuration	83
3.2.1 Phase method	84
3.2.2 Amplitude method	84
3.3 Experimental setup for transverse PBD	85
3.3.1 Pump source	85
3.3.2 Probe source	85

3.3.3 Chopper	86
3.3.4 Sample cell	86
3.3.5 Position sensitive detector	87
3.3.6 Preamplifier	87
3.3.7 Lock-in amplifier	87
3.4 Thermal diffusivity measurements	89
3.4.1 Polyaniline	90
3.4.2 Polypyrrole	95
3.4.3 Poly N-methyl pyrrole	104
3.4.4 Poly thiophene	104
Conclusions	109
References	110

**Chapter 4 Photoacoustic investigations on conducting
Polymers 113 - 127**

4.1 Introduction	113
4.1.1 Theoretical outline	114
4.2 Experimental setup	116
4.2.1 Laser source	116
4.2.2 Photoacoustic cell	116
4.2.3 Mechanical chopper	116
4.2.4 Lock in amplifier	117
4.3 Preparation of polymer samples	118
4.4 Thermal diffusivity measurements	118
4.5 Results and discussion	118
Conclusion	126

References	127
------------	-----

Chapter 5	Heat diffusion in conducting polymer Composites	129 - 140
------------------	--	------------------

5.1 Introduction	129
5.1.1 Tailoring processability of polymers	129
5.1.2 Open photoacoustic cell configuration	131
5.2 Preparation of polymer composites	131
5.2.1 Preparation of PANI/PVC	131
5.2.2 Preparation of PPy/PVC	132
5.3 Thermal diffusivity measurements	132
5.4 Electrical conductivity measurements	133
5.5 Results and discussion	133
Conclusion	140
References	140

Chapter 6	Summary and Conclusions	143 - 149
------------------	--------------------------------	------------------

Preface

The last few decades witnessed a surge in advanced techniques for material characterization with the availability of intense coherent sources of radiation. Photothermal science deals with a wide range of techniques and phenomena based on the conversion of absorbed optical energy into heat. Optical energy is absorbed and eventually converted into thermal energy by a variety of materials in the solid, liquid and gaseous states. Although the initial absorption process in many materials are selective, it is common for excited electronic states in atoms or molecules to give away its excitation energy by a series of non-radiative transitions that result in a general heating of the material. Photothermal heating can result in different effects which, in turn, provide various detection mechanisms. Photothermal heating can provide convenient and sensitive methods for detecting optical absorptions in matter. It can also provide information concerning various de-excitation mechanisms. Photothermal methods enjoy the advantage of being non-destructive. This optical diagnostic technique can provide information that is not obtainable by other conventional methods. Thus photothermal technique gained wide acceptance in the study of various optical and thermal parameters. Of the various photothermal methods in use, two techniques – the transverse probe beam deflection method and the open photoacoustic cell technique are employed for thermal characterization in the present work.

The discovery of highly conducting polyacetylene in 1977 by Shirakawa et. al has revolutionized the field of conducting polymers. The conductivity of this conjugated polymer could be increased by about fourteen orders by the process of doping. Since this Nobel Prize winning discovery, much of the work has been centered on synthesis and characterization of novel

polymers with π - conjugated backbone due to their highly promising optical, electrochemical and conducting properties. Conducting polymers are generally synthesized by chemical or electrochemical methods. Another technique used for obtaining polymer films is plasma polymerization. This technique makes use of molecules occurring in various plasma environments. Pin hole-free films with good adhesion to the substrate can be deposited using this method. The advantage of this technique lies in the easy control of polymerization reaction to any desired surface. The distinguishing feature of plasma deposited films is its highly cross-linked nature. On the other hand chemical synthesis produces polymers with an ordered structure. The electrical conductivity of these polymers can be tuned from the insulating regime to the highly conducting regime by suitable doping. The combination of conductivity and polymeric properties such as flexibility, processability and a reduction in weight and cost makes this class of polymers suitable for wide ranging applications.

In the present study, radio frequency plasma polymerization technique is used to prepare thin films of polyaniline, polypyrrole, poly N-methyl pyrrole and polythiophene. The thermal characterization of these films is carried out using transverse probe beam deflection method. Electrical conductivity and band gaps are also determined. The effect of iodine doping on electrical conductivity and the rate of heat diffusion is explored.

Bulk samples of polyaniline and polypyrrole in powder form are synthesized by chemical route. Open photoacoustic cell configuration is employed for the thermal characterization of these samples. The effect of acid doping on heat diffusion in these bulk samples of polyaniline is also investigated. The variation of electrical conductivity of doped polyaniline and polypyrrole with temperature is also studied for drawing conclusion on the

nature of conduction in these samples. In order to improve the processability of **polyaniline** and **polypyrrole**, these polymers are incorporated into a host **matrix** of poly vinyl chloride. Measurements of thermal diffusivity and **electrical conductivity** of these samples are carried out to investigate the **variation** of these quantities as a function of the content of polyvinyl chloride.

Chapter 1 is an introduction to the photothermal science. The various **photothermal effects** with the corresponding detection schemes are discussed in this chapter. A brief outline of the theory behind photothermal deflection and photoacoustic effect is also given.

An introduction to conducting polymers is presented in the first half of chapter 2. The second half explains the preparation techniques along with **optical and electrical characterization** of the conducting polymer samples used in this study. A brief description of the radio frequency plasma polymerization technique used for the preparation of polymer films is given. Methods adopted for **chemical synthesis** of polymer samples are outlined. Direct and indirect **band gaps** of pure and iodine doped films are obtained from the uv-vis-NIR measurements. The results of the **electrical conductivity** measurements of pure and iodine doped films are also presented.

An outline of the present experimental arrangement for **transverse probe beam deflection** configuration is presented in chapter 3. The observed **variation of phase and amplitude** of the photothermal signal with pump – probe offset is shown graphically for the four different thin film samples under investigation. The value of thermal diffusivity of each film is extracted from these plots. The effect of iodine doping on heat diffusion in these films is also investigated and the results are presented.

Chapter 4 describes the photoacoustic measurements on bulk samples. A brief theoretical outline and the details of our experimental setup of open

photoacoustic cell configuration are given. The variation of the phase of the photoacoustic signal with modulation frequency is represented graphically for each of the bulk polymer samples - chemically prepared polyaniline and polypyrrole. The effect of doping on heat diffusion in polyaniline is also investigated by carrying out photoacoustic measurements on polyaniline doped with hydrochloric acid, sulphuric acid and camphor sulphonic acid. Thermal diffusivity is computed by theoretical fit taking into account the effect of thermo-elastic bending.

The photoacoustic determination of thermal diffusivity of conducting polymer composites is presented in chapter 5. The preparation techniques for two conducting polymer composites - polyaniline-poly vinyl chloride and polypyrrole-poly vinyl chloride - are outlined. Open photoacoustic cell method is used to determine the thermal diffusivity values for three different compositions. The room temperature electrical conductivity values for the same compositions are also determined as an attempt to obtain the correlation between electrical and heat transport processes.

The summary of the important findings of the present work and the conclusions arrived at based on the results obtained are presented in the last chapter.

Publications / Seminars

1. 'Thermal diffusivity of plasma-polymerized polyaniline films by transverse probe beam deflection' – Accepted for publication in the 'International Journal of Polymeric Materials', Taylor and Francis, NJ (U S A).
2. 'Study of heat transport in polypyrrole by probe beam deflection and photoacoustic techniques' - Communicated to 'Thermochimica Acta', Elsevier
3. 'Study of heat diffusion in polyaniline by photothermal and photoacoustic techniques'- Communicated to 'Physica B – Condensed Matter', Elsevier.
4. 'Study of heat diffusion in polyaniline by open photoacoustic cell technique' Communicated to 'International Journal of Polymeric Materials', Taylor and Francis, NJ (U S A).
5. 'Probe beam deflection technique applied to study heat diffusion in polyaniline films' – International Conference on Optoelectronic Materials and Thin Films for Advanced Technology' October 24 – 27, 2005; Organized by Department of Physics, Cochin University of Science and Technology, Kochi – 22.

Chapter 1

Photothermal Effects – An Overview

1.1 Introduction

The evolution of our understanding of the nature of the interaction between electromagnetic radiation and matter forms the basis of some of the fascinating developments in the history of science.

The various effects arising out of the interaction of electromagnetic radiation with matter paved the way for a better understanding of the macroscopic as well as microscopic structure of matter. The last few decades witnessed a surge in advanced techniques for material characterization with the availability of intense coherent sources of radiation. Photothermal science deals with a wide range of techniques and phenomena based on the conversion of absorbed optical energy into heat. Optical energy is absorbed and eventually converted into thermal energy by a variety of materials in the solid, liquid and gaseous states. Although the initial absorption process in many materials are selective, it is common for excited electronic states in atoms or molecules to give away its excitation energy by a series of non-radiative transitions that result in a general heating of the material. Although photothermal science seems to have had a remarkably late start, the discovery of photothermal effect dates back to 1880, when Alexander Graham Bell observed that audible sound is produced when sunlight is incident on optically absorbing materials.

Photothermal heating can result in different effects which, in turn, provide various detection mechanisms. Photothermal heating can provide

convenient and sensitive methods for detecting optical absorptions in matter. It can also provide information concerning various de-excitation mechanisms. Photothermal heating of a sample is usually produced with the use of laser beams, Xe arcs, or other intense light sources. Photothermal generation has three types of applications – photothermal material probing, photothermal material processing and photothermal material destruction. The most significant among these is photothermal material probing and characterization, since it enjoys the advantage of being non-destructive. This optical diagnostic technique can provide information that is not obtainable by other conventional methods. Thus photothermal technique could get wide acceptance in the study of various optical and thermal parameters.

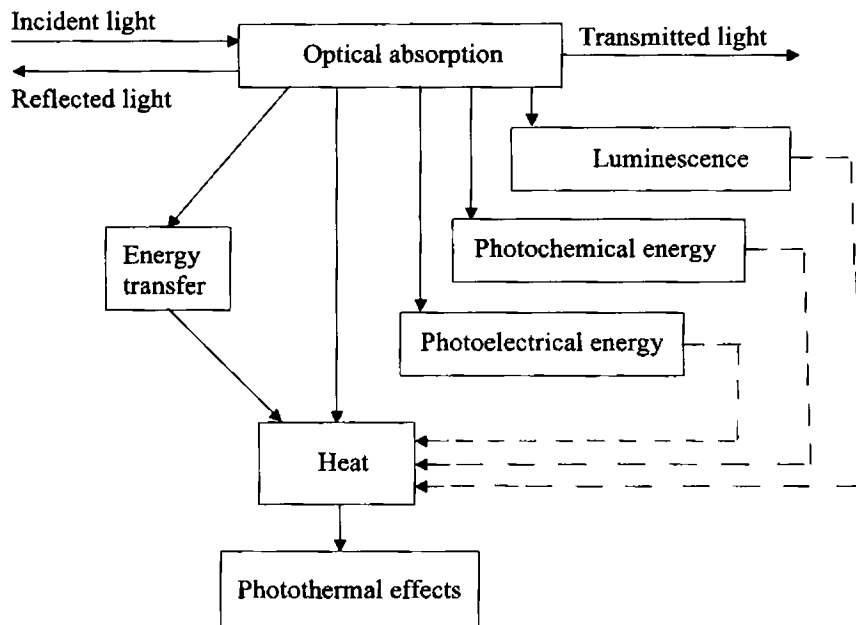


Figure 1.1 Results of optical absorption leading to prompt and delayed heat production.

Some of the most common photothermal heating effects are shown in

figure 1.1. Optical excitation of a sample can result in the generation of various forms of energy – heat, luminescence, chemical energy or electrical energy. The thermal generation is effected either directly or indirectly at various time delays due to energy transfer mechanisms. Photothermal heating induces changes in a material as well as in the adjacent medium. The various effects usually referred to as photothermal effects, arising out of this are valuable tools in material characterization [1, 2].

1.2 Photothermal effects and detection

Photothermal heating of a sample in air results in temperature rise, photoacoustic waves and refractive index changes in the sample and the adjacent medium. The choice of a photothermal effect for detection will depend on the nature of the sample and its environment, the light source used and the purpose of the measurement. Detection methods for the various

Table 1.1 Photothermal effects caused by heating of a sample by optical absorption and corresponding detection techniques

Photothermal effects	Detection methods (applicable to sample S or adjacent fluid F)
Temperature rise	Laser calorimetry (S or F)
Pressure change	Direct photoacoustic detection (S) Indirect photoacoustic detection (F)
Refractive index change (thermal or acoustic)	Probe beam refraction (S or F) Probe beam diffraction (S or F)
Surface deformation (thermal or acoustic)	Probe beam deflection (S) Optical interference (S)
Thermal emission change	Photothermal radiometry (S)
Reflectivity/absorptivity change	Transient thermal reflectance (S) Transient piezo reflectance (S) Optical transmission monitoring (S or F)

photothermal effects are generally classified into two depending on whether the detection methods are applied to the sample itself (direct detection scheme) or to the surrounding medium (indirect detection scheme). The various photothermal effects and the corresponding detection schemes are shown in table 1.1.

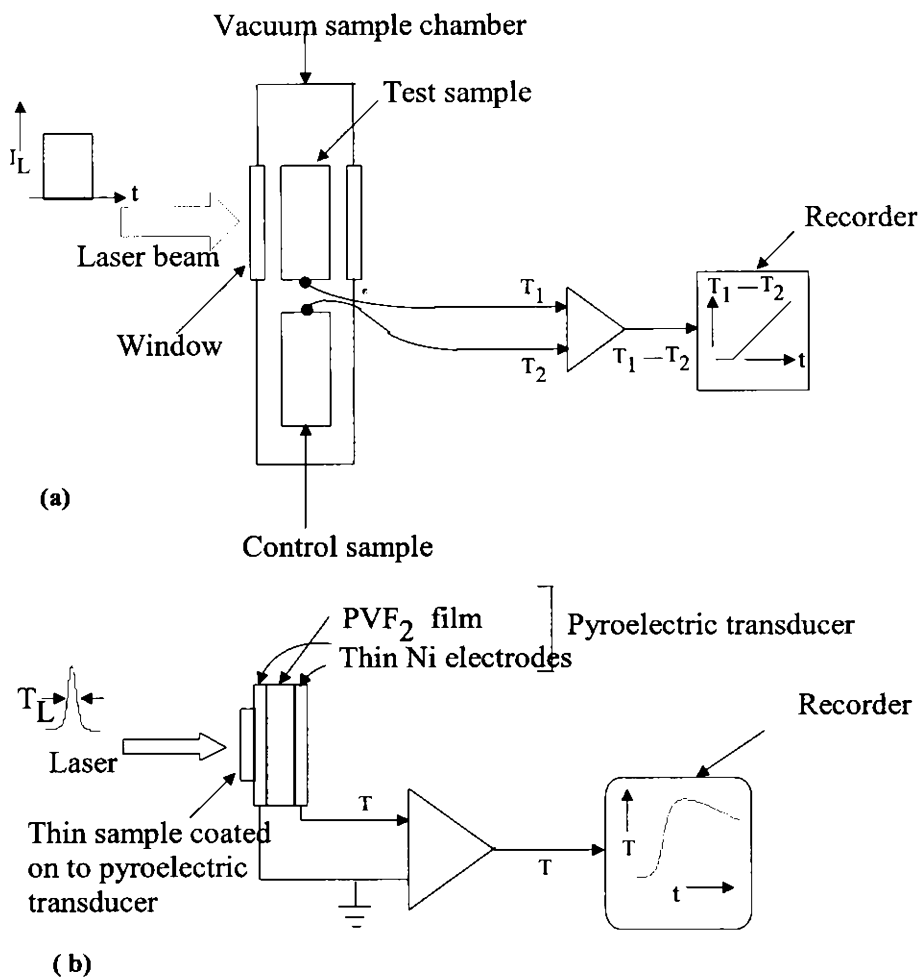


Figure 1.2 Laser calorimetric measurements (a) Step heating of an isolated sample. (b) Pulsed heating of a thin film sample in contact with a thin film pyrometer.

The various photothermal effects can be outlined as follows:

1.2.1 Temperature rise

Heating of a sample due to optical absorption can be detected by monitoring the rise in temperature. This technique is called optical calorimetry or laser calorimetry [3-5]. Laser-induced temperature rise can be directly measured using thermocouples or thermistors. Higher sensitivity is achievable with pyroelectric detectors. The method has the advantage of the readily available absolute calibration. The observed temperature rise can be directly measured and related to the physical parameters like the absorption coefficient. The main drawbacks of this technique are that the response is usually slow and the sensitivity is typically low compared to other methods. Also heat leakage from the sample must be minimized by elaborate thermal isolation. Improved techniques with high sensitivity have been developed for thin film samples, in which case the film sample is directly coated on to a thin film pyroelectric detector [6, 7].

1.2.2 Pressure change

Pressure variations resulting from absorption of modulated light from a sample is termed as photoacoustic or optoacoustic generation [8, 9]. Photoacoustic generation can be direct or indirect. In direct photoacoustic generation the acoustic wave is produced inside the sample whereas in the indirect case it is generated in a coupling medium adjacent to the sample.

Figure 1.3 shows an experimental setup used for direct photoacoustic measurements [1]. An intensity-modulated laser beam is incident on a sample in a cell and the pressure variations are monitored by a sensitive microphone. Photoacoustic method has higher sensitivity than thermocouple techniques and has wide ranging applications in the field of material characterization and nondestructive evaluation.

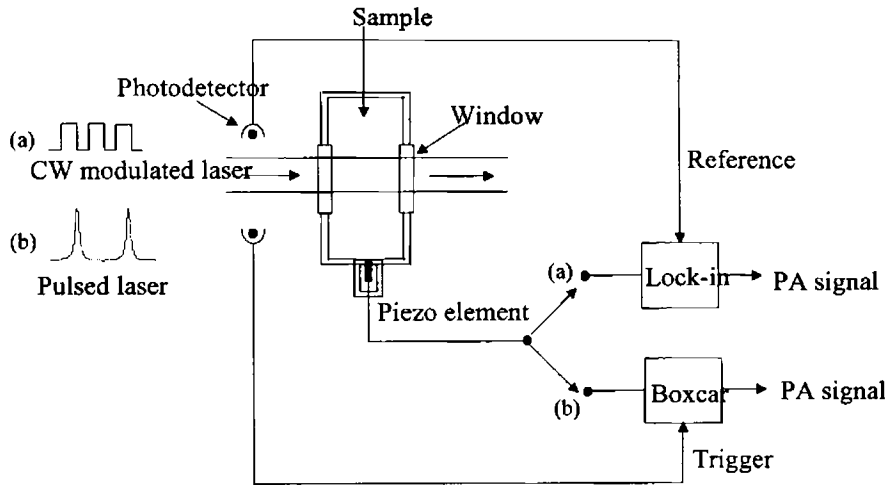


Figure 1.3 Direct PA measurement using (a) continuous modulated excitation (b) pulsed excitation.

1.2.3 Refractive index gradient

A refractive index gradient (RIG) occurs in the sample or in an adjacent medium due to photothermal heating. Basically there are two types RIG - thermal RIG and acoustic RIG - produced by photothermal heating of a sample. Thermal RIG is produced by the decreased density of the medium caused by the local temperature rise and decays in time following the diffusional decay of the temperature profile. The acoustic RIG is associated with the density fluctuations of the medium consequent to the propagation of a photoacoustic wave. The thermal refractive index gradient generated by the excitation beam affects its own propagation, resulting in self defocusing or thermal blooming [10 -12]. Self defocusing is generally observed instead of self focusing because the derivative of the refractive index with respect to temperature is usually negative, so that the temperature gradient results in a negative lens. The refractive index gradient caused by the excitation beam (pump beam) also affects the propagation of another weak probe beam in the vicinity of the excitation beam. A probe beam parallel to the pump beam with

a displacement of one beam radius gives largest probe deflection. But in the case of opaque samples the parallel configuration can not be used. For this orthogonal probe beam detection (PBD) is employed [13, 14]. The photothermal techniques involving bending of light path are in general referred to as photothermal deflection (PTD) or PBD methods [15-19]. Some experimental arrangements are designed for sensing the combined effects of deflection and lensing. Such methods are generally classified as photothermal refraction techniques [20]. Photothermal interferometric methods employ the principle of changes in optical path-lengths caused by refractive index variations.

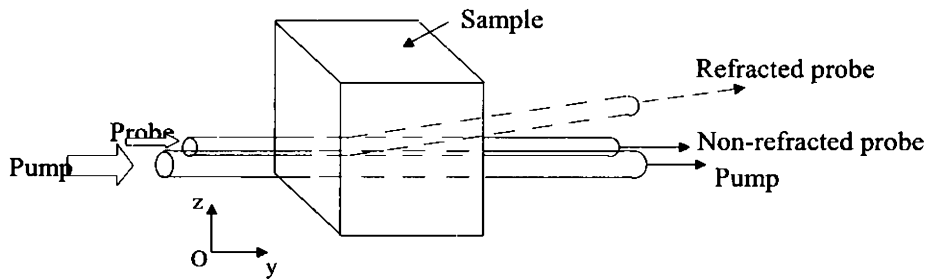


Figure 1.4a Parallel probe beam refraction

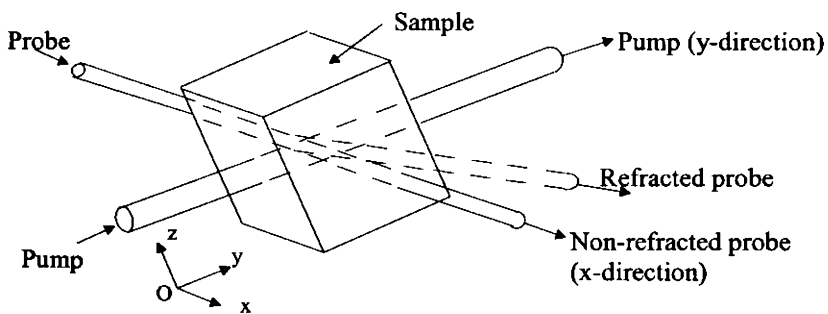


Figure 1.4b Perpendicular probe beam refraction

A periodic refractive index modulation can result in volume phase diffraction

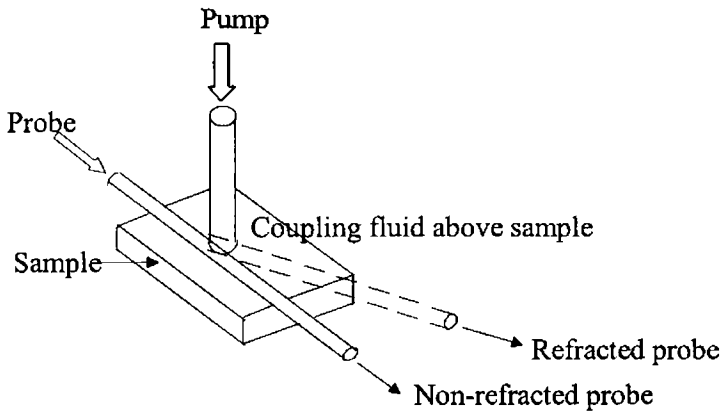


Figure 1.4c Perpendicular probe beam refraction outside the sample (mirage effect)

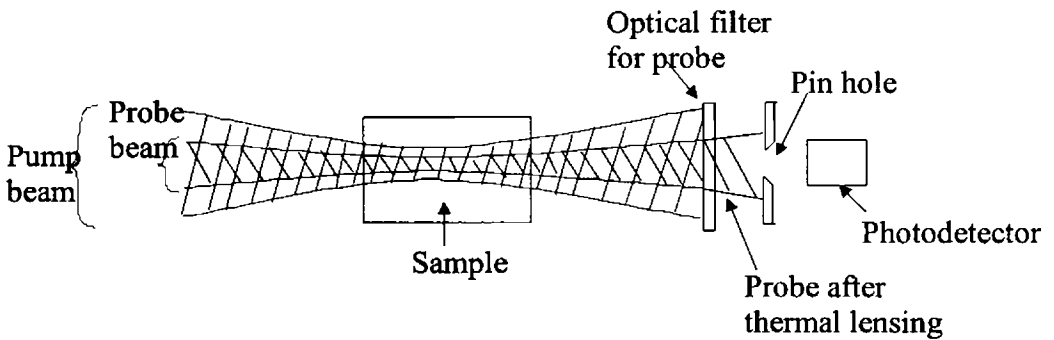


Figure 1.4d Thermal lensing

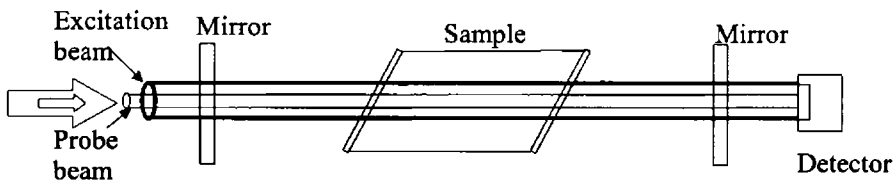


Figure 1.4e Interferometry

grating. The amount of light diffracted is proportional to the refractive index change. Methods used to measure spectroscopic signals based on volume

phase grating formed by the photothermal heating are called photothermal diffraction spectroscopy [21, 22]. The various configurations involving refractive index variations are illustrated in figures 4(a) - 4(e).

1.2.4 Surface deformation

The deformation of a sample surface resulting from photothermal excitation can be of two types – thermal and acoustic deformation. Although these two deformations are related, the thermal one decays in time as thermal diffusion, whereas the acoustic one propagates into the sample bulk and also along the sample surface as bulk and surface acoustic waves respectively.

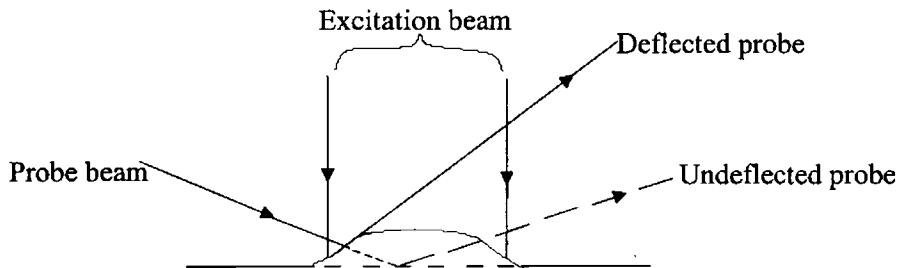


Figure 1.5 Surface deformation

The photothermal heating of a surface causes distortions due to thermal expansion [Fig 1.5]. The distortions can be very small, as low as 10^{-4} nm. Such very small surface deformations can be detected and techniques based on this form part of the photothermal displacement spectroscopy [23-25]. It is not always possible to totally separate surface deformation effects from refractive index gradient effects.

1.2.5 Infrared emission

Detection of variations in the infrared thermal radiation emitted from a sample that is excited by electromagnetic radiations of varying intensity or wavelength leads to a branch called photothermal radiometry (PTR). An

excitation spectrum called the PTR spectrum can be obtained by monitoring the PTR signal for various excitation wavelengths. The excitation beam is either continuously modulated with 50% duty cycle or pulse modulated with a very low duty cycle having high peak power. Depending on the observation point relative to the excitation region, two distinct configurations – back scattering PTR and transmission PTR - are in use. In the former emission is detected in the backward direction with respect to the excitation spot, whereas in the latter detection is in the forward direction through the sample. Thus depending on the excitation mode and the detection configuration, there are, in general, four variations of PTR as illustrated in figure 1.6. Applications of PTR include detection of voids inside opaque solids, sensitive spectroscopic absorption measurements due to less than a monolayer of molecules on a surface, spectroscopic measurements on materials at high temperature, measurement of thermal diffusivity of hazardous materials like nuclear fuels, remote sensing applications like measurements absolute absorption

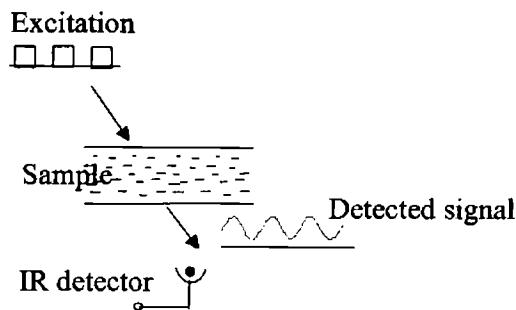


Figure 1.6a Continuously modulated transmission PTR

coefficients, monitoring thickness of layered structure and detection of degree of aggregation in powdered materials [26 -33].

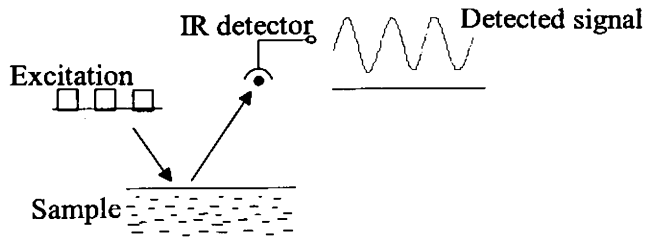


Figure 1.6b Continuously modulated back emission PTR

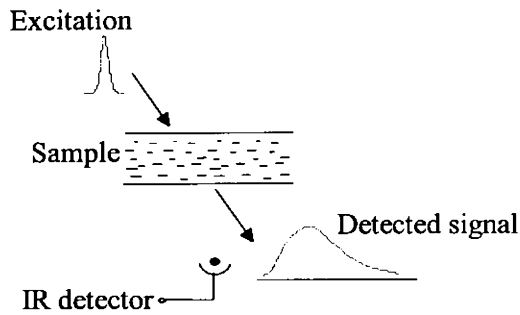


Figure 1.6c Pulsed transmission PTR

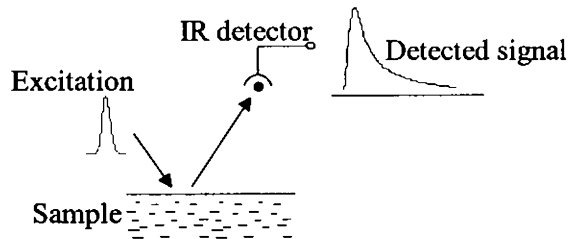


Figure 1.6d Pulsed back emission PTR

1.3 Transverse probe beam deflection methods

Transverse PBD is one of the most popular non-destructive techniques used in the thermal and optical characterization of a wide variety of materials. Its contactless nature makes it most suitable for delicate samples such as thin

films and single crystals. The underlying principle of this method is the thermal RIG resulting from the absorption of radiation.

In transverse PBD method the pump and probe are perpendicular to each other. The probe beam can be directed to the sample surface in two different ways [34- 36]. In the skimming configuration the probe beam just grazes the sample surface. In the bouncing configuration or surface reflection scheme, the probe beam is incident on the sample surface at an angle and the deflection of the reflected beam is noted.

Thermal diffusivity measurements constitute one of the most successful applications of PBD technique. The method is based on the periodic heating produced by an intensity modulated laser beam (pump beam) focused to the sample surface. The induced oscillating temperature distribution gives rise to thermal waves in the sample. The thermal waves have the same frequency as the modulated pump beam and have wavelengths determined by the modulating frequency and the thermal diffusivity of the sample. The thermal waves propagating along the surface of the sample gives rise to refractive index gradient in the nearby fluid medium adjacent to the sample surface. A second laser beam (probe beam) directed parallel to the surface of the sample in the RIG field is deflected due to mirage effect at the same frequency as the thermal wave. The magnitude and phase of the deflection is closely related to the thermal wave. The photothermal deflection signal can be resolved into two components – (i) the normal component ϕ_n in a direction normal to the sample surface and (ii) the transverse component ϕ_t along the direction tangential to the sample surface. Various schemes have been reported to analyse the mirage signal for thermal diffusivity measurement by the transverse PBD method.

1.3.1 Zero crossing method

This method, suggested by Kuo et. al. [37, 38], measures the transverse component of the photothermal signal as a function of the transverse offset. The thermal wavelength λ_{th} can be obtained from the separation x_0 between the points corresponding to a phase shift of $\pm\pi/2$ with respect to the spot centre $x=0$. Taking into account the effect of pump beam diameter, the parameter x_0 is obtained as $x_0 = \frac{\lambda_{th}}{2} + d$; where λ_{th} is the thermal wavelength and d is a constant that is related to the heating beam diameter. $x_0 = \sqrt{\frac{\pi\alpha}{f}} + d$, as $\lambda_{th} = 2\pi(2\alpha/\omega)^{1/2}$; where α is the thermal diffusivity of the sample and f is the modulating frequency. α is obtained from the slope of the plot between x_0 and $1/\sqrt{f}$. This method, although simple, fails in situations where the thermal diffusivity of the coupling fluid is greater than that of the sample.

1.3.2 Thermal wave coupling method

Wong et. al. suggested a modified PBD technique for thermal diffusivity measurements in thin films. For a film coated on a substrate, if the film is thermally thin, then a significant portion of pump power may be absorbed by the substrate [39, 40]. In this case the film-substrate combination is to be considered as a layered structure.

1.3.3 Phase method

This is the most popular transverse PBD technique used in the thermal characterization of a variety of materials ranging from semiconductors to polymers [41]. This method provides results with sufficient accuracy in the

case of materials whose thermal diffusivity is greater than that of the coupling fluid.

The tangential (transverse) component of the photothermal signal can be expressed as $\phi_t = \phi_0 \exp\left[-j\omega t - j\left(\frac{y}{l_t} + \phi\right)\right]$, where l_t is called the characteristic length which is the distance corresponding to one radian phase shift. ϕ is term depending on the pump beam spot size and the vertical offset of the probe with respect to the sample surface. The above relation implies that the phase of the PBD signal varies linearly with the pump-probe offset y . The characteristic length can be taken to be equal to the thermal diffusion length $\mu = \sqrt{\frac{\alpha}{\pi f}}$ for samples whose thermal diffusivity is greater than that of the coupling fluid. The thermal diffusivity can be obtained from the slope of the plot between phase and the pump-probe offset. A detailed theoretical treatment of the probe beam deflection is presented in section 1.4.

For materials with very low thermal diffusivity, the characteristic length differs from the thermal diffusion length $\mu = \sqrt{\frac{\alpha}{\pi f}}$ and has a strong dependence on the vertical offset of the probe beam relative to the sample surface. In this case the characteristic length is related to the thermal diffusion length as $l_t = \mu + kz$, where k is the term depending on the ratio of the diffusivities of the coupling fluid and the sample and z is the vertical offset [41]. Thermal diffusivity can be computed by plotting l_t against $1/\sqrt{f}$, thus eliminating the effect of vertical offset of the probe above the sample surface.

1.3.4 Amplitude method

Similar to the phase method, the amplitude method accounts for the variation of amplitude A_t of the tangential component of the PBD signal with pump-probe offset. It can be shown that $\ln A_t$ varies linearly with the offset y and the thermal diffusivity can be obtained from the slope of the plot [42]. For materials with low thermal diffusivity, the effect of vertical offset can be eliminated as described in section 1.3.3.

1.4 Probe beam deflection – A theoretical approach [1, 16-18]

The heat diffusion equation in cylindrical geometry [43] is given by

$$\frac{\partial T}{\partial t} = D \left[\frac{\partial^2 T}{\partial r^2} + \frac{1}{r} \frac{\partial T}{\partial r} + \frac{1}{r^2} \frac{\partial^2 T}{\partial \theta^2} + \frac{\partial^2 T}{\partial z^2} \right]; \quad 1.1$$

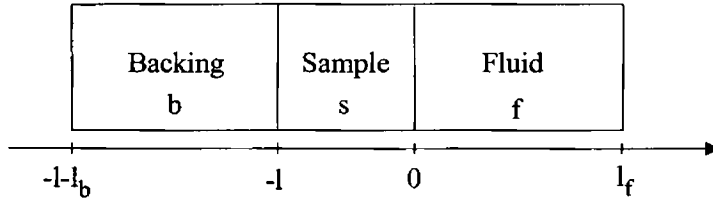


Figure 1.7: Geometry of Rosencwaig and Gersho model

where D is the thermal diffusivity. When heat flow takes place in planes through z-axis then the heat diffusion equation becomes

$$\frac{\partial T}{\partial t} = D \left[\frac{\partial^2 T}{\partial r^2} + \frac{1}{r} \frac{\partial T}{\partial r} + \frac{\partial^2 T}{\partial z^2} \right] \quad 1.2$$

Assuming that the homogeneous sample is absorbing and the backing and adjacent fluid are transparent, the heat diffusion equations in the three regions can be written as

$$\frac{\partial^2 T_f}{\partial r^2} + \frac{1}{r} \frac{\partial T_f}{\partial r} + \frac{\partial^2 T_f}{\partial z^2} = \frac{1}{D_f} \frac{\partial T_f}{\partial t}; \quad 0 \leq z \leq l_f \quad 1.3$$

$$\frac{\partial^2 T_s}{\partial r^2} + \frac{1}{r} \frac{\partial T_s}{\partial r} + \frac{\partial^2 T_s}{\partial z^2} = \frac{1}{D_s} \frac{\partial T_s}{\partial t} - A(r,t) \exp(\alpha z) [1 + \exp(j\omega t)]; \quad -l \leq z \leq 0. \quad 1.4$$

$$\frac{\partial^2 T_b}{\partial r^2} + \frac{1}{r} \frac{\partial T_b}{\partial r} + \frac{\partial^2 T_b}{\partial z^2} = \frac{1}{D_b} \frac{\partial T_b}{\partial t}; \quad -(l+l_b) \leq z \leq -l. \quad 1.5$$

The relevant boundary conditions are

$$k_s \frac{\partial T_s}{\partial z}(z=0) = k_f \frac{\partial T_f}{\partial z}(z=0) \quad 1.6a$$

$$k_s \frac{\partial T_s}{\partial z}(z=-l) = k_b \frac{\partial T_b}{\partial z}(z=-l) \quad 1.6b$$

$$T_s(z=-l,t) = T_b(z=-l,t); \quad T_s(z=0,t) = T_f(z=0,t) \quad 1.6c$$

$$T_f(\infty,t) = T_b(-\infty,t) = 0 \quad \text{with } l_f : \infty, l_b : -\infty \quad 1.6d$$

Heat deposited per unit volume is

$$A(r,t) = \frac{\eta P \alpha}{k_s \pi a^2} \exp(-2r^2/a^2) (1 + \cos \omega t); \quad 1.7$$

where P is the power of the exciting beam, α is the optical absorption coefficient, η is the light conversion efficiency and a is the beam radius at $1/e^2$ -intensity. It is assumed that l_f and l_b are very large compared to the heated area and backward heat propagation in these two regions is neglected. k_i is the thermal conductivity of the material i with $i = s, b$ and f .

The above partial differential equations are reduced to simple partial differential equations using Hankel transformation. Laplace transformation is used to convert the resulting equations to ordinary differential equations. The analytical expressions for the temperature field can be obtained from the resulting differential equations replacing the modulated source by a unit source $A(r)\delta(t)$.

Applying the Hankel transformation $T(r, z, t) \rightarrow T_0(\lambda, z, t)$, the partial differential equations for the three regions are reduced to the form,

$$-\lambda^2 T_0(\lambda, z, t) + \frac{\partial^2 T_0}{\partial z^2}(\lambda, z, t) = \frac{1}{D} \frac{\partial T_0}{\partial t}(\lambda, z, t) \quad 1.8$$

$$\text{or } -\lambda^2 T_0(\lambda, z, t) + \frac{\partial^2 T_0}{\partial z^2}(\lambda, z, t) = \frac{1}{D} \frac{\partial T_0}{\partial t}(\lambda, z, t) - A_0(\lambda) \exp(\alpha z) \delta(t); \quad 1.9$$

where $A_0(\lambda)$ is the Hankel transform of $A(r)$. Equation 1.9 is valid for the sample region where a heat source exists.

Use of Laplace transformation $T_0(\lambda, z, t) \rightarrow F(\lambda, z, p)$ yields equations of the form

$$-\lambda^2 F_0(\lambda, z, p) + \frac{\partial^2 F_0}{\partial z^2}(\lambda, z, p) = \frac{p}{D} \frac{\partial F_0}{\partial t}(\lambda, z, p) \quad 1.10$$

$$-\lambda^2 F_0(\lambda, z, p) + \frac{\partial^2 F_0}{\partial z^2}(\lambda, z, p) = \frac{p}{D} \frac{\partial F_0}{\partial t}(\lambda, z, p) - A_0(\lambda) \exp(\alpha z) \quad 1.11$$

$$F_0(\lambda, z, p) = A(\lambda, p) \exp\left(-\sqrt{\lambda^2 + \frac{p}{D}} z\right) + B(\lambda, p) \exp\left(\sqrt{\lambda^2 + \frac{p}{D}} z\right) \quad 1.12$$

$$F_0(\lambda, z, p) = A'(\lambda, p) \exp\left(-\sqrt{\lambda^2 + \frac{p}{D}} z\right) + B'(\lambda, p) \exp\left(\sqrt{\lambda^2 + \frac{p}{D}} z\right) + C'(\lambda, p) A_0(\lambda) \exp(\alpha z) \quad 1.13$$

$$\text{where } C'(\lambda, p) = \frac{1}{\lambda^2 + (p/D) - \alpha^2}$$

Use of Hankel inversion gives

$$F_0(r, z, p) = \int_0^\infty \left[A(\lambda, p) \exp\left(-\sqrt{\lambda^2 + \frac{p}{D}} z\right) + B(\lambda, p) \exp\left(\sqrt{\lambda^2 + \frac{p}{D}} z\right) \right] \times J_0(\lambda r) \lambda d\lambda$$

and

$$F_0(r, z, p) = \int_0^{\infty} \left[A'(\lambda, p) \exp\left(-\sqrt{\lambda^2 + \frac{p}{D}} z\right) + B'(\lambda, p) \exp\left(\sqrt{\lambda^2 + \frac{p}{D}} z\right) + C'(\lambda, p) A_0 \lambda \exp(\alpha z) \right] \times J_0(\lambda r) \lambda d\lambda$$

1.15

The periodic steady state is obtained from

$$T(r, z, t) = F_0(r, z, p)_{p=j\omega} \exp(j\omega t) \quad 1.16$$

where the constants are determined by the boundary conditions. The modulated temperature field in the three regions is obtained as

$$T_f(r, z, t) = \int_0^{\infty} T_s(\lambda) \exp(-\beta_f z) \exp(j\omega t) J_0(\lambda r) \lambda d\lambda \quad 1.17$$

$$T_b(r, z, t) = \int_0^{\infty} W(\lambda) \exp[\beta_b(z+l) + j\omega t] J_0(\lambda r) \lambda d\lambda \quad 1.18$$

$$T_s(r, z, t) = \int_0^{\infty} [U(\lambda) \exp(\beta_s z) + V(\lambda) \exp(-\beta_s z) - E(\lambda) \exp(\alpha z)] \exp(j\omega t) J_0(\lambda r) \lambda d\lambda \quad 1.19$$

$$\text{where } E(\lambda) = \frac{P\eta}{\pi k_s} \frac{\exp\left(\frac{-\lambda^2 a^2}{8}\right)}{\left(-\lambda^2 - j\frac{\omega}{D_s} + \alpha^2\right)} \quad 1.20$$

$$a^2 \exp\left(\frac{-\lambda^2 a^2}{8}\right) = \int_0^{\infty} \exp(-2r^2/a^2) J_0(r\lambda) r dr$$

$$\text{and } \beta_i^2 = \lambda^2 + \frac{j\omega}{D_i} \quad 1.21$$

The final temperature distribution is obtained by substituting the following expressions in the above equations:

$$T_s(\lambda) = -E(\lambda) + U(\lambda) + V(\lambda)$$

$$W(\lambda) = -E(\lambda)\exp(-\alpha l) + U(\lambda)\exp(-\beta_s l) + V(\lambda)\exp(\beta_s l)$$

$$U(\lambda) = \left[(1-g)(b-r)\exp(-\alpha l) + (g+r)(1+b)\exp(\beta_s l) \right] \frac{E(\lambda)}{H(\lambda)}$$

$$V(\lambda) = \left[(1+g)(b-r)\exp(-\alpha l) + (g+r)(1-b)\exp(-\beta_s l) \right] \frac{E(\lambda)}{H(\lambda)}$$

1.22

$$\text{where } g = \frac{k_f \beta_f}{k_s \beta_s} \quad b = \frac{k_b \beta_b}{k_s \beta_s} \quad r = \frac{\alpha}{\beta_s} \quad 1.23$$

$$\text{and } H(\lambda) = (1+g)(1+b)\exp(\beta_s l) - (1-g)(1-b)\exp(-\beta_s l) \quad 1.24$$

The surface temperature can be written as

$$T_s(0, t) = \int_0^{\infty} \overline{T_s(\lambda)} J_0(\lambda r) \lambda d\lambda \exp(j\omega t); \quad 1.25$$

where

$$\overline{T_s(\lambda)} = E(\lambda) \left[\frac{-(1+b)(1-r)\exp(\beta_s l) + (1-b)(1+r)\exp(-\beta_s l) - 2(r-b)\exp(-\alpha l)}{(1+g)(1+b)\exp(\beta_s l) - (1-g)(1-b)\exp(-\beta_s l)} \right]$$

1.26

The term in the bracket in $\overline{T_s(\lambda)}$ describes the thermal response of the three media to a unit spatial pulse. For thermally thick samples the term reduces to

$\frac{r-1}{g+1}$ and for thermally thin samples the term is given by

$$\frac{(r-b)[1-\exp(-\alpha l)] + \sigma_s l (rb-1)}{b+g} \quad 1.27$$

Consider the case of a transverse probe beam deflection configuration.

Let the probe beam be propagating in the fluid f along the x-direction. The probe beam deflection in the two directions z and y are given by

$$\theta_n = \frac{1}{n_0} \frac{dn}{dT} \int_{-\infty}^{+\infty} \frac{\partial T_f}{\partial z} dx \quad \text{and} \quad \theta_t = \frac{1}{n_0} \frac{dn}{dT} \int_{-\infty}^{+\infty} \sin \alpha \frac{\partial T_f}{\partial r} dx . \quad 1.28$$

θ_n is the normal deflection parallel to z whereas θ_t is the transverse (tangential) deflection parallel to y. Using the Hankel spectrum of surface temperature as given by equation 1.26, θ_n and θ_t can be expressed as

$$\theta_n = \frac{2}{n_0} \frac{dn}{dT} \exp(j\omega t) \int_0^{\infty} \overline{T_s(\lambda)} \beta_f \exp(-\beta_f z) \cos(\lambda y) d\lambda \quad 1.29$$

$$\theta_t = \frac{2}{n_0} \frac{dn}{dT} \exp(j\omega t) \int_0^{\infty} \overline{T_s(\lambda)} \beta_f \exp(-\beta_f z) \sin(\lambda y) d\lambda \quad 1.30$$

θ_n is related to the heat diffusion process normal to the sample surface while θ_t is a measure of the heat diffusion parallel to the sample surface. An account of the thermal diffusivity of a sample can be obtained from the measurements of these deflections.

1.5 Photoacoustic Effect - Rosencwaig-Gersho Theory

A one dimensional analysis of the production of photoacoustic signal in a cylindrical cell is presented by the Rosencwaig and Gersho theory [44,45].

Consider a cylindrical cell of length L and diameter D as shown in figure 1.8. Assume that the length L is small compared to the wavelength of the acoustic signal. The sample is considered to be in the form of a disk having diameter D and thickness l . The sample is mounted so that its front surface is exposed to the gas (air) within the cell and its back surface is a poor thermal conductor of thickness l_b . The length l_g of the gas column in the cell is then

given by $l_g = L - l - l_b$. Further assumption is that the gas and backing material are not light absorbing.

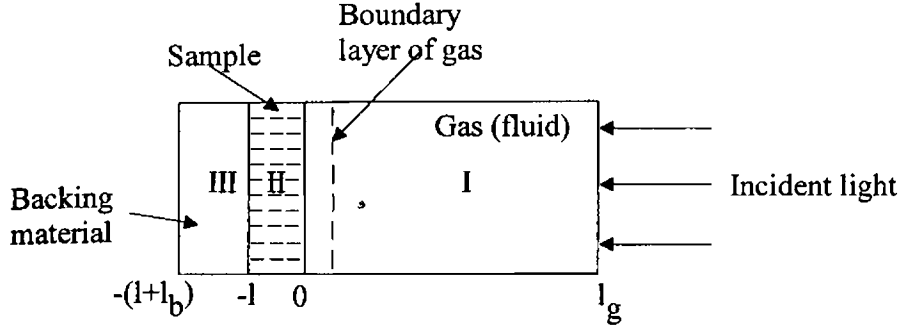


Figure 1.8 Rosencwaig and Gersho ID model

Let k_i , ρ_i , C_i and α_i represent the thermal conductivity, density, specific heat capacity and thermal diffusivity respectively of the material i .

$a_i = \left(\frac{\omega}{2\alpha_i} \right)^{1/2}$ is the thermal diffusion coefficient and $\mu_i = \frac{1}{a_i}$ is the thermal diffusion length of the material. The subscript i can be s , g and b for solid, gas and backing material respectively. ω denotes the chopping frequency of the incident light beam in radians per second.

Assume that the sinusoidally chopped monochromatic light source with wavelength λ is incident on the solid with intensity $I = \frac{1}{2} I_0 (1 + \cos \omega t)$

The thermal diffusion equation in the three regions can be written as [43]

$$\frac{\partial^2 \theta}{\partial x^2} = \frac{1}{\alpha_b} \frac{\partial \theta}{\partial t}; \quad -l - l_b \leq x \leq -l \quad (\text{Region III}) \quad (1.31)$$

$$\frac{\partial^2 \theta}{\partial x^2} = \frac{1}{\alpha_g} \frac{\partial \theta}{\partial t}; \quad 0 \leq x \leq -l_g \quad (\text{Region I}) \quad (1.32)$$

$$\frac{\partial^2 \theta}{\partial x^2} = \frac{1}{\alpha_s} \frac{\partial \theta}{\partial t} - A \exp(\beta x) [1 + \exp(j\omega t)]; \quad -l \leq x \leq 0 \quad (\text{Region II})$$

$$(1.33)$$

with $A = \frac{\beta I_0 \eta}{2k_s}$. θ is the temperature, η is the light conversion efficiency and

β is the optical absorption coefficient. The real part of the complex-valued solution $\theta(x, t)$ of the above equations is the solution of physical interest and represents the temperature in the cell relative to the ambient temperature as a function of position and time. Thus, the actual temperature field in the cell is given by $T(x, t) = \text{Re}[\theta(x, t) + \phi_0]$; where ϕ_0 is the ambient temperature.

The complex amplitude of the periodic temperature distribution, $\theta(x, t)$ at the solid-gas boundary ($x = 0$) is given by

$$\theta_0 = \frac{\beta I_0}{2k_s (\beta^2 - \sigma_s^2)} \times \left(\frac{(r-1)(b+1)\exp(\sigma_s l) - (r+1)(b-1)\exp(-\sigma_s l) + 2(b-r)\exp(-\beta l)}{(g+1)(b+1)\exp(\sigma_s l) - (g-1)(b-1)\exp(-\sigma_s l)} \right)$$

$$(1.34)$$

$$\text{where } b = \frac{k_b a_b}{k_s a_s}, \quad g = \frac{k_g a_g}{k_s a_s}, \quad r = (1-j) \frac{\beta}{2a_s} \text{ and } \sigma_s = (1+j)\alpha_s.$$

The main source of acoustic signal arises from the periodic heat flow from the solid to the surrounding gas. The periodic heating causes the boundary layer of gas to expand and contract periodically. This can be thought of as the action of an acoustic piston on the rest of the gas column, producing an acoustic pressure signal that travels through the entire gas column. The

displacement of the gas piston due to the periodic heating can be estimated using the ideal gas law,

$$\delta x(t) = \frac{\theta_0 \mu_g}{\sqrt{2} T_0} \exp \left[j \left(\omega t - \frac{\pi}{4} \right) \right] \quad (1.35)$$

$T_0 = \phi_0 + F_0$; where ϕ_0 is the ambient temperature at the cell walls and F_0 is the increase in temperature due to the steady state component of the absorbed heat. Assuming that the rest of the gas responds to the action of the piston adiabatically, the acoustic pressure in the cell due to the displacement of the gas piston can be obtained from the adiabatic gas law, $PV^\gamma = \text{constant}$, where P is the pressure, V is the gas volume in the cell, and γ ratio of the specific heats. Thus the incremental pressure is

$$\delta P(t) = \frac{\gamma P_0}{V_0} \delta V = \frac{\gamma P_0}{l_g} \delta x(t) \quad (1.36)$$

where P_0 and V_0 are the ambient pressure and volume respectively and δV is the incremental volume. Then from equations (1.35) & (1.36)

$$\delta P(t) = Q \exp \left[j \left(\omega t - \frac{\pi}{4} \right) \right]; \quad (1.37)$$

where $Q = \frac{\gamma P_0 \theta_0}{\sqrt{2} l_g a_g T_0}$

The actual physical pressure variation is given by the real part of $\delta P(t)$ and Q specifies the complex envelope of the sinusoidal pressure variation.

Substituting for θ_0 ,

$$Q = \frac{\beta I_0 \gamma P_0}{2\sqrt{2} k_s l g_a T_0 (\beta^2 - \sigma_s^2)} \times \left(\frac{(r-1)(b+1)\exp(\sigma_s l) - (r+1)(b-1)\exp(-\sigma_s l) + 2(b-r)\exp(-\beta l)}{(g+1)(b+1)\exp(\sigma_s l) - (g-1)(b-1)\exp(-\sigma_s l)} \right) \quad (1.38)$$

Thus, equation $\delta P(t)$ can be evaluated for obtaining the amplitude and phase of the acoustic pressure wave produced in the cell by photoacoustic effect. It can be observed that interpretation of the full expression for $\delta P(t)$ is difficult because of the complex expression of Q . Physical insight can be gained easily if certain special cases according to the optical opaqueness of solids are examined. For each category of optical opaqueness, three cases arise depending on the values of thermal diffusion length μ_s , the physical length l and the optical absorption length μ_β . The equation 1.38 can be reduced to a simpler form for each of these categories.

1.6 Open photoacoustic cell (OPC) method

The generation of acoustic waves in a material when a modulated beam of light is incident on it is referred to as the photoacoustic effect. Ever since the theory of PA effect was developed by Rosencwaig and Gersho, this effect has been effectively used in diverse areas of physics, chemistry and medicine [46 - 47]. With the availability of sophisticated data acquisition systems and high quality tunable light sources, the versatility of the PA technique paved the way to several innovative experimental configurations. Photoacoustic methods can, in general, be divided into two – (i) direct and (ii) indirect. In direct photoacoustic signal generation, the acoustic wave is

produced in the sample whereas in the indirect method it is in the coupling medium adjacent to the sample.

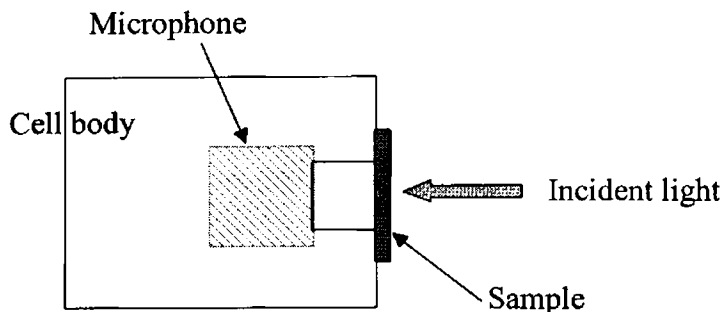


Figure 1.8 Basic OPC configuration

The open photoacoustic cell (OPC) configuration is a more convenient and compact form of PA detection scheme [48 – 59]. It is also referred to as minimal volume photoacoustic configuration. In this method a solid sample is mounted directly on the top of the detector (microphone), leaving a small volume of air in between the sample and the microphone. Being a minimal volume PA detection scheme, the strength of the PA signal will be much higher than that in a conventional PA method. The main advantage of the OPC method is that samples having large area can be studied, whereas in a conventional PA cell the sample size is restricted by the cavity dimensions.

1.6.1 OPC configuration – Theory

The expression for the PA signal from the 1-D heat flow model of Rosencwaig and Gersho is given by

$$\delta P = \frac{\gamma P_0 I_0 (\alpha_g \alpha_s)^{1/2}}{2\pi l_g T_0 k_s f \sinh(l_s \sigma_s)} \exp\left[j\left(\omega t - \frac{\pi}{2}\right)\right] \quad 1.39$$

where γ is the specific heat ratio of air, P_0 and T_0 are the ambient pressure and temperature respectively, I_0 is the incident light intensity, f is the modulation frequency, and l_i , k_i and α_i are the respective length, thermal conductivity and thermal diffusivity of material i . Here the subscript i denotes the sample (s) and gas (g) and $\sigma_s = (1+j)a_s$, with $a_s = (\pi f / \alpha_s)^{1/2}$ is the complex thermal diffusion coefficient of the sample.

If the sample is optically opaque and thermally thick,

$$\delta P; \frac{\gamma_0 P_0 I_0 (\alpha_g \alpha_s)^{1/2} \exp[-l_s (\pi f / \alpha_s)^{1/2}]}{\pi l_g T_0 k_s f} \exp\left[j \left(\omega t - \frac{\pi}{2} - l_s a_s \right) \right] \quad 1.40$$

where l_s and a_s are the thickness and thermal diffusion coefficient of the sample. According to equation (1.40) the phase of the PA signal varies with modulation frequency as $l_s (\pi f / \alpha_s)^{1/2}$. Thus thermal diffusivity can be obtained from the phase data. If there is thermo-elastic bending due to the temperature gradient generated within the sample across its thickness, then the phase will not vary linearly with square root of modulation frequency [60, 61]. In such a case,

$$\delta P = \frac{3\alpha_T R^4 \gamma P_0 I_0 \alpha_s}{4\pi R_c^2 l_s^2 l_g k_s f} \left[\left(1 - \frac{1}{x} \right)^2 + \frac{1}{x^2} \right]^{1/2} e^{j(\omega t + \pi/2 + \Phi)}, \quad 1.41$$

$$\text{where } x = l_s (\pi f / \alpha_s)^{1/2}, \quad 1.42$$

$$\Phi = \tan^{-1} \left[\frac{1}{x-1} \right] \quad 1.43$$

and α_r is the thermal expansion coefficient of the sample. R and R_c are the radii of the front hole of the microphone and OPC air chamber respectively. Now the thermal diffusivity can be obtained from the phase data by fitting the following equation,

$$\phi = \phi_0 + \tan^{-1} \left\{ \left[I_s (\pi f / \alpha_s)^{1/2} - 1 \right]^{-1} \right\} \quad 1.44$$

In the present work the two photothermal techniques – probe beam deflection and OPC, whose theoretical background is described above, are successfully applied for the non-destructive thermal characterization of some of the important electrically conducting polymers. Thermal diffusivity of some of the conducting polymers with conjugated structure is determined using OPC technique whereas that of plasma polymerized thin films is evaluated applying transverse probe beam deflection method.

References

1. Jeffrey A Sell, Photothermal Investigations of Solids and Liquids, Academic Press Inc, New York (1988).
2. Stephen E Bialkowski, Photothermal Spectroscopy Methods for Chemical Analysis, John Wiley & Sons, Inc.
3. M.Bass, L.Liou, J.appl.Phys.56 (1984)184
4. G.H. Brilmyer, A Fujishima, K S V Santhanam, A J Bard, Anal.Chem.49, (1977) 2057.
5. M Bass, E W Van Stryland and A F Steward, Appl. Phys. Lett. 34 (1979) 142.
6. H Coufal, P Hefferle, Appl. Phys A, 38 (1985)213.
7. H Coufal, Appl Phy Lett 44 (1984) 59.

8. A Rosencwaig, *Photoacoustics and Photoacoustic spectroscopy*, Wiley, New York (1980).
9. A Rosencwaig, J B Willis, *J. Appl. Phys.* 51(8), (1980) 4361.
10. R C Leite, R.S.Moore, J R Whinnery, *Appl. Phys. Lett.*, 5 (1964) 141.
11. R L Swofford, M E Long, A C Albrecht, *J. Chem. Phys.*, 65 (1976)179.
12. Howard L Fang, Robert L Swofford, *J. Appl. Phys.*50 (11) (1979) 6609.
13. D A Fournier, A C Boccara, N M Amer and R Gerlach, *Appl Phys Lett* 37 (1980) 519.
14. M J D Low, C. Morterra, A G Severdia and M Lacroix, *Appl. Surf. Sci.* 13 (1982) 429.
15. A C Boccara, D Fournier, J Badoz, *Appl. Phys. Lett.* 36, (1979)130.
16. J C Murphy, L C Aamodt, *J. Appl. Phys* 51(9) (1980) 4580.
17. L C Aamodt, J C Murphy, *J. Appl. Phys.* 52(8) (1981)4903.
18. J C Murphy, L C Aamodt, *Appl. Phys. Lett* 39(7) (1981) 519.
19. A C Boccara, D Fournier, W Jackson, D Fournier, *Opt. Lett* 5(9) (1980) 377.
20. N J Dovichi, T G Nolan, W A Weimer, *Anal. Chem.* 56 (1984) 1700.
21. J F Power, M A Schweitzer, *Opt. Eng.* 36(2), (1997) 521.
22. S E Bialkowski, A Chartier, *Appl. Opt.* 36(27), (1997) 6711.
23. M A Olmstead and N M Amer, *Phy. Rev. Lett*, 52, (1984) 1148.
24. N M Amer, *J. Phys (Paris) Colloq C6* (1983) 185.
25. M. A. Olmstead, N. M. Amer, S E Kohn, D Fournier and A C Boccara, *Appl. Phys. A* 32 (1983) 141.
26. G Busse, *Infrared Phys.* 20 (1980) 419.
27. G Busse and P Eyerer, *Appl. Phys. Lett.* 43 (1983) 355.
28. G Busse and K F Renk, *Appl. Phys. Lett.* 42 (1983) 366.
29. P E Nordal, S O Kanstad, *Appl. Phys. Lett.* 38 (1981) 486.

30. H W Deem and W D Wood, *Rev. Sci. Instrum.* 33 (1962) 1107.
31. A C Tam and B Sullivan, *Appl. Phys. Lett.* 43 (1983) 333.
32. W P Leung and A C Tam, *Opt. Lett.* 9 (1984) 93.
33. W P Leung and A C Tam, *J. Appl. Phys.* 56 (1984) 153.
34. A Salazar, A Sanchez-Lavega, J Fernandez, *J. Appl. Phys.* 69(3), (1991)1216.
35. M Bertolotti, G L Liakhou, R Li Voti, S Paoloni, C Sibilìa, *J. Appl. Phys.* 83 (2) (1998) 966.
36. M Bertolotti, G L Liakhou, R Li Voti, S Paoloni, C Sibilìa, *Appl. Phys. B* 67 (1998) 641.
37. P K Kuo, M J Lin, C B Reyes, L D Favro, R L Thomas, D S Kim, Shu-yi Zhang, L J Inglehart, D Fournier, A C Boccara, N Yacoubi, *Can. J. Phys.* 64 1165 (1986).
38. P K Kuo, E D Sandler, L D Favro, R L Thomas, *Can. J. Phys.* 64 1168 (1986).
39. P K Wong, P C W Fung, H L Tam, J Gao, *Phys. Rev. B* 51(1) (1995) 523.
40. P K Wong, P C W Fung, H L Tam, *J. Appl. Phys* 84(12) (1998) 6623.
41. M Bertolotti, R Li Voti, G Liakhou, C Sibilìa, *Rev. Sci. Instrum* 64(6) 1576 (1993).
42. X Quelin, B. Perrin, G Louis, P Peretti, *Phys. Rev. B* 48 (6) (1993) 3677.
43. H S Carslaw and J C Jaeger, *Conduction of Heat in Solids*, Oxford, Clarendon (1959).
44. A Rosecwaig, A Gersho, *J. Appl. Phys.* 47 (1976) 64.
45. A Rosecwaig, *Photoacoustics and Photoacoustic Spectroscopy*, John Wiley & Sons, New York, (1980).
46. H Vargas, L C M Miranda, *Rev. of Sci. Instrum.* 74(1) (2003) 794.

47. Werner Faubel, Stefan Heissler, Ute Pyell, Natalia Ragozina, *Rev. Sci. Instrum.* 74(1) (2003) 491.
48. S O Kanstad, P E Nordal, *Opt. Comm.* 26, (1978) 367.
49. L F Perondi, L C M Miranda, *J. Appl. Phys.* 62 (1987) 2955.
50. M V Marquezini, N Cella, A M Mansanares, H Vargas, L C M Miranda, *Meas. Sci. Technol.* 2 (1991) 396.
51. A P Neto, H Vargas, N F Leite, L C M Miranda, *Phy. Rev. B*, 40 (1989) 3924.
52. A P Neto, H Vargas, N F Leite, L C M Miranda, *Phy. Rev. B*, 41 (1990) 9971.
53. A M Mansanares, H Vargas, F Galembeck, J Buijs, D Bicanic, *J. Appl. Phys.* 70 (1991) 7046.
54. P M Nikolic, D M Todorovic, A J Bojicic, K T Radulovic, D Urosevic, J Elzar, V Blagojevic, P Mihajlovic, M Miletic, *J. Phys: Condens. Matter*, 8 (1996) 5673.
55. C G Segundo, M V Muniz, S Muhl, *J. Phys. D: Appl. Phys.* 31 (1998) 165.
56. E Marin, H Vargas, P Diaz, I Reich, *Phys. Stat. Sol. (a)* 179 (2000) 387.
57. O D Vasallo, A C Valdes, E Marin, J A P Lima, M G Silva, M Sthel, H Vargas, S L Cardoso, *Meas. Sci. Technol.* 11, (2000) 412.
58. O D Vasallo, E Marin, *J. Phys. D: Appl. Phys.* 32 (2000) 593.
59. B Lopez, D A Avalos, J J Alvarado, J Angel, F S Sinencio, C Falcony, F Orea, H Vargas, *Meas. Sci. Technol.* 6 (1995) 1163.
60. N F Leite, C Cella, H Vargas, L C M Miranda, *J. Appl. Phys* 61 (8) (1987) 3025.
61. G Rousset, F Lepoutre, L Bertrand, *J. Appl. Phys.* 54 (1983) 2383.

Chapter 2

Conducting Polymers

2.1 Introduction

Conducting polymers have been extensively studied during the last two decades because of their highly significant contributions in the field of applied as well as basic sciences. The excellent mechanical properties and intriguing electronic properties of this class of polymeric materials make them ideal candidates to be used in many device applications. Until the early sixties the carbon based polymers were extensively used as insulators in the electronic industry. Researches in the beginning of the 1960s at BASF, Germany revealed new structural properties of polymers made by oxidative coupling. This work yielded conducting polymers like polyphenylene and polythiophene exhibiting electrical conductivities up to 0.1 S.cm^{-1} . The highly sophisticated microelectronics industry channeled adequate resources for encouraging research and development of novel polymers possessing good physical and electrical properties.

A significant discovery in the development of conducting polymers was the finding in 1973 that the inorganic polymer polysulphur nitride, $(\text{SN})_x$ is as good as a metal with room temperature conductivity of the order of 10^3 Scm^{-1} compared to $6 \times 10^5 \text{ Scm}^{-1}$ for copper and $10^{-14} \text{ Scm}^{-1}$ for polyethylene [1]. A major breakthrough in the field of electrically conducting polymers occurred in 1977 with discovery of conducting polyacetylene by Shirakawa et al [2]. Polyacetylene containing conjugated single and double bonds in its structure becomes electrically conducting with a structural

modification consequent to a process called 'doping'. Since this Nobel Prize winning discovery, much of the work has been centered on synthesis and characterization of novel polymers with π - conjugated backbone due to their highly promising optical, electrochemical and conducting properties.

2.1.1 π - conjugated polymers

Last two decades witnessed a resurgence in field of π - conjugated polymers owing to increased interest from different applied science sectors. Hectic activities in this field resulted in a large family of π - conjugated polymers which exhibits a series of promising properties such as tunable electrical conductivity, photoconductivity, charge storage capacity, photoluminescence and electroluminescence [3 - 10]. Conjugated polymers are organic semiconductors that are similar to their inorganic counterparts in their electronic levels. Both have their electrons organized in bands rather than discrete levels [3, 4]. Typical band gap between conduction and valence bands is about 1 to 3 eV. Having such an energy gap suggests that this class of polymers are normally insulators or at best semiconductors. The electrical conductivity of π - conjugated polymers can be enhanced to a large extent by doping it with either an electron donor or an electron acceptor. Introduction of dopants results in strong electron-phonon interactions leading to the generation of polarons, bipolarons and solitons in the system [11 - 14].

The charge carriers contributing to conductivity in conjugated polymers are solitons, polarons and bipolarons. Figure 2.1 shows some of the popular conducting polymers. The basic structural motif of conjugated polymer is an alternating sequence of single and double bonds. Trans-polyacetylene has a degenerate ground state in which there is no preferred sense of bond alternation. Most of the conjugated polymers possess a non-degenerate ground state with a preferred sense of bond alternation. Oxidation

~~When~~ polyacetylene generates a cation radical. As there is no preferred sense of bond alternation, the positive charge and the unpaired electron of the cation can move independently along the polymer chain, forming domain walls between two identical parts of bond alternation. In solid state physics a charge associated with a boundary or domain wall is called a soliton [15 - 18]. Figure 2.2 shows soliton formation in polyacetylene.

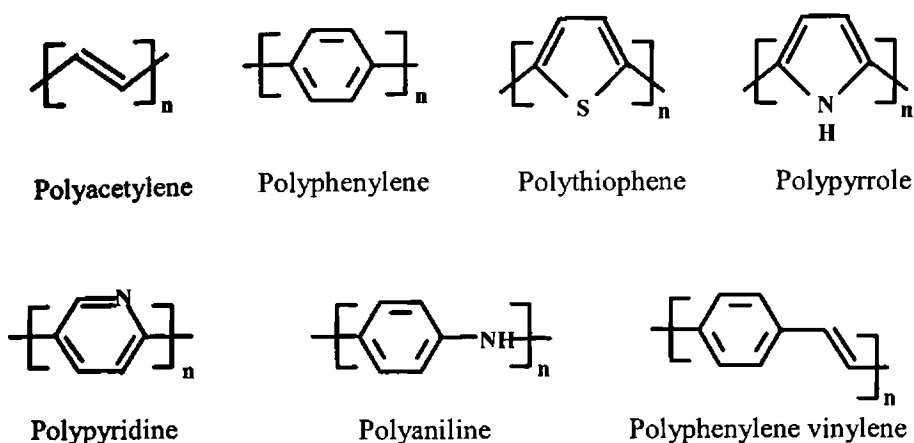


Figure 2.1: Structure of some conjugated polymers

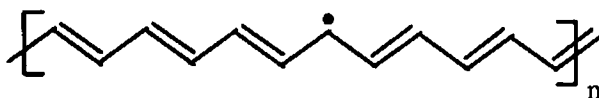


Figure 2.2: Soliton in Polyacetylene

In the case of oxidation and reduction of non-degenerate ground state polymers such as polythiophene and polypyrrole, a different mechanism occurs. The initially formed cation radical possesses both spin and charge and can not move independently [19]. A polaron is either a positively charged hole site (radical cation) or a negatively charged electron site (radical anion). It has

a lattice relaxation (distortion) around the charge. Theoretical models demonstrate that two radical ions (polarons) on the same chain interact to produce a dication or dianion called a bipolaron, which accounts for spinless conductivity in these polymers. Figure 2.3 illustrates formation of polarons and bipolarons in polymer chains.

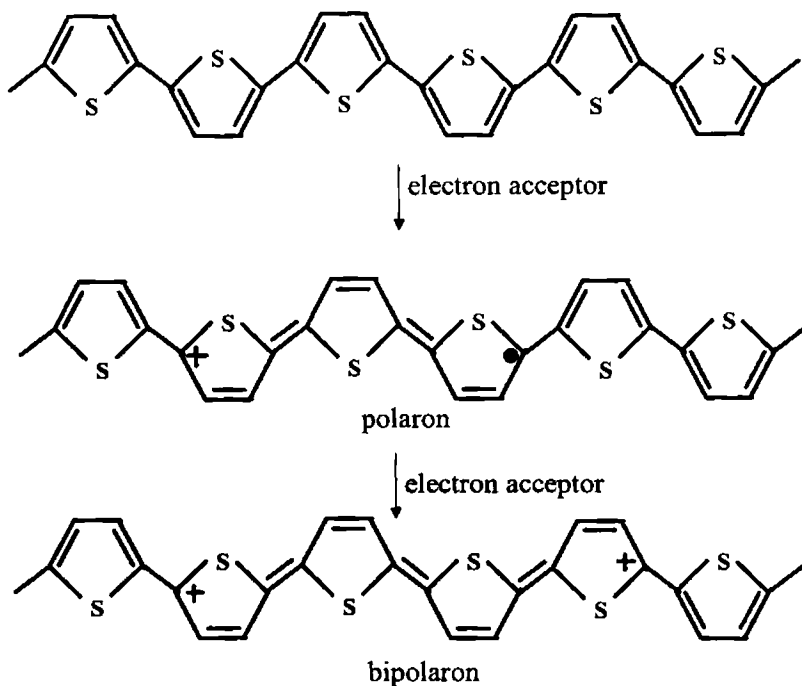


Figure 2.3 Polaron and bipolaron

2.1.2 Electrically conducting polymers

As the band gap of typical conjugated polymers ranges from 1 to 3 eV, the electrical conductivity is low and the material can be at best a semiconductor. The electrical conductivity can be considerably enhanced by the introduction of charge into these polymer chains by various methods like oxidation, reduction, acid doping, etc. It was discovered in 1977 that

polyacetylene could be readily oxidized by electron acceptors such as iodine or **arsenic pentafluoride** or reduced by donors such as lithium [2, 20, 21]. The **conductivity** of this modified polyacetylene was several orders higher than the **original sample**. The redox reaction can be carried out in

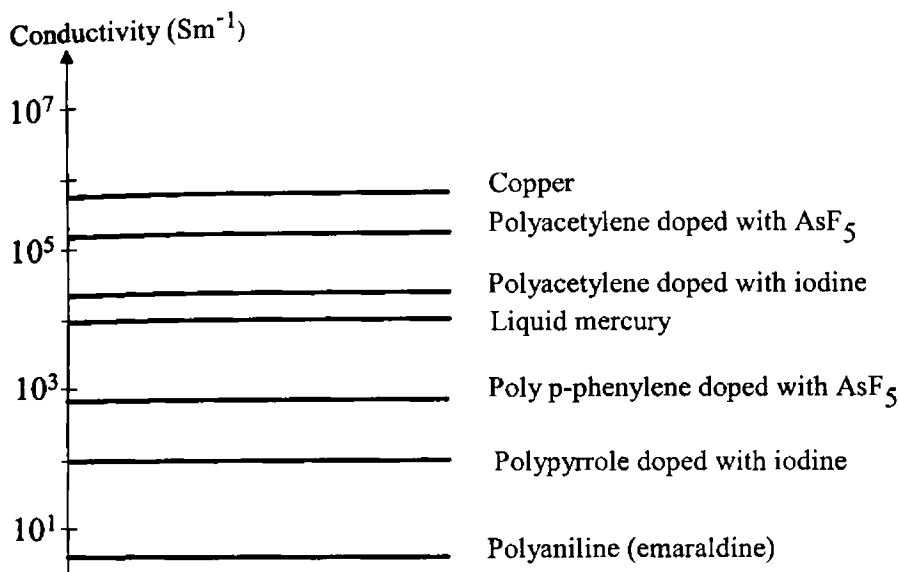


Figure 2.4: The conductivity ladder

vapour phase, in solution or electrochemically. A similar significant finding was reported in 1979 in the case of polyphenylene[22]. Many poly-aromatics and polyheterocyclics are now known to exhibit this enhanced electrical conductivity upon doping. Typical examples are polypyrrole, polythiophene, polyfuran, polyindole, polycarbazole, polyaniline, etc. [23 – 29]. These polymers, because of their high electrical conductivity and ease of preparation, assume great significance in potential technological applications. A comparison of the electrical conductivity of various conducting polymers with that of mercury and metallic copper are given in figure 2.4.

Table 2.1: Conductivity and nature of doping in typical polymers.

Polymer	Maximum conductivity (S.cm ⁻¹)	Type of doping
Polyacetylene	200 -1000	n, p
Polyparaphenylene	500	n, p
Polyparaphenylene vinylene	1 -1000	p
Polypyrrole	40 - 200	p
Polythiophene	10 - 100	p
Polysothianaphthene	1 -50	p
Polyaniline	10	p

2.1.3 Conduction mechanisms

The concepts of band structure are applicable to conducting polymers also. The conductivity is dependent on the conjugation length of the polymer [30, 31]. The increase in conjugation length increases the carrier mobility, resulting in increased conductivity. The charge carriers have to move along the extended π system of the conjugated backbone (intra-chain conductivity) as well as between the individual molecules (inter-chain conductivity). In conducting polymers like trans-polyacetylene two energetically equivalent resonance structures are possible. Unpaired electrons called solitons are present at the conversion points. This conversion point is actually spread out over several bonds. Solitons introduce a localized electronic state in the middle of the energy gap between the conduction band and valence band of polyacetylene. Conjugated polymers like polypyrrole, polythiophene, etc do not have a degenerate ground state, but different resonance structures can be present and unpaired electrons are formed at conversion points. These electrons polarize the local environment resulting in two electronic states in the

band gap, which then contributes to conductivity. The combination of charge carrier and its distorted environment is called a polaron. Its chemical equivalent is a charged radical.

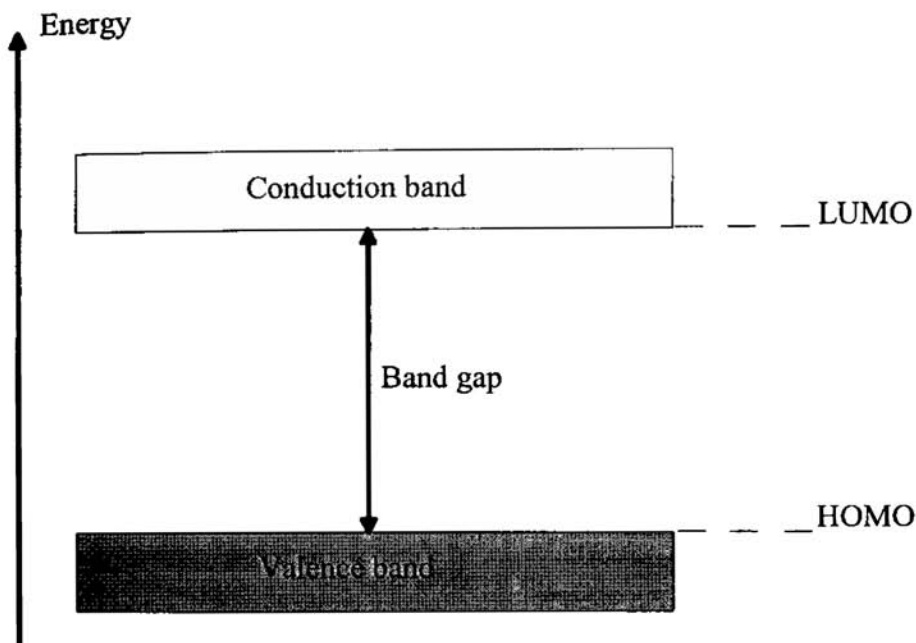


Figure 2.5 Band structure in an electrically conducting polymer

Although conjugated structures are favourable for conduction due to high charge mobility, low carrier concentration reduces the conductivity. Charge carriers are produced by oxidation or reduction of the polymer and the process is called doping. Oxidation of polymer results in a hole-conducting polymer (p-type), whereas on reduction electron-conducting polymer is formed [4]. The increase in conductivity on doping can be as high as about 13 to 14 orders of magnitude for different dopant combinations [32, 33]. Conductivity caused by n-type doping is less than that produced by p-type doping.

The evolution of polymer band structure with doping is shown in figure 2.6.

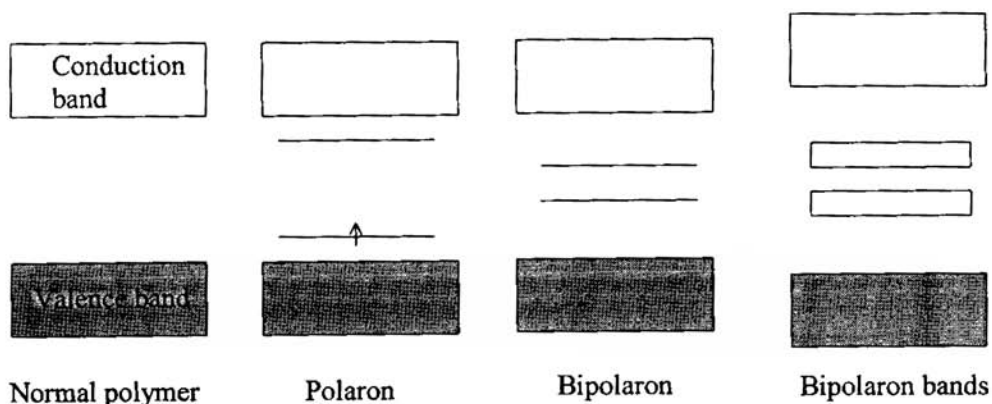


Figure 2.6: Evolution of polymer band structure on doping

2.1.4 Applications of conducting polymers

▪ Polymer rechargeable batteries

Conducting polymers are used as electrode material for rechargeable batteries [34]. The electrochemical doping process constitutes the basic electrochemistry of battery. The reversibility of electrochemical doping provides a rechargeable battery system.

▪ Sensors

Conducting polymers are widely used in biological and chemical sensors [35 – 37]. Sensors employing conducting polymers are used in different modes such as pH-based mode, conductometric mode, and potentiometric mode. Heteroaromatic polymers can act as gas and solution sensors. Polypyrrole and polythiophene exhibit conductivity changes upon exposure to both oxidizing and reducing gases. Polyaniline, polythiophene and polypyrrole are the most commonly used conducting polymers used for the fabrication of sensors.

- **Electroluminescent devices**

Polymeric light emitting diodes (PLED) have aroused much interest worldwide since the discovery of electroluminescence in a thin layer of poly p-phenylene vinylene by Friend and co-workers in 1990 [38]. The device is prepared by sandwiching the conducting polymer between an electron-injecting metal (Al or Ca) and hole-injecting material (Indium-Tin-Oxide). Electroluminescence has been reported in many conducting polymers [38 - 41].

- **Antistatic coatings**

Build up of static electricity on an insulator can be prevented by coating it with a thin layer of conducting polymer. Delicate integrated circuits can be protected from static discharge by providing a thin conductive polymer coating.

- **Printed circuit boards**

Conducting polymer coated printed circuit boards are a better alternative to the conventional ones because of their relatively lower cost and better adhesion.

- **Molecular electronics (ME)**

ME is an interdisciplinary field evolving from physics, chemistry, biology, electronics and information technology. Among organic materials conducting polymers have attracted most attention for possible application in ME devices because of their unique properties and versatility [42 - 46]. The conductivity of these polymers can be tuned from insulating regime to superconducting regime by the degree and nature of doping. These polymers offer the advantages of light weight, flexibility, corrosion-resistivity, high chemical inertness and ease of processing. The progress in the field of ME is dependent on the synthetic routes and molecular tailoring. Conducting

polymers can be prepared both by chemical and electrochemical methods. By varying the nature of the groups, specific interactions with external physical and chemical phenomena can be developed in these materials leading to molecular devices such as transducers, memories and logic operators.

Conducting polymers like polyaniline, polypyrrole, polyacetylene and poly 3-alkyl thiophene are used in Schottky diodes [47 - 50]. Many conjugated polymers are used for the fabrication of organic thin film field effect transistors [51 - 57].

- **Microwave engineering**

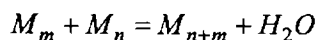
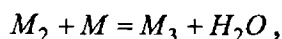
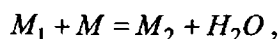
The response of conducting polymers to microwave frequencies has been extensively studied because of their use in reflector antenna coating, electromagnetic interference shielding, frequency selective surfaces, radar absorbing materials, etc.

2.2 Polymerization Techniques

Conducting polymers are prepared by a variety of polymerization methods such as chain growth (addition), step growth (condensation), electrochemical, ring opening and plasma polymerization.

2.2.1 Step-growth polymerization

In step-growth polymerization, a polymer is formed by the step-wise repetition of the same reaction. If the monomer is represented by M and the growing molecules by M_1 , then step growth polymerization can be represented by

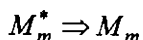
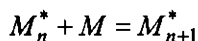
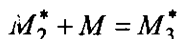
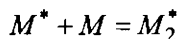


It is seen that the reaction at each step is identical to the first reaction.

2.2.2 Chain-growth polymerization

In chain-growth polymerization, a long chain molecule is formed by a series of consecutive steps that is completed in a very short time. In this case, products are only final polymers. Unlike the case of step growth polymerization, intermediate size molecules cannot be isolated. Consequently, entire polymer formation can be essentially considered a one step process, as long as the concept of chemical reaction that relies on the identification of reactants and products is concerned.

If the chain carrying species is indicated by M^* and the monomer by M , the chain growth mechanism can be shown by



The first three reactions represent the propagation reaction and the last reaction in which the chain carrying species is lost is the termination reaction. In the step growth polymerization, each growth step is a chemical reaction between two molecules whereas in chain growth polymerization, each individual growth step is a chemical reaction between a chain carrying species and a molecule.

A typical example of the chain growth polymerization is the addition polymerization. Depending on the nature of the reactive species, the addition polymerization can be classified as free radical polymerization, cationic polymerization and anionic polymerization.

2.2.3 Radiation polymerization

Polymerization initiated by ionizing radiation such as γ rays from ^{60}Co or high-energy beams is somewhat similar to plasma polymerization. For elucidating the mechanism of plasma polymerization, an understanding of radiation polymerization is helpful.

The significant difference between radiation polymerization and the polymerizations discussed so far is that no initiator is employed in radiation polymerization. The chain carrying species are created by ionization of a monomer molecule. Radiation induced polymerization differs from the polymerization by an initiator in that (i) free radical and ionic polymerization co-exist, (ii) ion radicals contribute to the initiator reaction and (iii) ionic sites have no counter ions.

2.2.4 Plasma polymerization

Plasma polymerization (glow discharge chemical vapour deposition) technique to prepare thin polymer films has been rapidly developing in the field of organic materials as well as in that of conventional inorganic ones [58 - 62]. Polymerization of molecules, inorganic or organic, saturated or unsaturated occurs in various plasma environments such as plasma jets, electron beams, ion beams, corona discharges, laser induced plasmas and non-equilibrium glow discharges. Plasma polymerization is a thin film process where thin films deposit directly on the surfaces of the substrate. In this process growth of low molecular weight molecules (monomer) into high molecular weight molecules (polymer) occurs with the assistance of plasma energy, which involves activated electrons, ions and radicals. In plasma polymerization, plasma acts as an energy source to initiate polymerization reactions. Ion-molecule and radical-molecule mechanisms are mainly

responsible for the dissociation of neutral species and subsequent polymerization. Introduction of inert gases as carriers enhances these reactions. Polymers formed by this technique are highly cross-linked and bear little resemblance to polymers prepared by conventional polymerization.

- **Mechanisms of plasma polymerization**

In view of the multitude of reactive species and parametrical factors affecting the nature of glow discharge, the polymerization mechanisms and the polymerization routes are highly complex. Numerous models have been proposed for the large variety of organic and inorganic substances in the presence or absence of other species, carriers and catalysts which involve ionic, radical or both mechanisms in polymerization. The explanation of the reaction mechanisms are usually based on qualitative observations and measurements of the overall deposition rates rather than the direct identification of the active species present. The neutral species entering the plasma reactor are transformed into reactive species as electric energy is given to the neutral species by the electrons. These active particles comprising of ions, free radicals, excited atoms and molecules and radical ions together with the neutral species may be involved in one of the following reaction schemes:

(i) They interact in the gas phase ionically or via radical mechanism at high rates to form polymers, usually powders before reaching a surface.

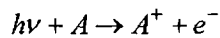
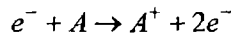
(ii) The active species tend to move to the surface where they are adsorbed or rebound into the gas phase. Each sorption represents a deposition step. The adsorbed particles subsequently interact and engage in ionic or radical polymerization on the surface and form a thin film.

- **Basic reactions in a glow discharge**

The primary processes in the generation of ions involve electron impact and photo-ionization. Similarly free radicals may be generated by electron

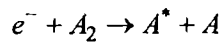
impact. Ionization process also takes place via collisions of metastable species and molecules or atoms. These processes are referred to as Penning ionization and treated in terms of metastable-normal and metastable - metastable collisions resulting in ionization. Some of the basic reactions are given below:

Primary ion production by electron impact and photo-ionization:

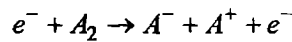


The following basic reactions control deposition of films in a glow discharge.

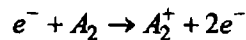
Excitation (rotational, vibrational, electronic):



Dissociative attachment:



Ionization:

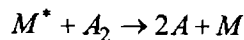


Dissociative ionization:

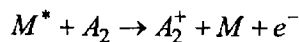


Inelastic collisions between heavy particles-

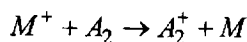
Penning dissociation:



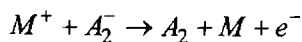
Penning ionization:



Charge transfer:



Collisional detachment:



Atom recombination:



In the presence of free radicals and ions, both are capable of inducing polymerization and both ionic and free radical mechanisms may operate depending on the conditions. Free radicals react at rates 10-100 times faster than ions.

▪ **Merits of plasma polymerization technique**

Polymers formed by plasma polymerization demonstrate unique chemical and physical properties. Many films can be deposited in plasma at low temperatures, whereas conventional vapour deposition would require prohibitively high temperatures. Plasma polymers are amorphous, hard, tough and insoluble in organic solvents. They are resistant to high temperatures. These unique properties result mainly from the chemical structure of the plasma polymer chains, which are highly crosslinked and branched. The polymer chains are not illustrated from the concept of a repeating unit. Such singularity of polymer chains is the result of the particular initiation reaction triggered by plasma energy, which is higher than that of conventional energy sources such as heat or ultra violet rays. Other advantages include better adhesion to the substrate, reduction of pinholes, smoothness of surfaces and improved chemical and wear resistance. This resulted in the worldwide application of this technology for thin film fabrication.

▪ **Applications of plasma polymerized films**

Pinhole-free polymer films prepared from glow discharge plasmas of organic vapours have wide ranging applications. The film structure and the composition depend primarily on the monomer, but are also affected by deposition parameters such as the power applied to the discharge, monomer

flow rate, system pressure and substrate temperature. Films suited for specific applications can be prepared by controlling these parameters.

Plasma polymers prepared from C_2H_2 - nitrogen discharges show low degree of cross linking with hydrophilicity and are used for reverse osmosis applications [63]. High quality conducting polymers have been prepared by plasma polymerization techniques. Flawless films prepared by this method are widely used in electronic device industry. Conducting polythiophene films were prepared by Sadhir et. al. [64]. The conductivity of polymerized films can be modified by co-polymerization [65]. Plasma polymerization has shown to be compatible with microelectronic fabrication process and has been used for the deposition of photoresistors [66, 67]. Plasma polymerized methyl methacrylate films are used for photonic applications [68]. Plasma deposited organic films are widely used as protective coatings for metals and other refractive surfaces.

▪ **Experimental setup for plasma polymerization**

Four elements are essential for any plasma polymerization setup. They are (i) electric power source for the initiation and maintenance of glow discharge, (ii) the reaction chamber, (iii) the vacuum system and (iv) the control system and the monomer gas flow.

Electric power source: The electric power source employed in plasma polymerization can be operated by both direct and alternating currents with frequencies ranging from 50 Hz to the microwave region. Depending on the power source used the methods are labeled as DC plasma polymerization, AC plasma polymerization, RF plasma polymerization and microwave plasma polymerization. Commercially available units employ a frequency of 13.56 MHz. The electric energy from the power source is transmitted into the

reaction chamber with inductive or capacitive coupling. The type of coupling system is restricted by the frequency and shape of the reaction chamber.

Reaction chamber: Various types of reaction chambers are in use for plasma polymer coating. Basically there are two types – a tubular type chamber and a bell jar type chamber. Tubular chamber is compact and convenient for laboratory use whereas bell jar designs are used for commercial applications.

Vacuum system: The reaction chamber must be maintained at a low pressure to obtain a stable glow discharge state. In most cases a combination of diffusion and rotary pumps is employed to reduce the pressure. A constant pressure must be maintained during the plasma polymerization process, since the operating pressure is one of the factors controlling the polymerization reactions.

Control system and monomer gas flow: The flow rate of the monomer gas is one of the factors that determine the appearance and the chemical composition of plasma polymers. Changes in the monomer flow rate during the polymerization process should be avoided. The monomer flow is carefully controlled using a needle valve or a mass flow controller.

- **RF plasma polymerization system**

At frequencies above 1MHz, direct contact between electrodes and plasma is no longer necessary. The energy can be fed to the plasma indirectly by capacitive or inductive coupling (Figure 2.7, 2.8). In the case of capacitive coupling the electrodes enclose the plasma tube. The tube lies on the axis of a coil for inductive coupling. For plasma deposition RF generators with fixed frequency and adjustable power are preferred.

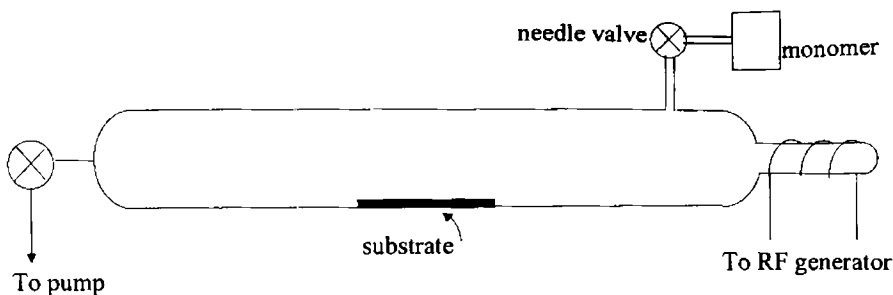


Figure 2.7 Inductively-coupled plasma polymerization unit

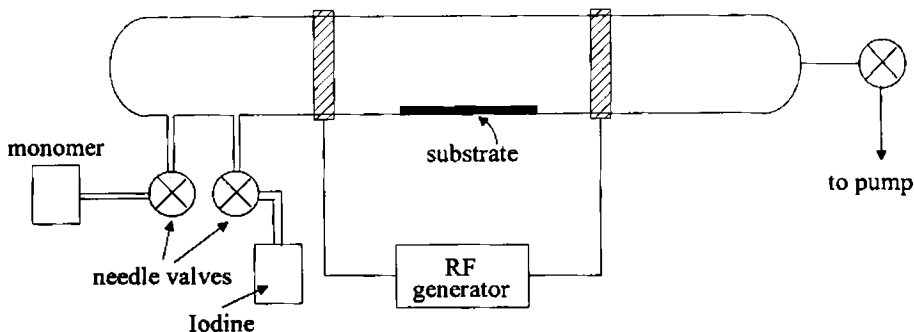


Figure 2.8: Capacitively-coupled plasma polymerization unit

2.3 Synthesis of conducting polymers

The polymers selected and prepared for the present study are polyaniline (PANI), polypyrrole (PPy), poly N-methyl pyrrole (MPy), polythiophene (PTh). Acid-doped forms of PANI are also prepared. Composites of PANI with poly vinyl chloride (PVC) and PPy with PVC are synthesized for their thermal characterization.

The polymer samples are prepared by chemical synthesis as well as radio frequency (RF) plasma polymerization. Powder samples are prepared by the chemical route whereas polymer thin films are coated on glass substrate by RF plasma polymerization technique.

2.3.1 Chemical synthesis

▪ Polyaniline (PANI)

Chemical oxidative polymerization of aniline is carried out using ammonium persulphate as initiator in the presence of 1M hydrochloric acid at 0 – 5°C. The reaction is allowed to continue for four hours. Polyaniline thus formed is vacuum-dried. It is dedoped by treating it with ammonium hydroxide for twenty four hours, and then doped with different dopants – 1M hydrochloric acid, 1M sulphuric acid and 1M camphor sulphonic acid. The powder samples are pelletized to form pellets of 1 cm diameter with a thickness of less than 1 mm.

To combine the electrical conductivity with the desirable physical properties of a polymer, conducting polymers can be introduced into a host polymer matrix. The resulting structure is an interpenetrating network. In this study chemical oxidative polymerization of aniline is carried out using ammonium persulphate as initiator in the presence of 1M HCl and emulsion grade polyvinyl chloride. The polymerization reaction is carried out for four hours at room temperature. It is then filtered, washed and dried. PANI/PVC composites are prepared in 3:1, 2:1 and 1:1 compositions. The powder samples are pressed into pellets of thickness less than 1mm.

▪ Polypyrrole (PPy)

PPy is chemically prepared by the polymerization of pyrrole with ferric chloride in the presence of methanol. The reaction is carried out for twenty minutes at 0 - 5°. It is then filtered, washed and dried in vacuum for sixteen hours. Pellets of less than 1mm thickness are prepared from the powder samples.

PPy/PVC composite is prepared by the polymerization of pyrrole with ferric chloride in the presence of methanol and emulsion grade polyvinyl chloride. The reaction is carried out for twenty minutes at 0 – 5°C. It is then filtered, washed and dried under vacuum for sixteen hours at room temperature. PPy/PVC compositions 3:1, 2:1 and 1:1 are prepared using the above procedure. The powder samples are pelletised.

2.3.2 Preparation of Plasma Polymerized Films

Capacitively coupled RF plasma polymerization unit is used for the preparation of polymer films in this study. The tubular chamber is of about 40 cm in length and 6 cm in diameter. The monomer container is connected to this tube through a needle valve. An inlet is also provided for admitting iodine vapour into the reaction chamber, so that in situ iodine doping may be performed. Aluminium foil rings are used to couple RF power to the reaction chamber. The chamber is attached to a rotary pump through a stop cock. The RF generator uses four RCA tetrodes. It is a tuned-plate tuned-grid RF oscillator designed to generate RF power at 7 MHz. The power can be adjusted over a limited range.

▪ Preparation of polyaniline films

The polymer thin films are prepared on optically flat glass slides of dimensions 75 x 25 x 1.4 mm. The glass plates are first cleaned in running water and are immersed in chromic acid for about 1 to 2 hours in order to remove alkaline impurities. The slides are then washed in distilled water and are cleaned ultrasonically. The microscopic impurities are stripped off by ultrasonic agitation in water. The glass slides are then dried and placed in the deposition chamber. The chamber is evacuated to a pressure of approximately 0.4 m bar keeping the monomer needle valve closed. The RF power is switched on and a glow appears in between the electrodes. About 1 ml of the

Monomer aniline is taken in a small glass container and the monomer vapour is supplied to the reaction chamber through a needle valve. The needle valve is fully opened and the monomer vapour is admitted into the chamber. The valve is closed after half a minute. The RF power is switched on. The distance between the aluminium rings is adjusted to get uniform glow. Now the needle valve is carefully adjusted to regulate the monomer flow. After a deposition time of about 15 to 25 minutes, a thin film of the polymer gets coated on to the glass plate.

PANI films are also prepared with in situ iodine doping. Films are coated under different pressure conditions of the reaction chamber. Films of different thickness are prepared by allowing different reaction time.

For the measurement of the dc conductivity of the PANI films, aluminium electrode is coated on glass substrate. PANI film is allowed to form on this lower electrode by placing this in the plasma reactor. The upper electrode is coated on this film with proper masking so as to form metal-polymer-metal structure of effective area 0.25 cm^2 . A similar structure is prepared with iodine doped PANI film.

▪ Preparation of polypyrrole films

About 1ml of analytical grade pyrrole monomer (Lancaster) is taken in the monomer container and is attached to the plasma reaction chamber through a needle valve. Films of different thickness are coated on ultrasonically cleaned glass substrate as in the case of PANI. Deposition time of 30 – 50 minutes is allowed.

Al-PPy-Al structure is prepared with and without iodine doping as in the case of PANI.

- **Preparation of poly N-methyl pyrrole films**

2 ml of N-methyl pyrrole monomer (Merck) is taken in the monomer container. Films of different thickness are coated on glass substrate by changing the deposition time. Iodine doped films are also prepared.

- **Preparation of polythiophene films**

Plasma polymerization of thiophene monomer (Merck) is carried out as described in the above cases. Relatively higher deposition time (45 minutes to 1 hour) has to be allowed to obtain films of suitable thickness. In situ iodine doping is carried out to obtain doped films. Al-PTh-Al structure is prepared for conductivity studies.

- **FTIR spectra of plasma polymerized films**

While the chemical synthesis of polymerization followed in the present study is a standard, well established and product specific route, the plasma polymerization technique is a more complex route of polymerization as already pointed in section 2.2.4. Hence the FTIR spectra of all the plasma polymerized samples are recorded to check whether the ring structure is completely lost under the plasma deposition conditions used in this study.

A comparison of the IR spectra of chemically prepared and plasma polymerized PPy shows that most of the peaks of chemically prepared PPy are present in the plasma polymerized sample also. A small shift is observed in many of the absorptions. The presence of ring vibrations points to the retention of the ring structure to some extent. In chemically prepared PPy, characteristic peaks of the pyrrole functional groups can be seen. The broad peaks at approximately 3450 cm^{-1} is typical of N-H stretch and the peak at approximately 1620 cm^{-1} corresponds to C=C and C=N in-plane vibrations in the pyrrole structure. The peak at approximately 1310 cm^{-1} is attributed to the

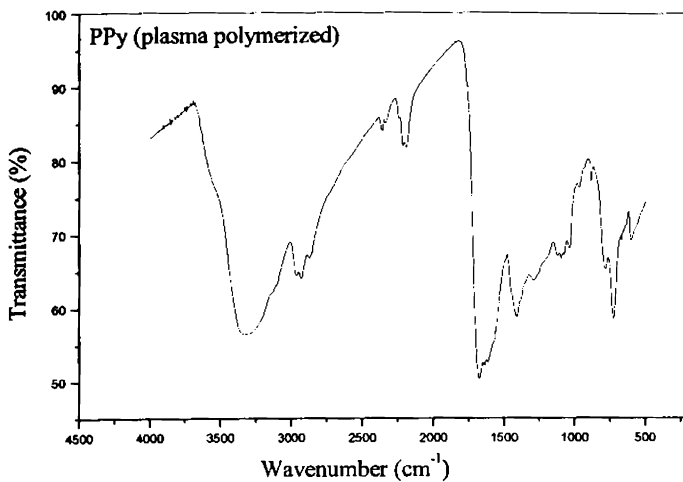


Figure 2.9 IR spectrum of plasma deposited PPy

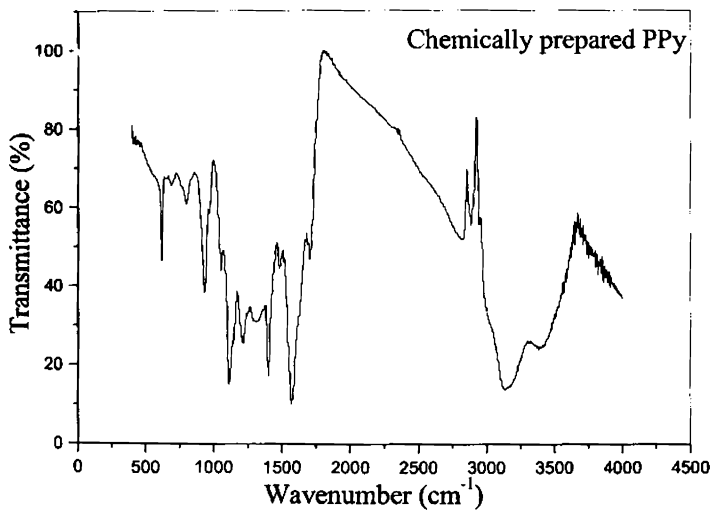


Figure 2.10 IR spectrum of chemically prepared PPy

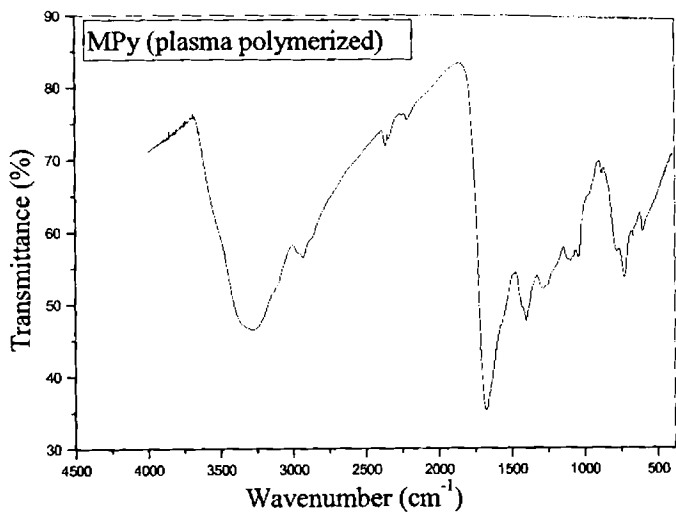


Figure 2.11 IR spectrum of plasma deposited MPy

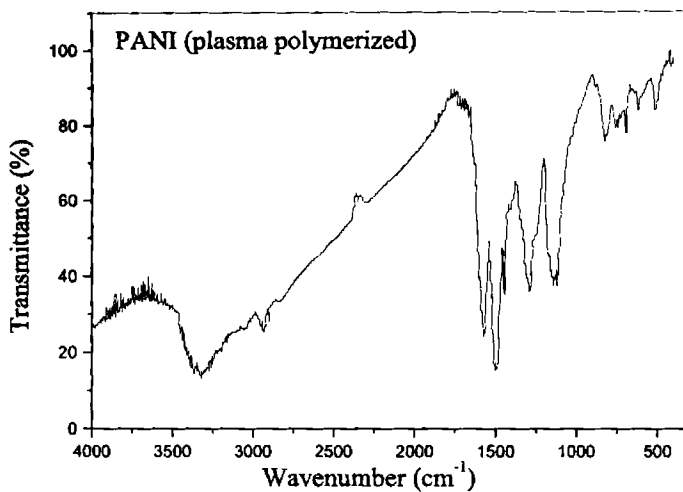


Figure 2.12 IR spectrum of plasma deposited PANI

secondary amine C-N stretching. The peaks at 790 cm⁻¹ and 920 cm⁻¹ are a combination of a number of absorptions corresponding to NH₂ wag, symmetric

N-C stretching or its deformation. In the FTIR spectrum of plasma polymerized pyrrole, different absorptions corresponding to alkenes resulting from broken rings also appear as peaks between 500 and 1000 cm^{-1} . When pyrrole rings are broken, branching and cross linking reactions tend to occur predominantly. Thus primary secondary or even tertiary amines may appear in the plasma polymerized sample. This tends to make absorptions in this region complicated.

The absorption in the IR region for plasma polymerized film of N-methyl pyrrole compares well with the spectrum of PPy film. The C-H stretching of methyl group is seen around 2930 cm^{-1} .

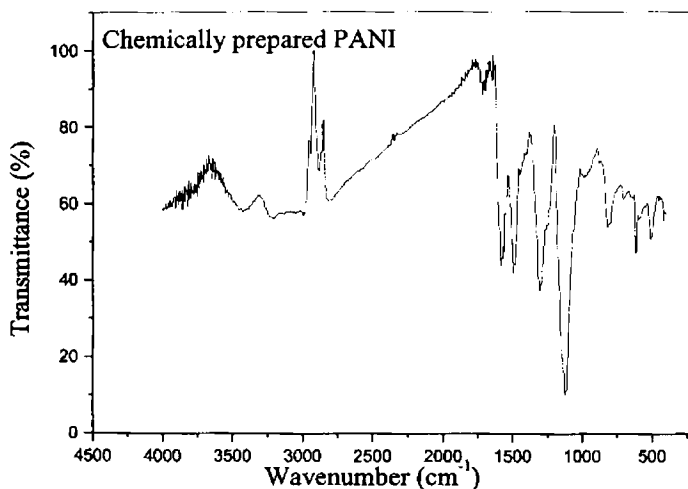


Figure 2.13 IR spectrum of chemically prepared PANI

In the case of plasma polymerized PANI the peak at 3356 cm^{-1} is assigned to the N-H asymmetric stretch of PANI. The absorptions at 1590 cm^{-1} and 1500 cm^{-1} belong to the C=C stretching. Peaks at 1240 cm^{-1} , 750 cm^{-1} and 689 cm^{-1} correspond to the C=N stretch and C-H out of plane deformations. The peaks corresponding to ring stretching are fairly strong,

which is indicative of the retention of the ring structure. The spectrum chemically prepared PANI is given for comparison.

In the IR spectrum of PTh, the peaks in the range of $2800 - 3100 \text{ cm}^{-1}$ is due to aliphatic and aromatic C-H stretching vibrations. The range

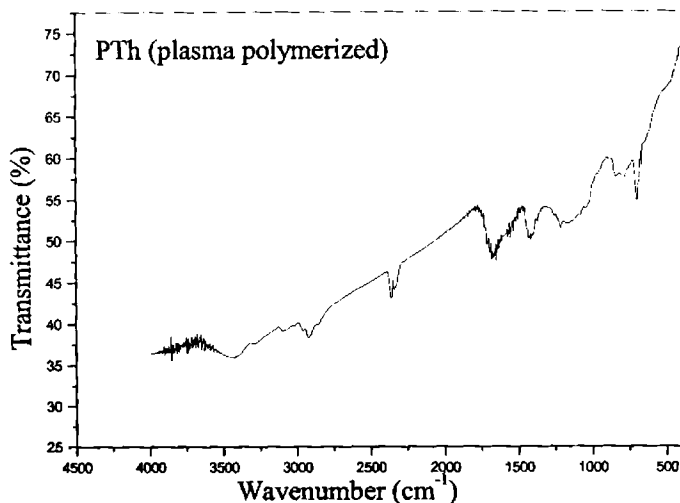


Figure 2.14 IR spectrum of plasma deposited PTh.

$600 - 1500 \text{ cm}^{-1}$ is the finger print region of of PTh. The peak at 830 cm^{-1} represents the aromatic C-H out of plane deformation mode whereas the other absorptions in this region are attributed to the ring stretching modes, aromatic C-H in-plane and out of plane deformations. The peak at 705 cm^{-1} is due to the aromatic C-H out of plane bending vibrations. The absorption at the 2320 cm^{-1} is the region where contributions from C=C stretching or S-H stretching appear. The broad peak at approximately 2925 cm^{-1} represents the stretching mode of methyl and methylene groups and aliphatic structures. The peak around 3275 cm^{-1} indicates the presence of some acetylene structures of plasma polymerized thiophene.

Electrical conductivity measurements

Chemically prepared polymer samples in the powder form is pelletised to form pellets of about 1cm diameter with thickness less than 1mm. Silver paste is coated on either side so as to serve as terminals for applying a DC voltage. V-I measurements are carried out keeping the pellets in conductivity cell using Keithley Source Measure Unit (SMU), Model: 236. Dependence of conductivity on temperature in the case of PANI and PPy is investigated by keeping the samples in a cryostat [C T I Cryogenics, Helix Tech Corporation and Cryo Industries America Inc. Atkinson Model: 22].

▪ **Chemically prepared PANI**

The variation of conductivity with temperature in the case of samples doped with 1M HCl and 1M camphor sulphonic acid, in the range 140 to 300 K is investigated keeping the pellet in a cryostat.

▪ **Chemically prepared PPy**

As in the case of PANI, variation of conductivity with temperature is investigated in the case of chemically prepared PPy by placing the PPy pellet in the cryostat.

▪ **Plasma polymerized aniline film**

Al-PANI-Al sandwich structure is prepared and V – I measurements are carried out using the Keithley Model 236 SMU, placing the sample in a conductivity cell. The measurements are taken for a film of thickness 630 nm in the voltage range of 0 - 20 volts. Conductivity of the sample is computed from the V – I plot.

Measurements are repeated for iodine-doped film of thickness 1230 nm in the voltage range 0 – 20 V.

- **Plasma polymerized pyrrole film**

V – I measurements for plasma polymerized pyrrole films in the undoped and doped forms are taken as in the case of PANI film.

- **Plasma polymerized N-methyl pyrrole film**

Room temperature conductivity of N-methyl pyrrole in the undoped and doped forms is obtained from the V - I measurements.

- **Plasma polymerized thiophene film**

V – I measurements on undoped iodine-doped thiophene films are carried out as outlined in the case of PANI.

2.4.1 Results and discussion

The variation of electrical conductivity of 1M HCl doped PANI, 1M camphor sulphonic acid PANI and PPy (as-prepared) with temperature are shown in figures 2.15 - 2.17. For a large variety of disordered materials the conductivity is described by the Mott's law for variable range hopping [69, 70]. The plots indicate variable range hopping conduction mechanisms in these specimens. As the thermal energy decreases with temperature, there are fewer nearby states with accessible energies, resulting in increase in the mean range of hopping. The expression for conductivity is given by $\sigma = \sigma_0 \exp\left(-\frac{T_0}{T}\right)^n$; where σ_0 and T_0 are constants. $n=1/2$ for 1-D hopping mechanism whereas $n=1/4$ corresponds to a 3-D variable range hopping conduction. In the present study the variation of conductivity of these samples with temperature can be fitted into a relation with $n=1/4$. This suggests that the major contribution to the conductivity is by 3-D variable range hopping in the samples under investigation.

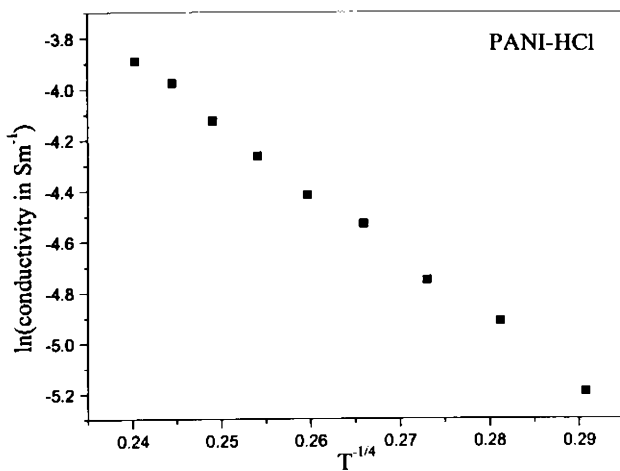


Figure 2.15 Variation of conductivity with temperature for HCl-doped PANI

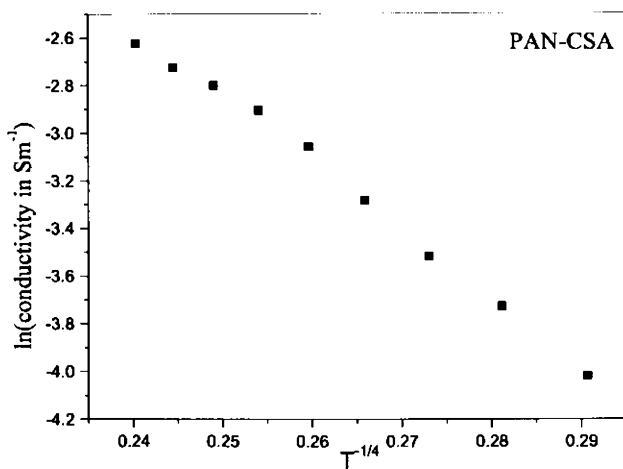


Figure 2.16 Variation of conductivity with temperature for CSA-doped PANI

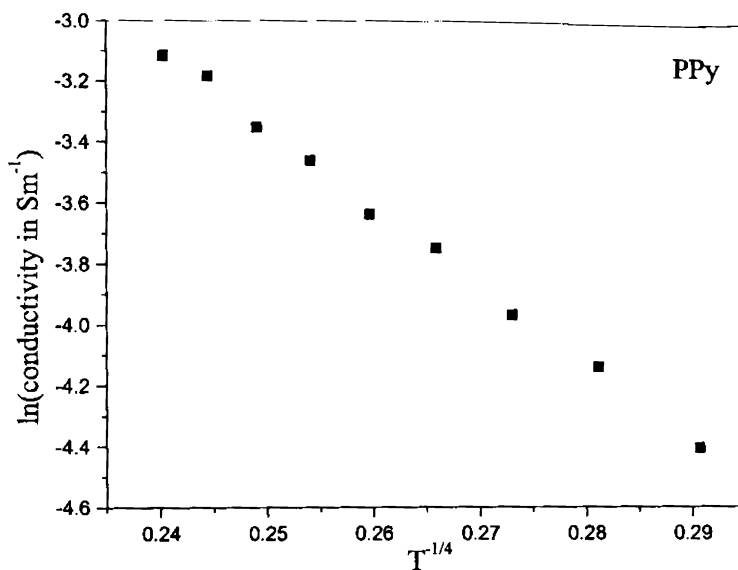


Figure 2.17 Variation of conductivity with temperature for PPy

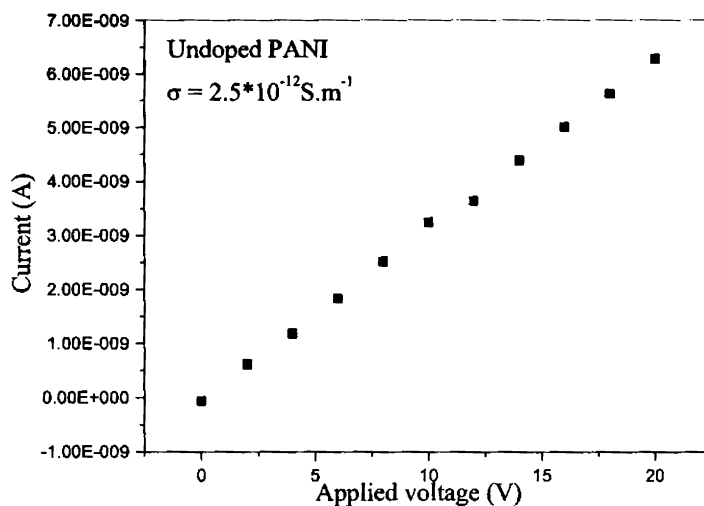


Figure 2.18 V-I plot for plasma polymerised PANI (undoped)

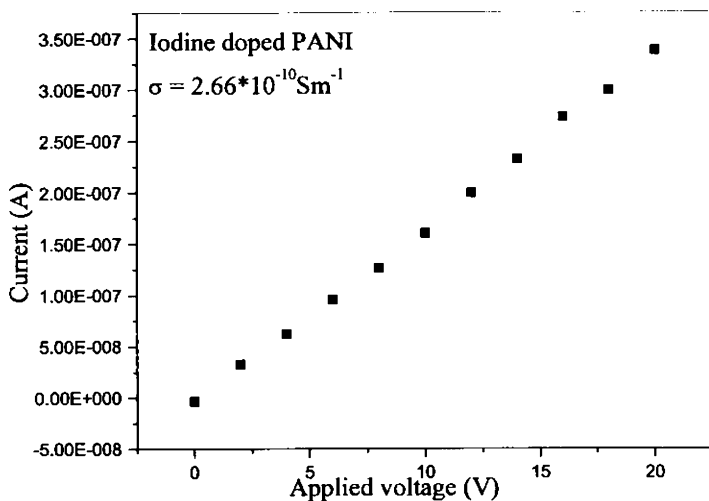


Figure 2.19 V - I plot for plasma polymerized PANI (iodine-doped)

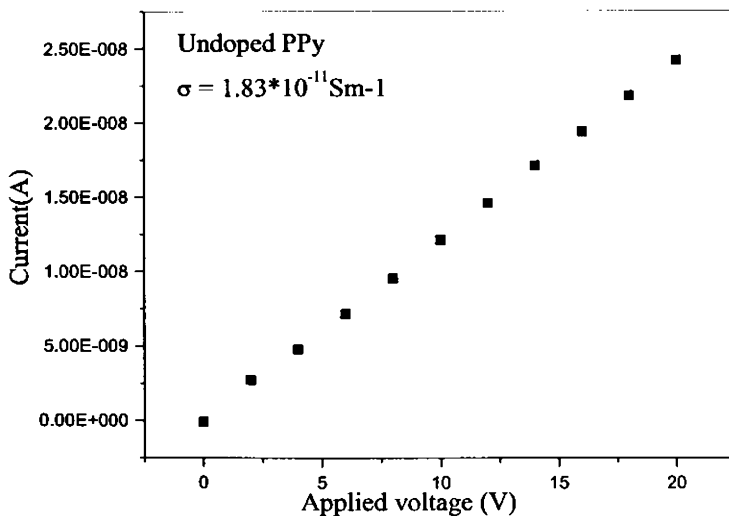


Figure 2.20 V - I plot for plasma polymerised PPy (undoped)

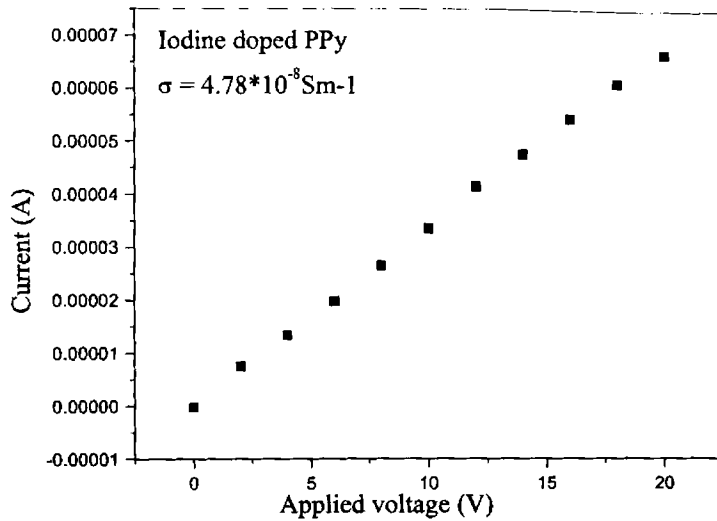


Figure 2.21 V - I plot for plasma polymerised PPy (iodine-doped)

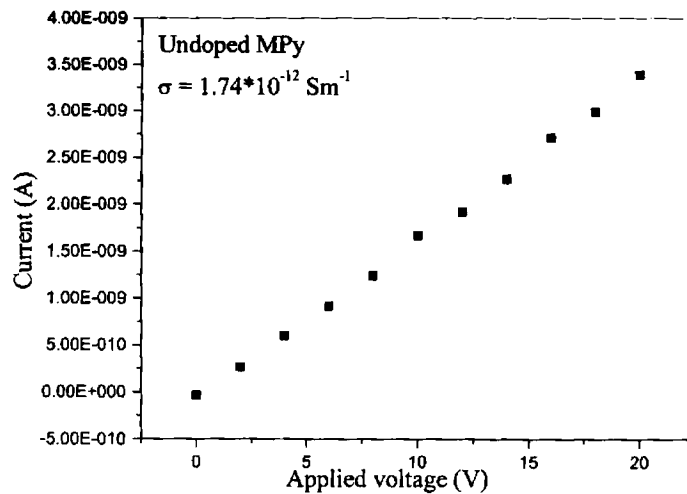


Figure 2.22 V - I plot for plasma polymerised MPy (undoped)

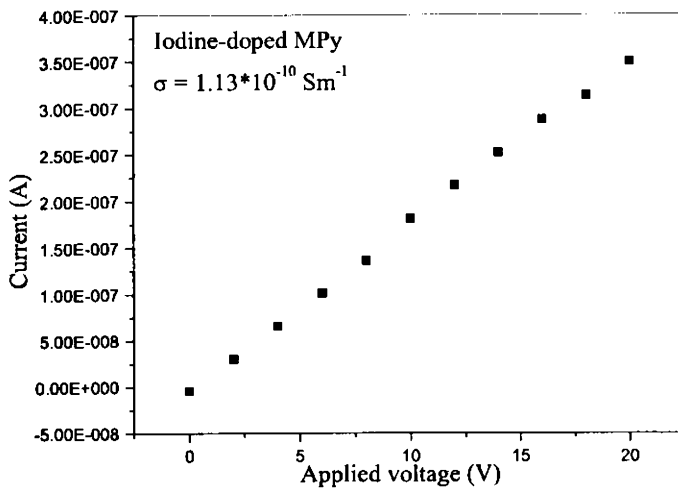


Figure 2.23 V - I plot for plasma polymerised MPy (iodine-doped)

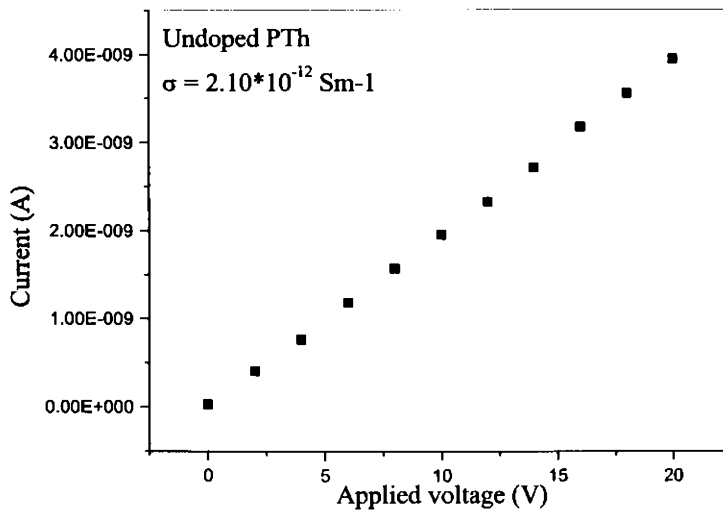


Figure 2.24 V - I plot for plasma polymerised PTh (undoped)

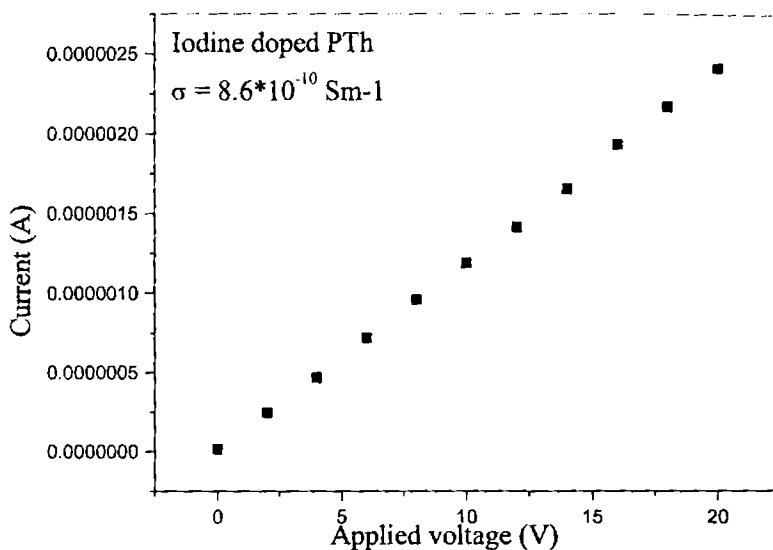


Figure 2.25 V - I plot for plasma polymerised PTh (iodine-doped)

Table 2.2 Conductivity of plasma polymerized films

Polymer film	Conductivity (Sm^{-1})	
	Undoped	Iodine doped
PANI	2.5×10^{-12}	2.6×10^{-10}
PPy	1.83×10^{-11}	4.78×10^{-8}
MPy	1.74×10^{-12}	1.13×10^{-10}
PTh	2.10×10^{-12}	8.65×10^{-10}

All the polymer samples show ohmic behaviour in the applied voltage range (Fig: 2.18 – 2.25). The values of conductivity for the different polymer samples are given in table 2.2. The conductivity shows an increase of two to three orders with iodine doping. Plasma polymerized films show a high degree of cross linking and side reactions. There is no local order in such films.

Iodine, being an electron acceptor contributes to the conductivity of the films to some extent.

2.5 Band gap measurements

Absorption of energy in the uv-visible region of the electromagnetic spectrum provides information about the electronic transitions in a solid. The electrons are excited from a filled band to empty band by the absorption of photons. This results in a sharp increase in the absorption coefficient and the onset of this rapid change in absorption coefficient is called the fundamental absorption edge. The corresponding energy is referred to as the optical energy-gap or the band gap energy. There are two kinds of optical transitions at the fundamental absorption edge of crystalline and amorphous solids - direct transition and indirect transition. For a direct transition from the valence band to the conduction band, the wave vector of the electron must be conserved. Only vertical transitions are allowed between the valence and conduction band. The bottom of conduction band and top of valence band lies at $k=0$ as shown in figure 2.26 so that electrons near the top of valence band can make direct transition to the states near the bottom of conduction band.

If the bottom of conduction band and top of valence band lies at the same k value, then absorption process do not require change in k and hence direct transition is possible. However, if the bottom of conduction band and top of valence band has different k , then the absorption process requires a change in k . In order to conserve momentum in such indirect transitions, participation of a phonon is required in the optical absorption process.

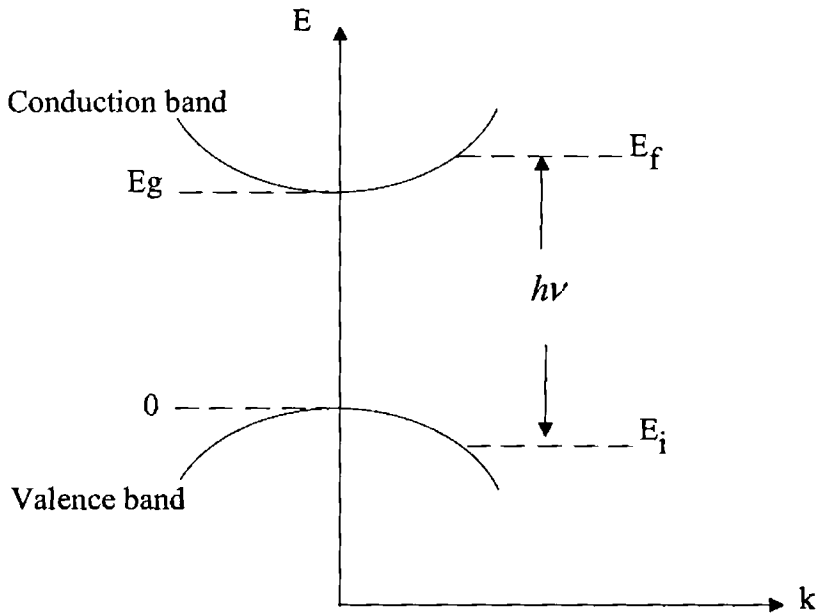


Figure 2.26 Direct absorption

Tauc, Bardeen, and Davis and Mott independently derived the following equation relating the absorption coefficient α with the photon energy $h\nu$ [71 – 73].

$\alpha h\nu = B(h\nu - E_g)^n$; where B is a constant reflecting the degree of randomness of the structure of the amorphous solid, E_g is the optical band gap of the absorption process. For direct allowed transitions $n=1/2$ and for indirect ones $n=2$.

The product of absorption coefficient and thickness of the film can be directly read from the uv-visible-NIR spectrophotometer. Knowing the thickness of the films the absorption coefficient of the samples can be

obtained. Direct and indirect transition energy gaps can be obtained from the plots of $(\alpha h\nu)^2$ versus $h\nu$, and $(\alpha h\nu)^{1/2}$ versus $h\nu$ respectively.

Absorbance of all the polymer samples are recorded using the uv-visible-NIR spectrophotometer (Varian Cary 5000).

The plots showing the variation of $(\alpha h\nu)^2$ and $(\alpha h\nu)^{1/2}$ with photon energy for the different polymer films are shown in figures 2.27 – 2.42.

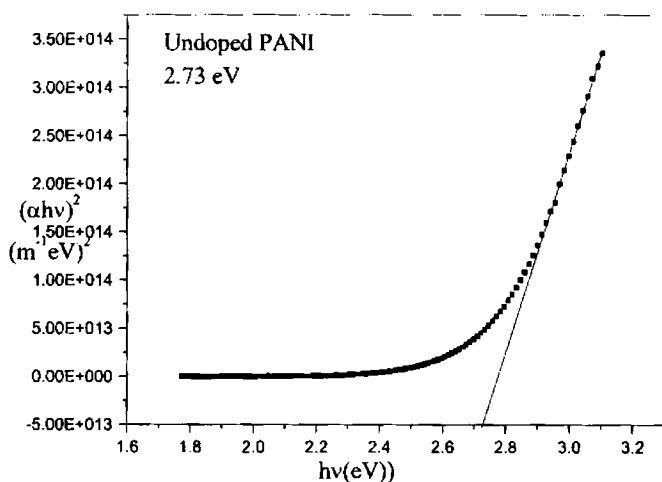


Figure 2.27. Variation of $(\alpha h\nu)^2$ with $h\nu$ for undoped PANI

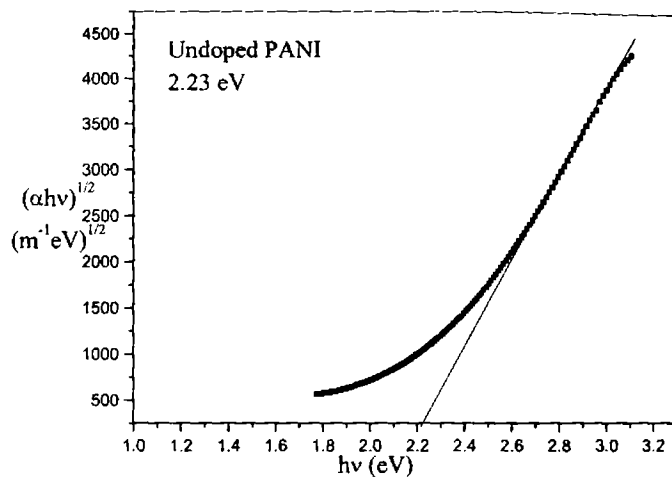


Figure 2.28. Variation of $(\alpha hv)^{1/2}$ with $h\nu$ for undoped PANI.

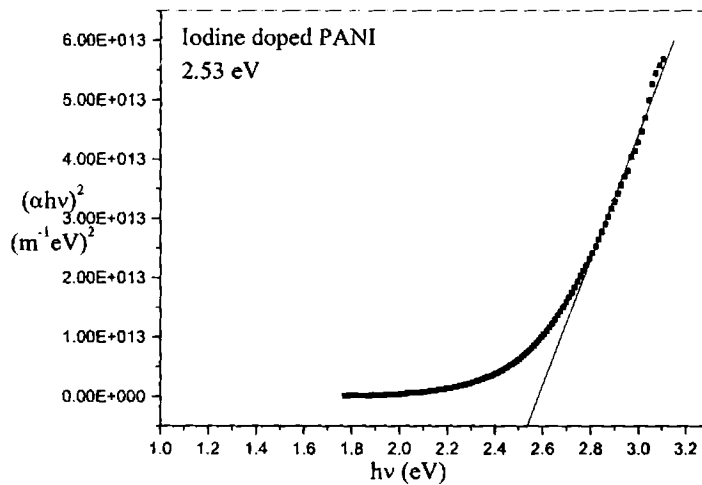


Figure 2.29. Variation of $(\alpha hv)^2$ with $h\nu$ for I-doped PANI

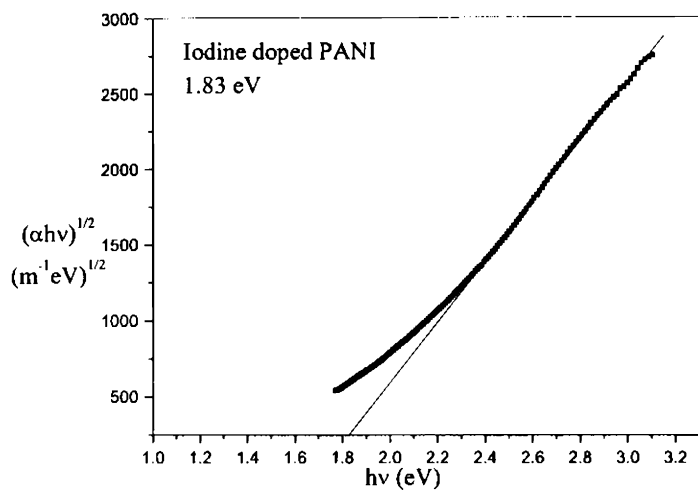


Figure 2.30. Variation of $(\alpha hv)^{1/2}$ with $h\nu$ for I-doped PANI.

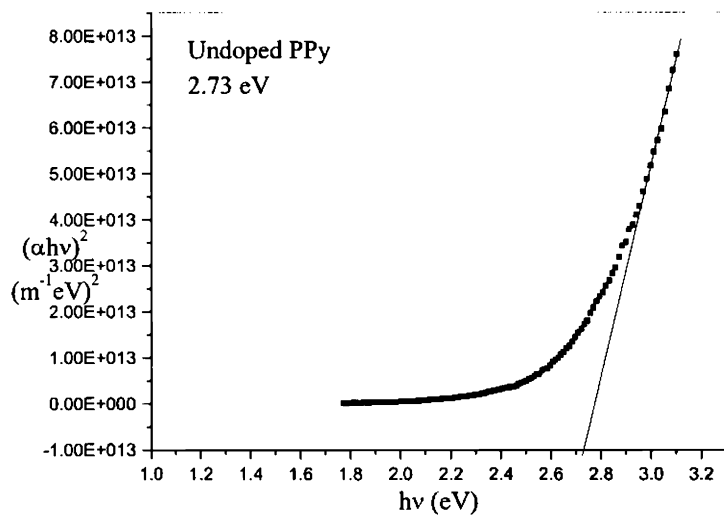


Figure 2.31. Variation of $(\alpha hv)^2$ with $h\nu$ for undoped PPy.

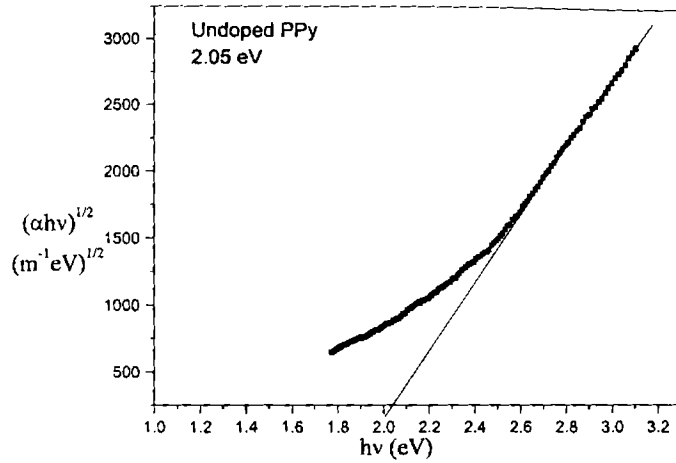


Figure 2.32. Variation of $(\alpha h\nu)^{1/2}$ with $h\nu$ for undoped PPy.

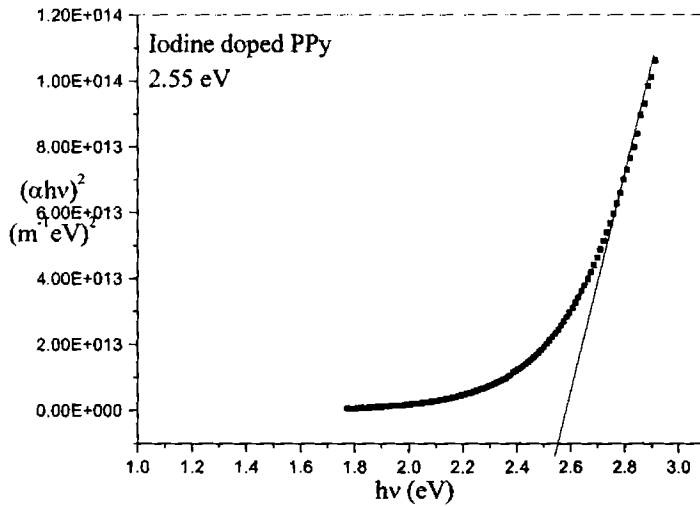


Figure 2.33. Variation of $(\alpha h\nu)^2$ with $h\nu$ for I-doped PPy.

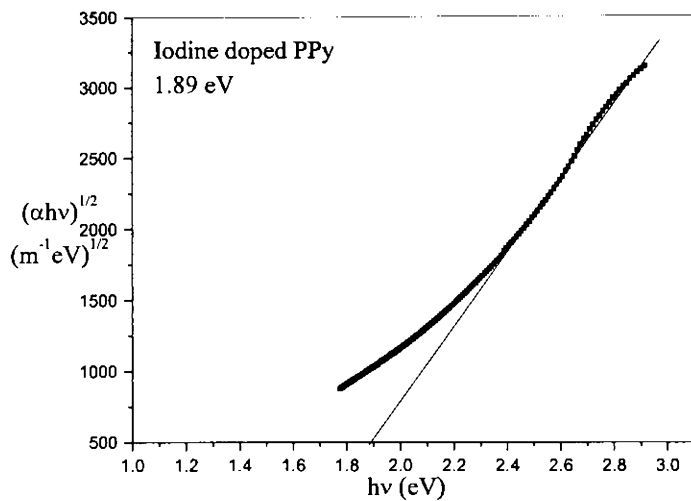


Figure 2.34. Variation of $(\alpha h\nu)^{1/2}$ with $h\nu$ for I-doped PPy.

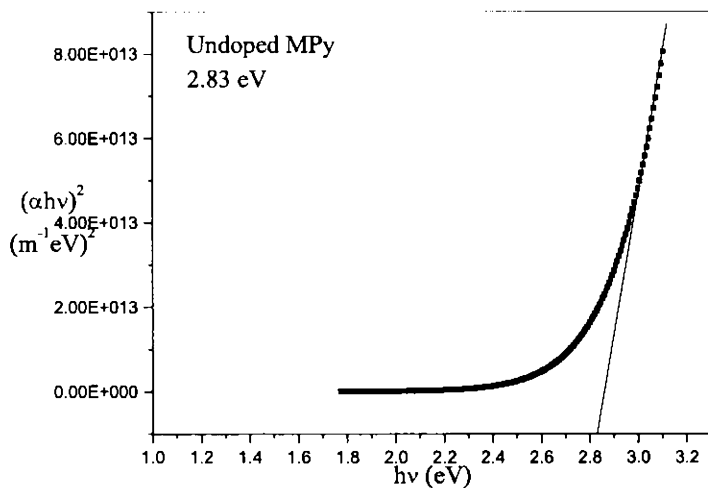


Figure 2.35. Variation of $(\alpha h\nu)^2$ with $h\nu$ for undoped MPy.

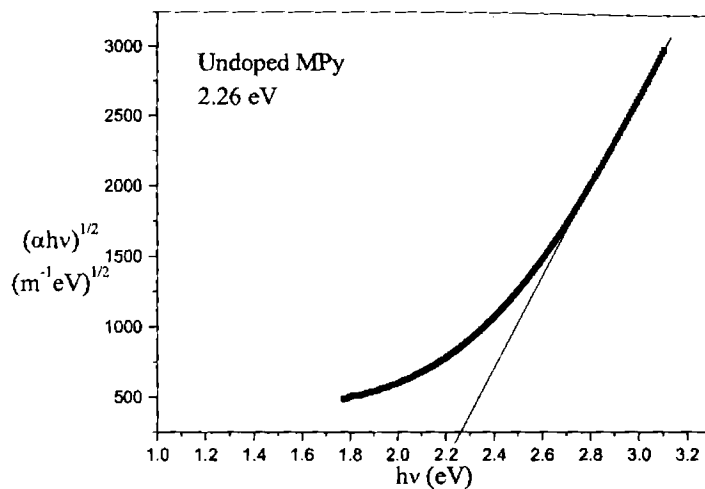


Figure 2.36. Variation of $(\alpha hv)^{1/2}$ with $h\nu$ for undoped MPy.

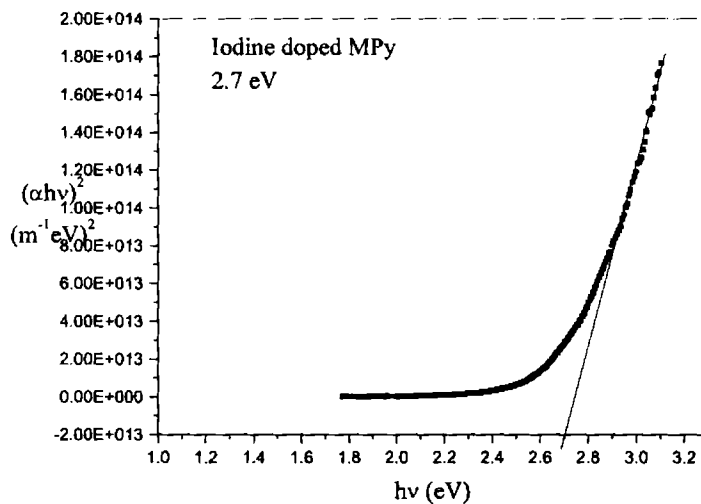


Figure 2.37. Variation of $(\alpha hv)^2$ with $h\nu$ for I-doped MPy.

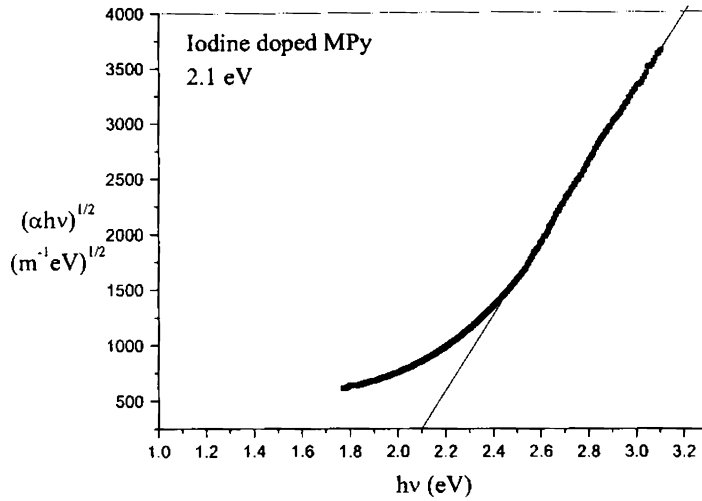


Figure 2.38. Variation of $(\alpha h\nu)^{1/2}$ with $h\nu$ for I-doped MPy.

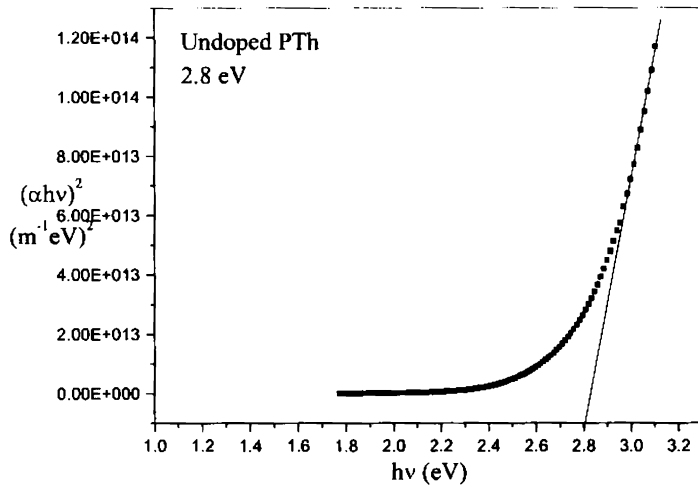


Figure 2.39. Variation of $(\alpha h\nu)^2$ with $h\nu$ for undoped PTh.

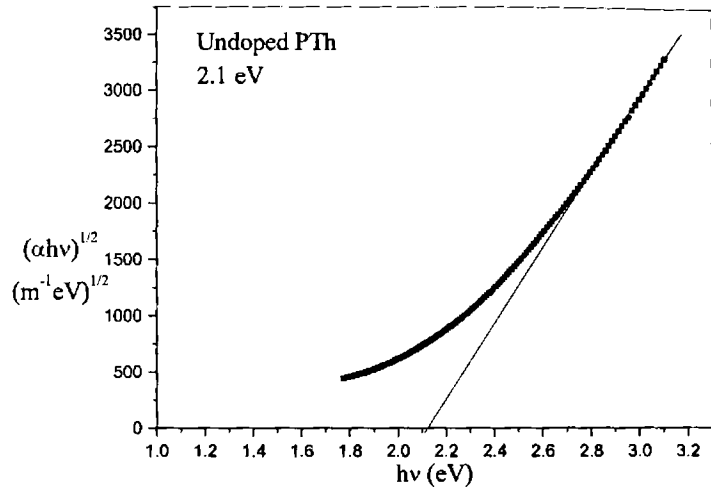


Figure 2.40. Variation of $(\alpha h\nu)^{1/2}$ with $h\nu$ for undoped PTh.

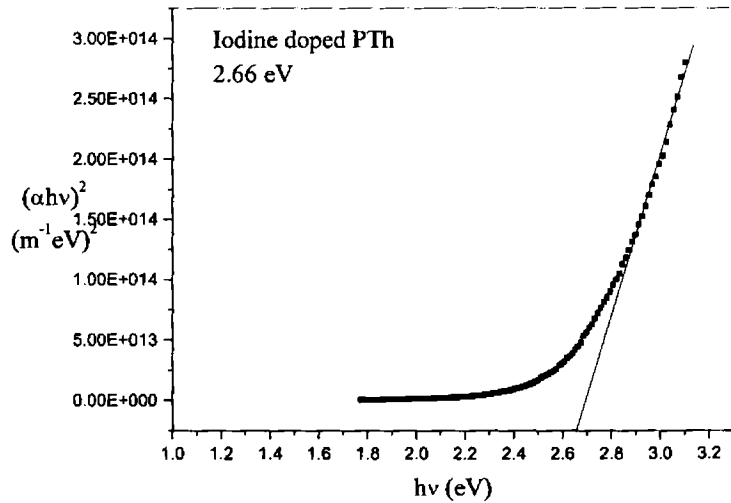


Figure 2.41. Variation of $(\alpha h\nu)^2$ with $h\nu$ for I-doped PTh.

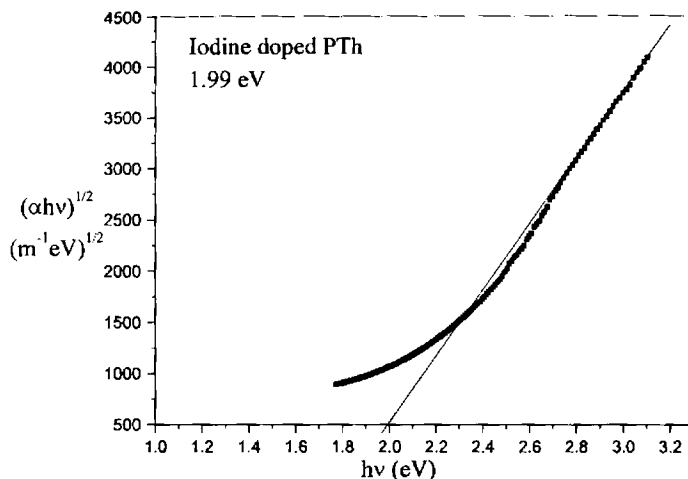


Figure 2.42. Variation of $(\alpha hv)^{1/2}$ with $h\nu$ for I-doped PTh.

Table 2.3 Direct and indirect transition gaps of the plasma polymerized films

Polymer film	Band gap (eV)			
	Undoped		Iodine doped	
	Direct	Indirect	Direct	Indirect
PANI	2.73	2.33	2.53	1.83
PPy	2.73	2.05	2.55	1.89
MPy	2.83	2.26	2.7	2.1
PTh	2.8	2.1	2.66	1.99

Direct and indirect transition gaps of the different films obtained from these plots are shown in table 2.3. It is observed that for all samples there is a reduction in direct and indirect band gaps on p-type doping with

iodine. This reduction, although not appreciable, is in agreement with theoretical predictions.

Conclusions

Chemically prepared polyaniline and polypyrrole powder samples show a variable range hopping conduction mechanism as illustrated in the respective plots. All the plasma polymer films under study show an ohmic behavior. There is no deviation from this behavior in the voltage and thickness ranges used.

Direct and indirect transition energy gaps are of comparable magnitudes for all the polymer films prepared by RF plasma polymerization [74]. On p-doping with iodine all samples show a reduction in the band gap.

References

1. V V Walatka, M M Labes, J H Perlstein, *Phys. Rev. Lett.* 31 (1973) 1139.
2. H Shirakawa, E G Lows, A G Mac Diarmid, C K Chiang, A J Heeger, *J. Chem. Soc. Chem. Commun.* 578 (1977).
3. T A Skotheim, R L Elsenbaumer, J R Reynolds, *Handbook of Conducting Polymers*, 2 Ed. Marcel Dekker, New York, Vol. 1-2, (1998).
4. H S Nalwa, *Organic conductive molecules and polymers*, John Wiley & Sons, Vol.2, England (1997).
5. W J Feast, J Tsibouklis, K L Pouwer, L Groenendual, E W Meijer, *Polymer*, 37, 5017 (1996).
6. J L Bredas, R Silbey, *Conjugated Polymers*, Kluwer, Dordrecht (1991).
7. K Y Law, *Chem. Rev.* 93 (1993) 449.
8. A Bohnen, H J Rader, K Mullen, *Synth. Met.* 47 (1992) 37.

9. N F Colaneri, D D C Bradley, R H Friend, P L Burn, A B Holmes, C W Spangler, *Phys. Rev. B* 42 (1990) 11670.
10. J H Burroughes, D D C Bradley, A R Brown, N Marks, K Mackay, R H Friend, P L Burn, A B Holmes, *Nature* 347 (1990) 539.
11. W P Su, J R Schrieffer, A J Heeger, *Phys. Rev. B* 22, (1981) 2099.
12. J L Bredas, J C Scott, K Yakushi, G B Street, *Phys. Rev. B* 30 (1984) 1023.
13. J L Bredas, *Mol. Cryst. Liq. Cryst.* 118 (1985) 49.
14. J L Bredas, B Themans, J G Fripiat, J M Andre, R R Chance, *Phys. Rev. B* 29 (1984) 6761.
15. W P Su, J R Schrieffer, A J Heeger, *Phys. Rev. Lett.* 42 (1979) 1698.
16. M J Rice, *Phys. Lett. A* 71 (1979) 152.
17. Y R Lin-Liu, K Maki, *Phys. Rev. B*, 26 (1982) 955.
18. J Tinka Gammel, J A Krumhansl, *Phys. Rev. B*, 24 (1981) 1035.
19. J L Bredas, R R Chance, R Silbey, *Phys. Rev. B*, 26 (1982) 5843.
20. C K Chiang, C R Fincher, Y W Park, A J Heeger, H Shirakawa, E J Louis, S C Gau, A G Mac Diarmid, *Phys. Rev. Lett.* 39 (1977) 1098.
21. H Shirakawa, S Ikeda, *Polym. J.* 2 (1971) 231.
22. D M Ivory, C G Miller, J M Sowa, R L Shacklette, R R Chance, R H Baughman, *J. Chem. Phys.* 71 (1979) 1506.
23. A F Diaz, K K Kanazawa, G P Gardini, *J. Chem. Soc. Chem. Commun.* (1979) 635.
24. A F Diaz, A Martinez, K K Kanazawa, M Salmon, *J. Electroanal. Chem.* 130 (1981) 181.
25. G. Tourillon, F Garnier, *J. Electrochem. Soc.* 130 (1983) 2042.
26. R J Waltman, J Bargon, A F Diaz, *J. Phys. Chem.* 87 (1983) 1459.
27. R J Waltman, A F Diaz, J Bargon, *J. Phys. Chem.* 88 (1984) 4343.

28. Y Shirota, N Noma, H Kaneza, H Mikawa, *J. Chem Soc. Chem. Commun.* (1984) 470.
29. T Osaka, Y Ohnuki, N Oyama, G Katagiri, K Kamisako, *J. Electroanal. Chem.* 161 (1984) 399.
30. F. Garnier, G Horowitz, F Deloffre, R. Hajlaoui, *Synth. Met.* 57 (2) (1993) 4747.
31. D. Fichou, G Horowitz, F. Garnier, *Synth. Met.* 39 (1) (1990) 125.
32. A G Mac Diarmid, A J Heeger, *Synth. Met.* 1(2) (1980) 101.
33. J M Tour, *Adv. Mater.* 6 (1994) 190.
34. D MacInnes Jr., M A Druvy, P J Nigrey, D P Nairns, A G Mac Diarmid, A J Heeger, *J. Chem. Soc. Chem. Comm.* (1981) 317.
35. J. Miasik, A Hopper, B Tofield, *J. Chem. Soc. Faraday Trans. I* 82 (1986) 1117.
36. T Hanawa, S Kuwabata, H Hashimoto, H Yoneyama, *Synth. Met.* 30(2) (1989) 173.
37. S Dong, Z Sun, Z Lu, *J. Chem Soc. Chem. Commun.* (1988) 993.
38. J H Bourroughes, D D C Bradley, A R Brown, R N Marks, K Mac Kay, R H Friend, P L Burn, A B Holmes, *Nature (London)* 347 (1990) 539.
39. G Grem, G Leditsky, B Ulrich, G Leising, *Adv. Mater.* 4 (1992) 36.
40. S Becker, C Ego, A C Grimsdale, E J W List, D Marsitzky, A Pogantsch, S Setayesh, G Leising, K Mullen, *Synth. Met.* 125(1) (2001) 73.
41. V Saxena, V Shirodkar, *J. Appl. Polym. Sci.* 77 (2001) 1050.
42. R L Greene, G B Street, L J Sutude, *Phys. Rev. Lett.* 34 (1975) 577.
43. H Shirakawa, E J Louis, A G Mac Diarmid, C K Chiang, A J Heeger, *J. Chem Soc. Chem. Commun.* (1977) 578.
44. T A Skotheim, *Handbook of conducting Polymers*, Marcel Dekker, New York, 1986.

45. K S V Srinivasan, *Macromolecules: New Frontiers* vol 1&2, Allied Publishers, India, 1998.
46. Ed. M Aldissi, *Intrinsically Conducting Polymers, An Emerging Technology*, Kluwer, Dordrecht, Netherlands, 1993.
47. J Lei, W Liang, C S Brumlik, C R Martin, *Synth. Met.* 47 (1992) 351.
48. M Narasimhan, M Hagler, V Commarata, M Thakur, *Appl. Phys. Lett.* 72 (1998) 1063.
49. T Tani, W D Gill, P M Grant, T C Clarke, G B Street, *Synth. Met.* 1 (1979) 301.
50. H Tomozawa, D Brown, S Phillips, A Heeger, H Kroemer, *Synth. Met.* 22 (1987) 63.
51. A Tsumura, M Koezuka, T Ando, *Appl. Phys. Lett.* 49 (1986) 1210.
52. J H Burroughes, C A Jones, R H Friend, *Nature*, 335 (1988) 137.
53. G Guilaud, M Al Sadoun, M Maitrot, J Simon, M Bouvet, *Chem. Phys. Lett.* 167 (1990) 503.
54. A Tsumura, H Fuchigami, H Koezuka, *Synth. Met.* 41 (1991) 1181.
55. A Tsumura, H Koeza, T Ando, *Appl. Phys. Lett.* 49 (1986) 1210.
56. F Garnier, R Hajlaoui, A Yassar, P Srivastava, *Science*, 265 (1994) 1684.
57. Y Yang, A J Heeger, *Nature* 372 (1994) 344.
58. J R Hollahan, A T Bell, *Techniques and Applications of Plasma Chemistry*, Wiley, New York, 1974.
59. R K Sathir, K F Schoch Jr, S Wood, *Synth. Met.* 26 (1988) 391.
60. H Yasuda, C E Lamaze, *J Appl. Polym. Sci.* 17 (1973) 201.
61. K Tanaka et. al. *J. Appl. Phys.* 70 (10) (1991) 5653.
62. S F Durrant et. al. *Thin Solid Films* 259 (1995) 139.
63. H Yasuda, T Hirotsu, *J Polym. Sci. Polym. Chem.* 15 (1977) 2749.
64. R K Sathir, K F Schoch Jr., *Thin Solid Films*, 223 (1993) 154.

65. T Nakano et al, J. Phys. D Appl. Phys.23 (1990) 711.
66. M. Yasuda et. al., Jpn. J. of Appl. Phys. 21 (1982) 768.
67. S. Morita et. al., J. Appl. Phys. 51 (1980) 3938.
68. J A Tobin, D D Denton, Appl. Phys. Lett. 60 (21) (1992) 2595.
69. J J Hauser, Phys. Rev. B 9 (1974) 2623.
70. N Motts, E A Davis, Electronic Processes in Non-crystalline Materials 2nd Ed. Oxford, Clarendon, 71.
71. J Tauc, Optical properties of solids, A Abeles, North Holland, Amsterdam (1970) 277.
72. J Bardeen, F J Blatt, L M Hall, Proc. Photoconductivity Cong. Wiley, New York, (1956) 146.
73. E A Davis, N F Mott, Phil. Mag. 22 ((1970) 903.
74. F U Z Choudhury, A H Bhuiyan, Thin Solid Films, 360 (2000) 69.

Chapter 3

Thermal Diffusivity Measurements of RF Plasma Polymerized Films by Probe Beam Deflection Method

3.1 Introduction

There has been tremendous growth in the field of smart materials with tailored properties over the past couple of decades. In this context, material characterization assumes high priority. For the thermal characterization of materials the conventional methods include Differential Scanning Calorimetry, Contact Transient Methods, etc. These techniques demand a relatively large size for the samples or are too complex and time consuming. In these conventional measuring methods the sample must be kept in contact with the detector, which produces fluctuations in the thermal field to be measured. Thermal wave physics emerged as an effective tool for the characterization of a wide variety of materials [1 – 4]. A detailed account of these methods is given in chapter 1. Major advantages of these methods are that they are non-destructive and non-contact techniques. The methods are in general referred to as photothermal techniques. A widely used and popular application of photothermal methods is the measurement of thermal diffusivity of materials. The choice of a particular photothermal technique depends on the thermo-optical properties and the structure of samples. Prominent among the

perpendicular and parallel to the sample surface. The normal component is related to heat diffusion process perpendicular to the sample surface whereas the transverse component describes the heat diffusion parallel to the surface.

3.2.1 Phase method

This is the most popular transverse PBD technique used in the thermal characterization of a variety of materials ranging from semiconductors to polymers [19]. This method provides results with sufficient accuracy in the case of materials whose thermal diffusivity is greater than that of the coupling fluid.

The tangential (transverse) component of the photothermal signal can be expressed as $\phi_t = \phi_0 \exp\left[-j\omega t - j\left(\frac{y}{l_t} + \phi\right)\right]$, where l_t is called the characteristic length which is the distance corresponding to one radian phase shift. ϕ is term depending on the pump beam spot size and the vertical offset of the probe with respect to the sample surface. The above relation implies that the phase of the PBD signal varies linearly with the pump-probe offset y . The characteristic length can be taken to be equal to the thermal diffusion length $\mu = \sqrt{\frac{\alpha}{\pi f}}$, for samples whose thermal diffusivity is greater than that of the coupling fluid. The thermal diffusivity can be obtained from the slope of the plot between phase and the pump-probe offset.

3.2.2 Amplitude method

The amplitude method accounts for the variation of amplitude A_t of the tangential component of the PBD signal with pump-probe offset. It can be shown that $\ln A_t$ varies linearly with the offset y and the thermal diffusivity

can be obtained from the slope of the plot for materials whose thermal diffusivity is greater than that of the coupling fluid [20].

3.3 Experimental setup for transverse PBD

The experimental configurations used in photothermal methods are in general simple and compact. The essential components of a transverse PBD setup are pump source, probe source, chopper, sample cell, position sensitive detector and data acquisition system.

3.3.1 Pump Source

The widely used pump source in photothermal methods is a laser. Lasers with fairly good Gaussian profile are used as pump source. In the present study of polymer films, a He-Ne laser (Melles Griot, 20 mW, 632.8 nm) with geometrical dimensions of length 50 cm and diameter 5 cm is used as the pump source. The $1/e^2$ beam diameter is 0.7 mm and the divergence is 1.2 milliradians. The beam is focused using a lens of focal length 10 cm. The He-Ne source is compact and economical compared to the Ar-ion laser used in conventional setups. It also meets the requirements of the pump source to be used in mirage experiments, in terms of coherence and directional properties in addition to the important condition that the sample absorbs at least a small portion of the energy of the pump source.

3.3.2 Probe source

Probe source in conventional setups is a low power He-Ne laser. In the present study, a diode laser (Melles Griot, 650 nm, 5mW) with beam diameter ~ 0.8 mm is used as the probe source. Since the power required for the probe source in PBD experiment is small, only a low power semiconductor laser

meets the requirement. The size of the laser is about 7 cm long and 1.5 cm diameter and is focused using a lens of focal length 5cm.

3.3.3 Chopper

In the transverse PBD method, the pump beam is intensity modulated using a suitable chopping mechanism. There are different chopping techniques like mechanical, electrical, electro-optic and acousto-optic. High quality, variable speed and low vibration noise chopper are available commercially. In this study a mechanical chopper (Stanford Model SR 540) is used. The chopping rate falls in the range of 4Hz - 4 kHz. The whole frequency range operation requires two blades - a 6-slot blade for operation in the frequency range 4Hz - 400 Hz and 30-slot blade for 400 Hz to 4 kHz.

Depending on the modulation the sample becomes thermally thick or thermally thin. This is due to the fact that the thermal diffusion length follows an inverse relation with the square root of modulation frequency. The sample is classified into thermally thick or thermally thin according as the thermal diffusion length is less than or greater than the thickness of the sample. Hence, by controlling the modulation frequency, the sample can be changed from thermally thick to thermally thin or vice versa. However, in the mirage measurements for thermal diffusivity, the technique can be applied irrespective of whether the sample is thermally thin or thermally thick.

3.3.4 Sample cell

A quartz cuvette of dimensions 10 mm x 10 mm x 5 mm is used in this study. High purity carbon tetrachloride is used as the coupling fluid surrounding the sample, mainly due to the high value of $\frac{dn}{dT}$ compared to air. This implies that for each degree temperature rise there will be considerable

change in the refractive index, which will lead to an appreciable beam deflection. The comparatively low values of thermal conductivity ($k = 0.099 \text{ Wm}^{-1}\text{K}^{-1}$), specific heat capacity ($C_p = 0.85 \text{ Jkg}^{-1}\text{K}^{-1}$) and thermal diffusivity ($0.731 \times 10^{-7} \text{ m}^2\text{s}^{-1}$) also make carbon tetrachloride an ideal coupling fluid for thermal diffusivity measurements.

3.3.5 Position sensitive detector

Silicon photodetectors can be used as position sensitive detectors (PSD) in photothermal applications. The position of beam with fractions of microns can be obtained using PSDs and hence are conveniently used in photothermal beam deflection experiments. In the present work, a bi-cell (SPOT 2D, UDT Sensors Inc.) serves as the position sensitive detector for the probe beam deflection measurements. The important features of this bi-cell include high accuracy, excellent resolution, high-speed response and ultra low dark current. Spectral response range is from 350-1100nm and it has excellent stability over time and temperature. It has fast response times necessary for high speed or pulsed operation and position resolutions of better than $0.1 \mu\text{m}$.

3.3.6 Pre-amplifier

A simple pre-amplifier of in-house design is used for amplifying the bi-cell output to the required level. The amplifier is standardized applying known signals.

3.3.7 Lock-in amplifier

Lock-in detection is employed for the amplified output from the pre-amplifier. The detection scheme has all the advantages of the phase sensitive detection. In the present work, the lock in amplifier SR830 (Stanford Research Inc.) is used. The SR 830 can measure voltages from 2 nV to 1 V.

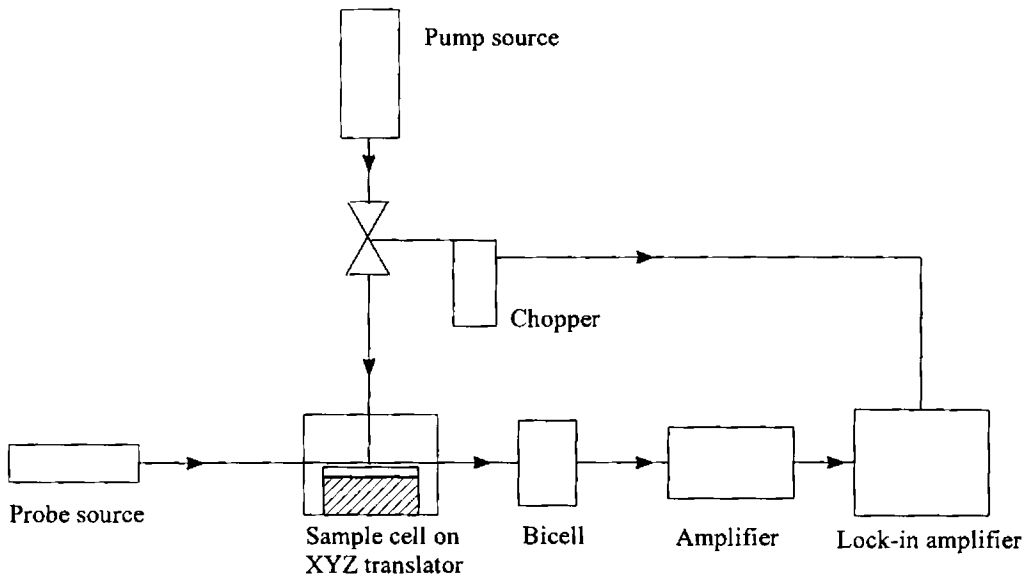


Fig 3.2 Block diagram of experimental setup for transverse PBD study

The block diagram of the experimental setup used for the PBD study is shown in figure 3.2. The transverse scan method is used in this study. In this case the distance between the pump and probe beams is gradually varied. In the experimental setup used, the pump beam is fixed and probe beam is made to scan the surface of the film. The probe source along with focusing arrangement is kept on a light platform fixed to an XYZ translator. The polymer film on glass substrate is arranged inside the sample cell containing carbon tetrachloride. The sample cell is kept on a translation stage. The pump laser and these two translation stages are fixed on an optical breadboard with honeycomb structure, placed on a granite table so as to minimize the errors due to mechanical vibrations.

The experimental setup is standardized for thermal diffusivity using InP wafer of thickness $350\mu\text{m}$ using the phase method as described. The thermal

diffusivity value obtained ($4.4 \times 10^{-5} \text{ m}^2 \text{ s}^{-1}$) is in good agreement with the literature value [21].

3.4 Thermal diffusivity measurements

Heat diffusion in different RF plasma polymerized thin films is investigated in this study. Both amplitude and phase methods described earlier are used for the determination of thermal diffusivity. The polymer samples selected for this study are polyaniline (PANI), polypyrrole (PPy), poly N-methyl pyrrole (MPy) and polythiophene (PTh). In situ iodine doping is carried out in these samples and the effect of doping on heat transport is examined.

It is well established that doping increases the electrical conductivity by several orders of magnitude. Iodine doping is a popular technique used in the case of conducting polymer films. The variation of heat diffusion properties with doping, though relevant in thermal design, is not much explored. Also in the case of thin polymer films, the preparation conditions play an important role in determining their structure and properties. Although the film structure and composition depend primarily on the monomer, in RF plasma polymerization, the deposition parameters such as monomer flow rate, the reactor pressure, RF power and substrate temperature are equally relevant in determining the structure as well as the thermo-physical properties of the film [22, 23]. The present study is focused on investigating heat diffusion in plasma polymerised films and also on the dependence of thermal diffusivity on iodine doping. The effect of reactor pressure on the thermal diffusivity of one of the polymer samples (PANI) is also examined.

3.4.1 Polyaniline

Polyaniline film on glass substrate is mounted on a sample holder and kept inside a quartz cuvette acting as the sample cell. Carbon tetrachloride is used as the coupling medium. Intensity modulated 632.8 nm radiation from the pump laser is allowed to fall on the sample. The probe beam runs parallel and close to the sample surface and is directed perpendicular to the pump beam. The probe beam gets deflected due to the thermal gradient induced in the coupling medium close to the sample surface, with deflection components both perpendicular and parallel to the sample surface. The transverse component, which is perpendicular to the pump beam and parallel to sample surface, describes the heat diffusion process parallel to the surface. This transverse component is detected by the position-sensitive detector.

The probe beam is made to scan a region on either side of the pump beam in the skimming configuration, recording the amplitude and phase of the photothermal signal. Thermal diffusivity α is obtained from the slopes of the phase-offset as well as the \ln (amplitude)-offset plots.

The phase-offset plots of PANI film prepared at different values of reaction chamber pressure are shown in figures 3.3 – 3.6. The graph obtained by amplitude method for undoped PANI prepared at 0.4 mbar pressure is shown in figure 3.7. Figures 3.8 and 3.9 illustrate the variation of amplitude and phase of the photothermal signal with transverse offset in the case of iodine doped PANI.

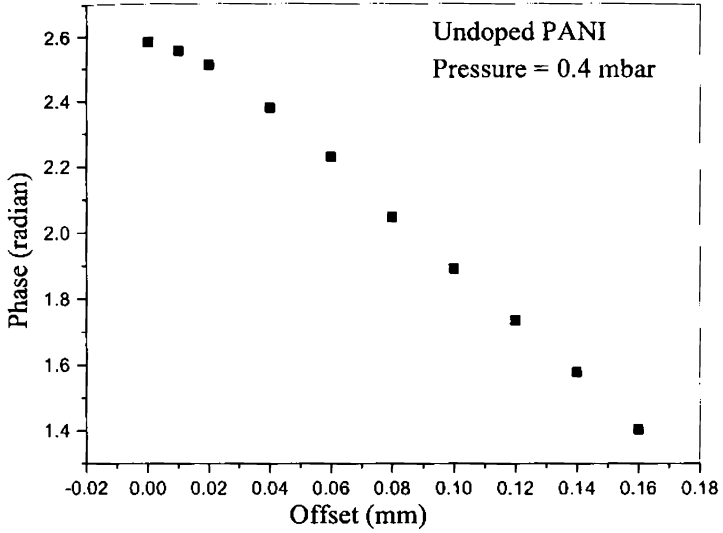


Figure 3.3: Phase-offset plot of PANI prepared at 0.4mbar

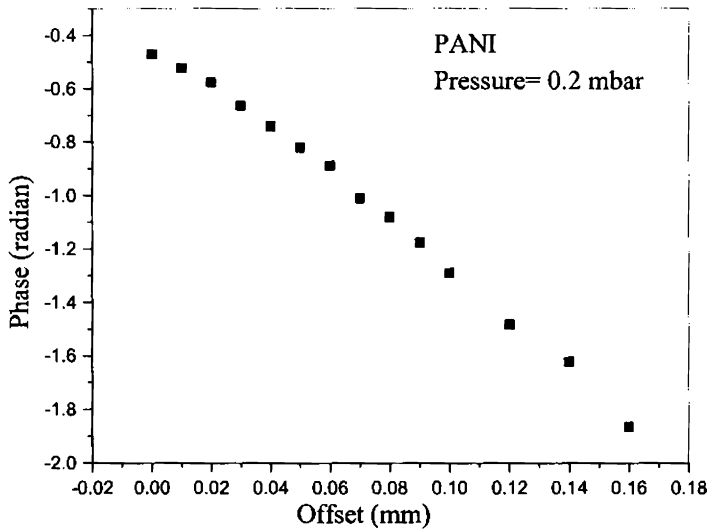


Figure 3.4 Phase-offset plot of PANI prepared at 0.2mbar

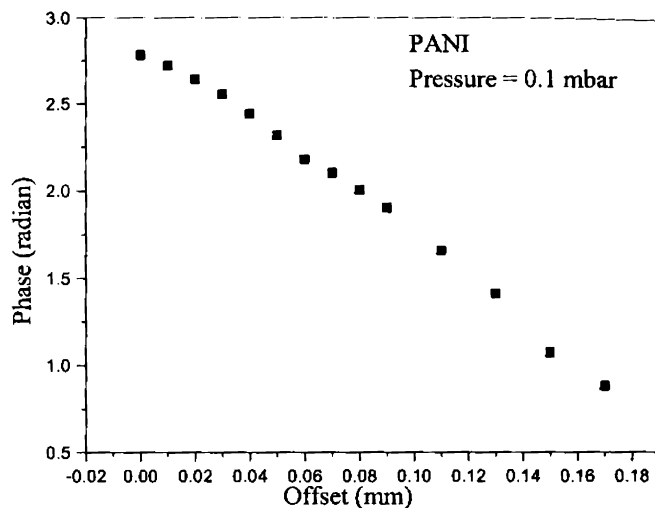
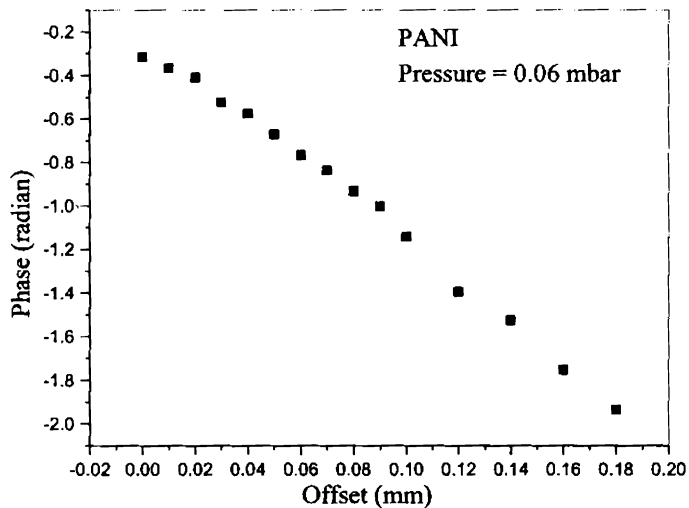


Figure 3.5 Phase-offset plot of PANI prepared at 0.1mbar



3.6 Phase-offset plot of PANI prepared at 0.06mbar

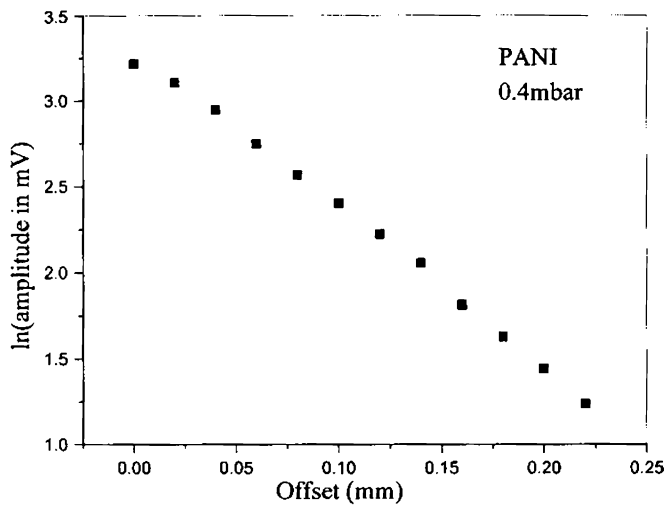


Figure 3.7 ln(amplitude) vs offset plot for PANI prepared at 0.4mbar

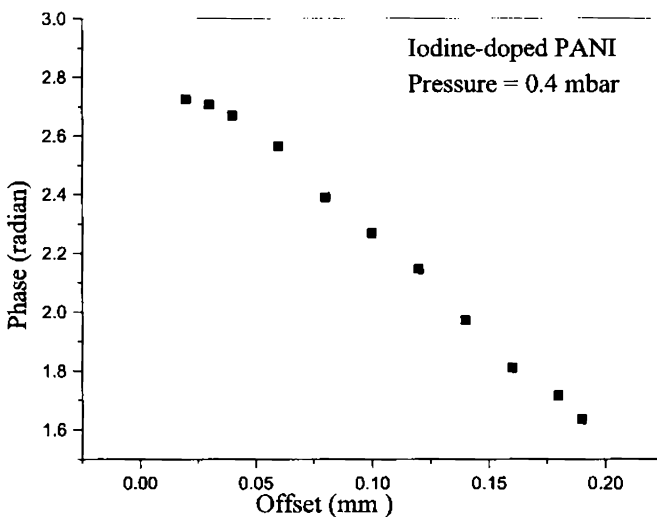


Figure 3.8 Phase-offset plot for iodine doped PANI

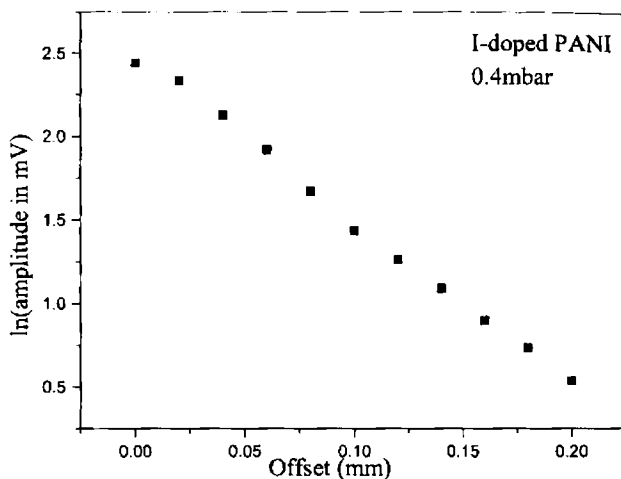


Figure 3.9 ln(amplitude) vs offset plot for iodine doped PANI

Table 3.1 Variation of thermal diffusivity with the reactor pressure.

Pressure (mbar)	0.4	0.2	0.1	0.06
α ($\times 10^{-7} \text{ m}^2 \text{ s}^{-1}$)	4.377	3.653	2.399	2.187

Tables 3.1 and 3.2 respectively show the variation of thermal diffusivity with the monomer pressure in the reaction chamber and with iodine doping.

Table 3.2 Effect of iodine doping on thermal diffusivity of PANI

Polymer film	Thermal diffusivity ($\times 10^{-7} \text{ m}^2 \text{ s}^{-1}$)	
	Phase method	Amplitude method
Undoped PANI	4.377 ± 0.02	4.491 ± 0.02
Iodine doped PANI	3.487 ± 0.03	3.55 ± 0.04

3.4.2 Polypyrrole

PPy film on glass substrate is mounted on a sample holder and kept inside a quartz cuvette sample cell. Recording of photothermal signal is carried out as in the case of PANI. Observations are repeated for the iodine doped sample.

Figures 3.10 - 3.12 show the variation of amplitude of the photothermal signal with pump-probe offset for three different frequencies - 6 Hz, 12 Hz and 18 Hz respectively. The corresponding plots obtained for iodine doped samples are given in figures 3.16 -3.18. The phase – offset plots for the three frequencies for undoped and iodine doped samples are shown in figures 3.13 – 3.15 and 3.19 – 3.21 respectively.

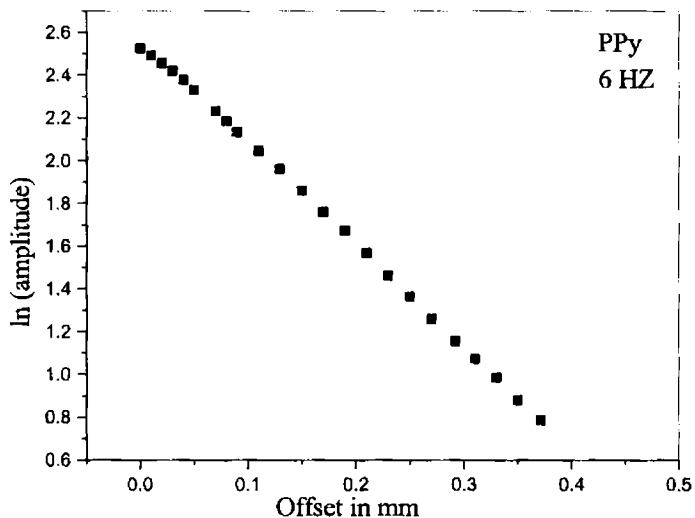


Figure 3.10 Variation of amplitude with offset for PPy at 6Hz modulation

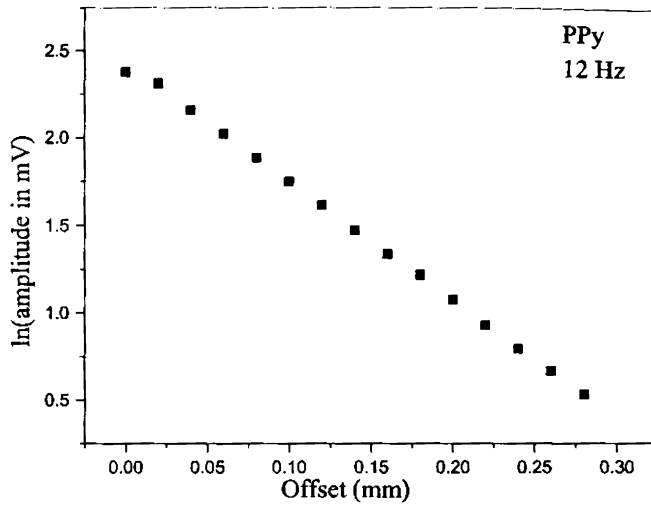


Figure 3.11 Variation of amplitude with offset for PPy at 12 Hz modulation

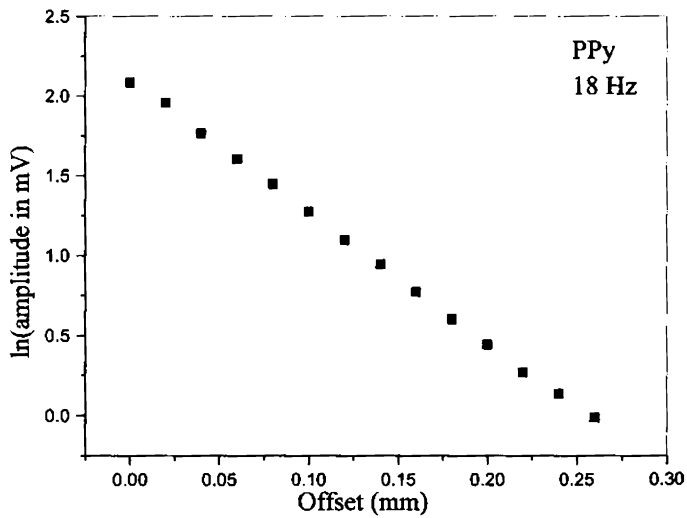


Figure 3.12 Variation of amplitude with offset for PPy at 18 Hz modulation

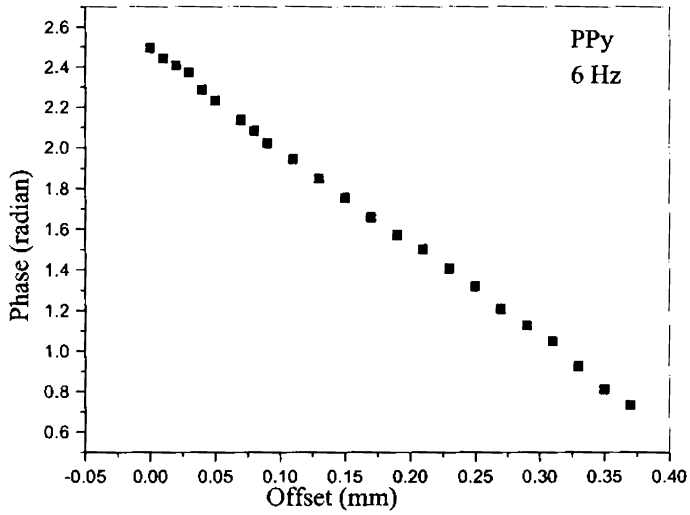


Figure 3.13 Variation of phase with offset for PPy at 6 Hz modulation

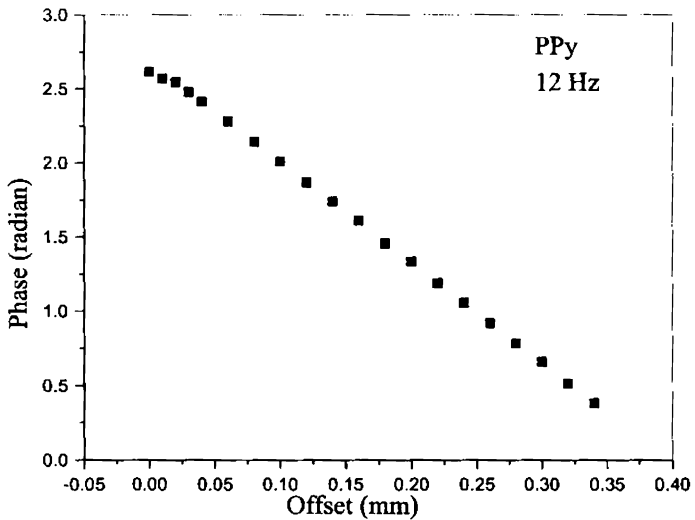


Figure 3.14 Variation of phase with offset for PPy at 12 Hz modulation

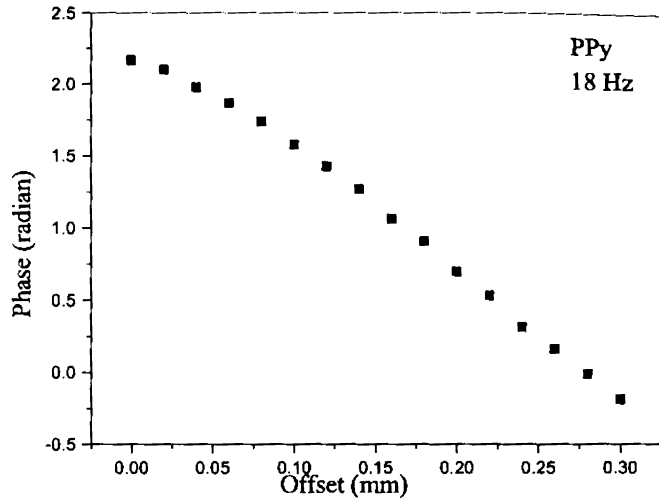


Figure 3.15 Variation of phase with offset for PPy at 18 Hz modulation

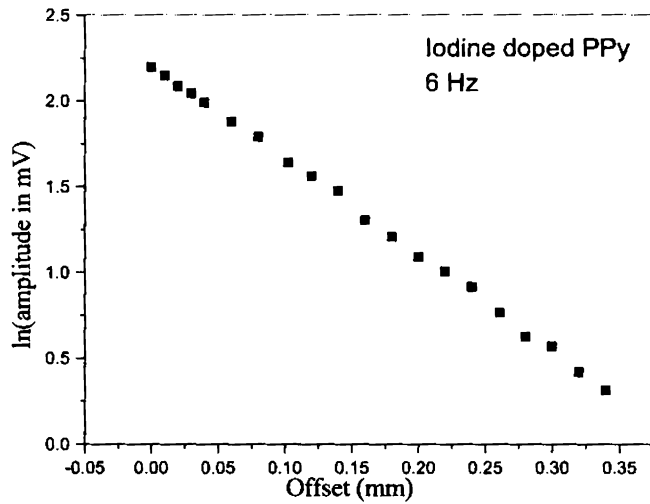


Figure 3.16 Variation of amplitude with offset for iodine doped PPy at 6 Hz modulation.

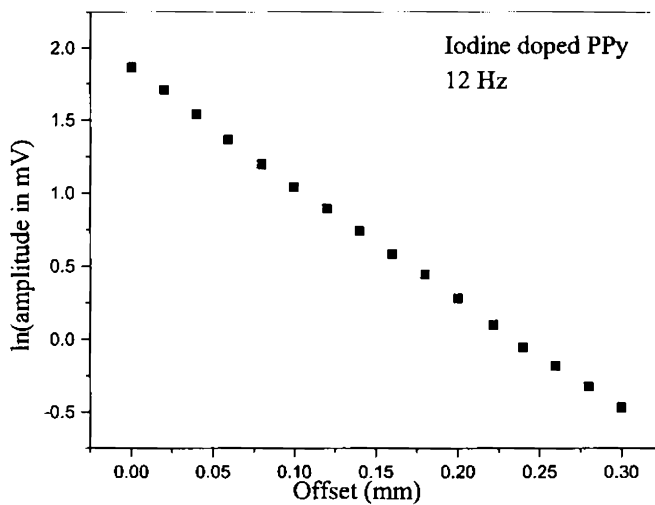


Figure 3.17 Variation of amplitude with offset for iodine doped PPy at 12 Hz modulation.

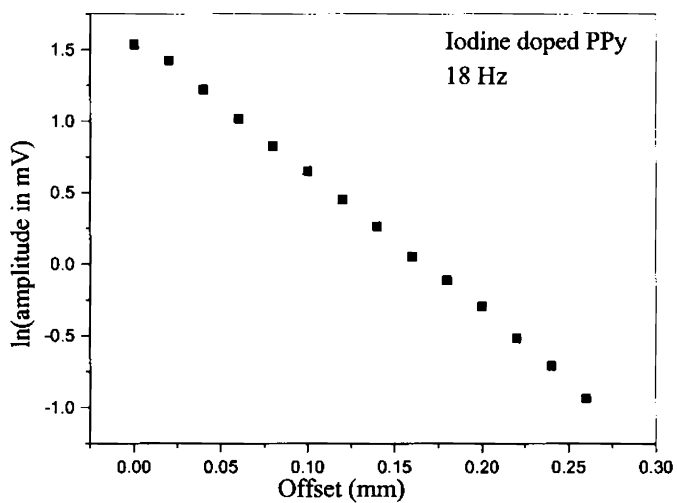


Figure 3.18 Variation of amplitude with offset for iodine doped PPy at 18 Hz modulation.



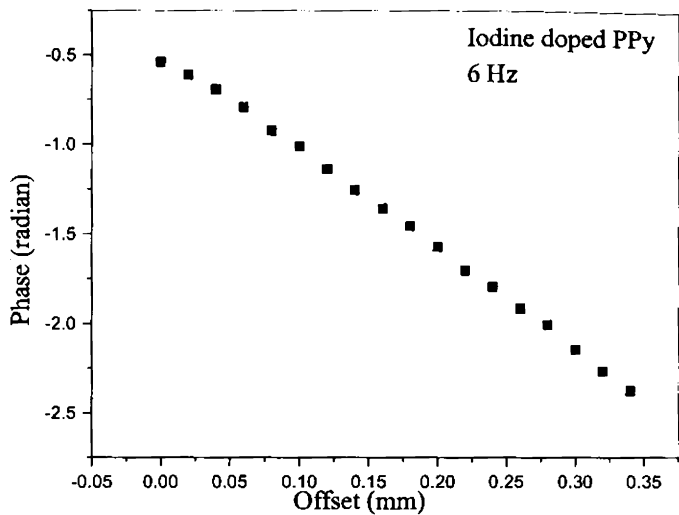


Figure 3.19 Variation of phase with offset for iodine doped PPy at 6 HZ modulation

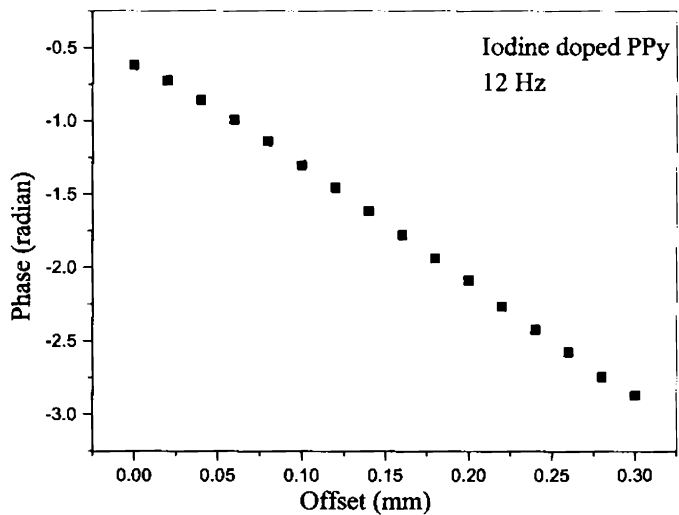


Figure 3.20 Variation of phase with offset for iodine doped PPy at 12 HZ modulation

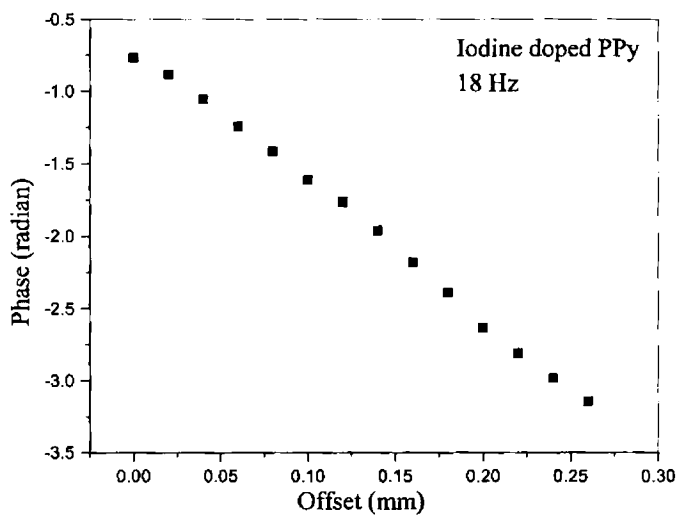


Figure 3.21 Variation of phase with offset for iodine doped PPy at 18 HZ modulation

The values of thermal diffusivity computed from the various plots for undoped and iodine doped PPy are listed in table 3.3.

Table 3.3 Thermal diffusivity values of pure and iodine-doped PPy.

PPy film	Modulation frequency (Hz)	Thermal diffusivity ($\times 10^{-7} \text{ m}^2 \text{ s}^{-1}$)	
		Phase method	Amplitude method
Pure	6	$8.49 \pm .06$	$8.28 \pm .03$
	12	$8.39 \pm .04$	$8.29 \pm .06$
	18	$8.45 \pm .03$	$8.38 \pm .04$
Iodine-doped	6	$6.23 \pm .03$	$6.12 \pm .05$
	12	$6.30 \pm .06$	$6.19 \pm .05$
	18	$6.28 \pm .06$	$6.17 \pm .03$

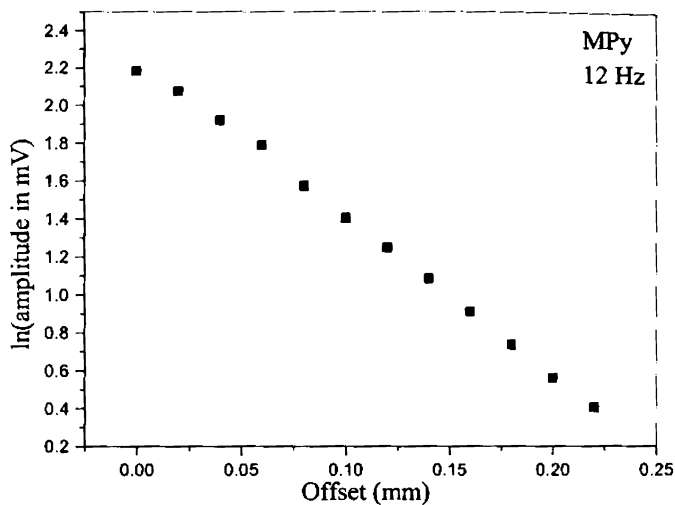


Figure 3.22 Variation of amplitude with offset for MPy at 12Hz modulation

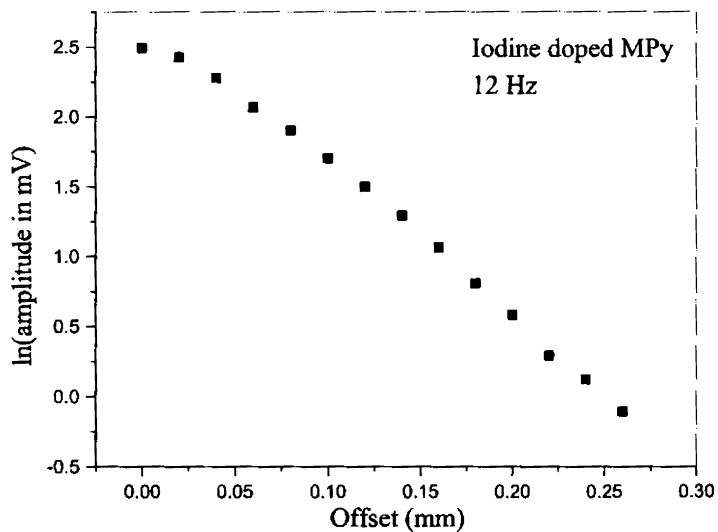


Figure 3.23 Variation of amplitude with offset for iodine doped MPy at 12Hz modulation

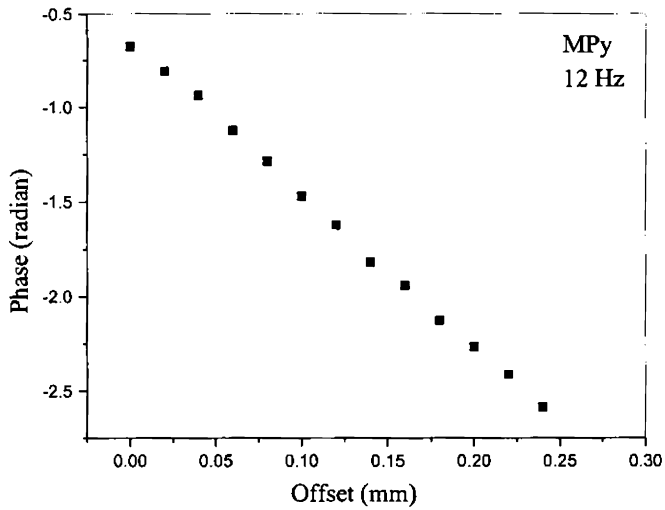


Figure 3.24 Phase-offset plot of MPy at 12Hz modulation

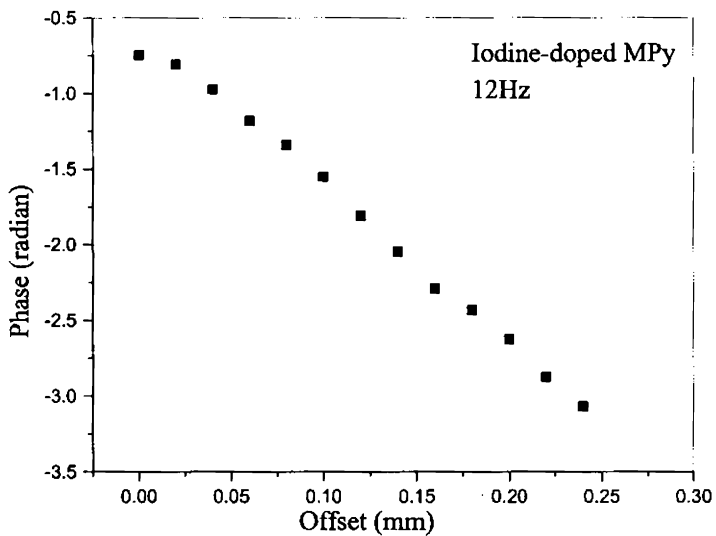


Figure 3.25 Phase-offset plot of iodine doped MPy at 12 Hz modulation

3.4.3 Poly N-methyl pyrrole

Thermal diffusivity of poly N-methyl pyrrole in the pure and iodine doped forms are determined by transverse PBD technique as outlined in the case of PPy.

Table 3.4 Thermal diffusivity values of pure and iodine-doped MPy.

MPy film	Modulation frequency (Hz)	Thermal diffusivity ($\times 10^{-7} \text{ m}^2 \text{ s}^{-1}$)	
		Phase method	Amplitude method
Pure	12	$5.75 \pm .02$	$5.47 \pm .04$
Iodine-doped	12	$3.62 \pm .03$	$3.48 \pm .02$

The variation amplitude and phase of the photothermal signal with offset in the pure and doped forms of the sample are shown in figures 3.22 – 3.25. The respective values of thermal diffusivity are given in table 3.4. It is observed that there is a reduction in thermal diffusivity on iodine doping as in the case of PANI film.

3.4.4 Polythiophene

Thermal diffusivity of plasma polymerized PTh film is determined by the PBD method as described in the above cases. Measurements are taken on films of different thickness to explore the possibility of any thickness dependence of diffusivity.

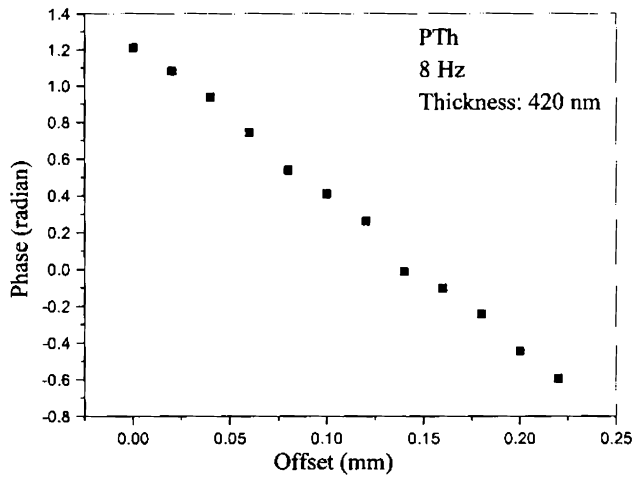


Figure 3.26 Phase-offset plot for PTh at 8 Hz modulation

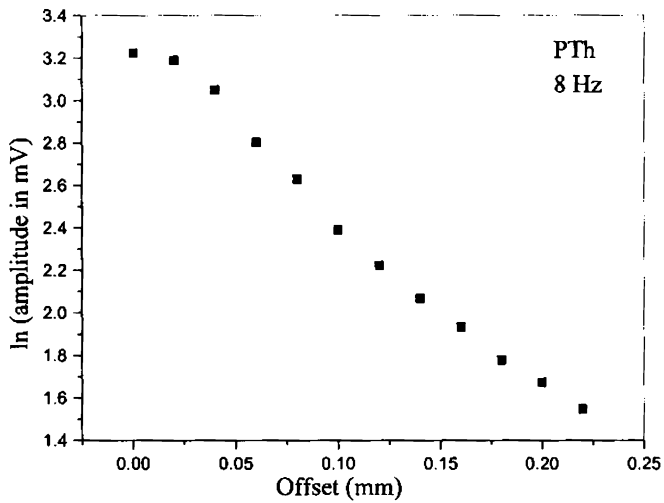


Figure 3.27 Variation of amplitude with offset for PTh at 8 Hz modulation

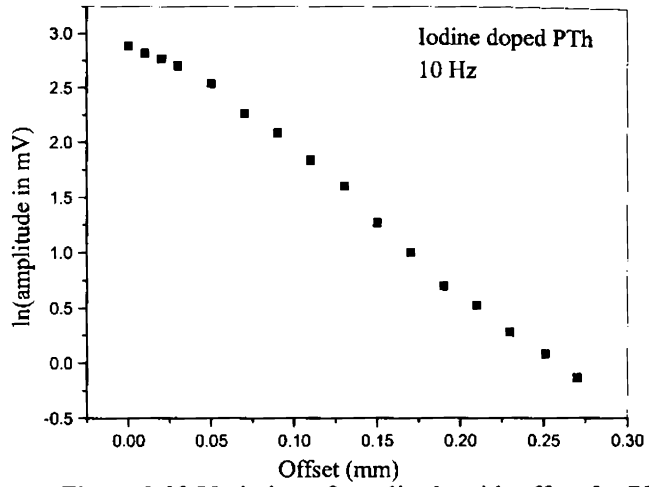


Figure 3.28 Variation of amplitude with offset for PTh at 10 Hz modulation

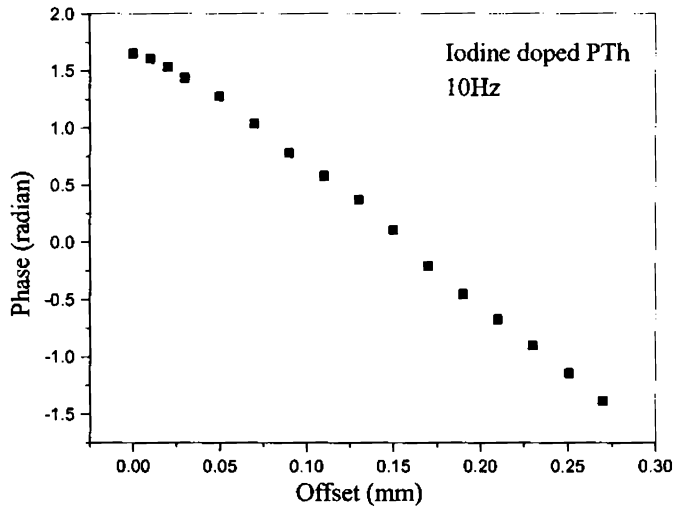


Figure 3.29 Phase-offset plot for iodine doped PTh at 10 Hz modulation

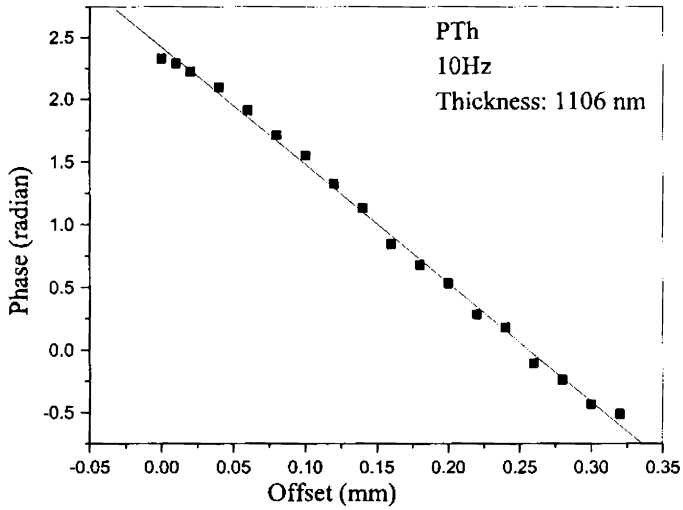


Figure 3.30 Phase offset plot for PTh film of thickness 1106 nm at 10 Hz modulation

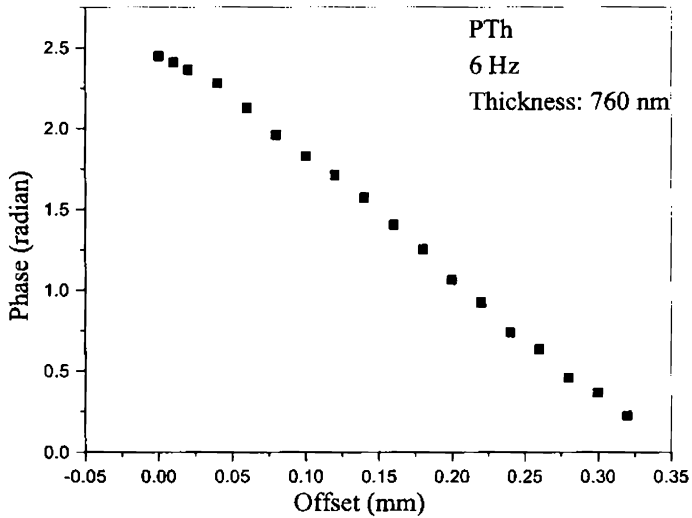


Figure 3.31 Phase-offset plot for PTh film of thickness 760 nm at modulation frequency 6 Hz

Table 3.5 Thermal diffusivity values of pure and iodine-doped PTh.

PTh film	Modulation frequency (Hz)	Thermal diffusivity ($\times 10^{-7} \text{ m}^2 \text{ s}^{-1}$)	
		Phase method	Amplitude method
Pure	8	$3.56 \pm .03$	$3.69 \pm .03$
Iodine-doped	10	$2.33 \pm .04$	$2.27 \pm .04$

Table 3.6 Thermal diffusivity values of PTh films of different thickness.

PTh Phase method	Thickness (nm)	Thermal diffusivity (cm^2/s)
	420	$3.56 \pm .03$
	760	$3.72 \pm .05$
	1106	$3.51 \pm .04$

The variation of PBD signal with offset is shown in figures 3.26 – 3.29. The corresponding diffusivity values obtained are shown in table 3.5.

The phase method is applied to determine the thermal diffusivity of three samples of PTh with different thickness. The phase-offset plots for film thickness 420nm, 1106nm and 760nm are given in figures 3.26, 3.30 and 3.31. It is seen that there is no dependence of this property on film thickness in the range 420nm – 1106 nm.

The accuracy of the results obtained in any transverse PBD method depends on the relative magnitudes of the thermal diffusivity of the sample and the coupling fluid. The method provides satisfactory results in cases where the

thermal diffusivity of the sample is greater than that of the coupling fluid. In the present study, although diffusivity of polymer films is low, the corresponding value ($7.31 \times 10^{-8} \text{ m}^2 \text{ s}^{-1}$) for the coupling fluid (carbon tetrachloride) is still lower by about an order. All the polymer samples under study are thermally thin in the range of frequencies used in this study. Consequently the substrate contribution to the photothermal signal becomes relevant. In the present study, the substrate material is glass which has negligible absorption at the frequency of the pump source. As the thermal expansion coefficients of polymers relatively large, there can be deformation of the film at the pump spot. Since a relatively low power laser is used the surface deformation can be neglected. The surface deformation can affect measurements in the bouncing configuration. In the present study, a skimming configuration is used.

Conclusion

Heat diffusion in four typical polymer films prepared by radio frequency plasma polymerization is investigated. As the deposition conditions can greatly affect the thermo-physical properties of the polymer films, the dependence of thermal diffusivity on one of the processing parameter (pressure) is examined. The results obtained suggest a reduction in diffusivity with decreasing pressure. This sort of behavior can be accounted for by the high degree of fragmentation and the cross linking occurring in the polymer structure at reduced pressure. Highly branched and cross linked nature is characteristic of any polymer deposited by RF plasma polymerization technique [24 - 27]. The structure is, in general, highly irregular and amorphous. The pressure in the reaction chamber affects the residence time of the molecules in the plasma atmosphere. It can influence the average energy

and the mean free path of the species in the reactor. The mean free path of the species will be less at higher values of pressure. This results in a lower average energy of collisions, resulting in lesser degree of fragmentation. A higher pressure means a higher flow rate. In this case the residence time of the species in the plasma is decreased. Or the different species are subjected to the plasma environment for a lesser time, resulting in reduced fragmentation. It is the reverse at lower values of pressure. As fragmentation and cross linking increases at low pressure, the film structure becomes highly disordered. This, in turn reduces the thermal diffusivity of films prepared at low pressure.

As doping, in general, increases the electrical conductivity of polymer films a corresponding behavior can be expected in the case of heat transport. The effect of p-type doping with iodine on the thermal diffusivity of the polymer samples is studied. In this study it is observed that heat diffusion in plasma polymerized films is dampened on iodine doping. The presence of iodine in an already disordered structure enhances phonon scattering resulting in a lower diffusivity.

Thermal properties of polymer films may differ from those of the bulk counterparts. The effect of thickness of the film on heat diffusion is explored in the case of PTh film. The results show that there is no thickness dependence of diffusivity in the range of 420nm to 1106 nm.

The values of thermal diffusivity obtained for all the polymer samples used in this study are of the order of that for other typical polymers [28].

References

1. Yu G Gurevich, G. Gonzalez de la Cruz, G Logvinov, M N Kasyanchuk, *Semiconductors*, 32(11) (1998)1179.
2. A Mandelis, *Physics Today*, August, (2000) 29.

3. G Biranbaum, B A Auld, Ed. Sensing for Materials Characterization, Processing and Manufacturing, The American Society for Nondestructive Testing Inc. Columbus, 1998.
4. A Mandelis, Ed., Principles and Perspectives of Photothermal and Photoacoustic Phenomena, Elsevier, Oxford, 1992.
5. A Rosencwaig, A Gersho, *J. Appl. Phys.* 47, (1976) 64.
6. A. Rosencwaig, *Photoacoustics and Photoacoustic Spectroscopy*, John Wiley & Sons, New York, (1980).
7. A Rosencwaig, T W Hindley, *Appl. Opt.* 20(4) (1981) 606.
8. J A Balderas Lopez, D A Costa-Avalos, J J Alvarado, O Zelaya-Angel, F Sanchez-Sinencio, C Falcony, A Cruz-Orea, H Vargas, *Meas. Sci. Technol.* 6 (1995) 1163.
9. J C Murphy, L C Aamodt, *J. Appl. Phys.* 51(9) (1980) 4580.
10. E Marin, H Vargas, P Diaz, I Riech, *Phys. Stat. Sol (a)* 179 (2000) 387.
11. C Garcia-Segundo, M Villagran-Muniz, S Muhi, *J. Phys. D: Appl. Phys* 31, (1988) 165.
12. L C Aamodt, J C Murphy, *J. Appl. Phys.* 52(8) (1981) 4903.
13. M A Schweitzer, J F Power, *Appl. Spectro.*, 48(9) (1994) 1054.
14. M A Schweitzer, J F Power, *Appl. Spectro.*, 48(9) (1994) 1076.
15. A Mandelis, Martin M Zver, *J. Appl. Phys.* 57(9) (1985) 4421.
16. P K Kuo, M J Lin, C B Reyes, L D Favro, R L Thomas, D S Kim, Shu-Yi-Zhang, L J Inglehart, D Fournier, A C Bocarra, N Yacoubi, *Can. J. Phys.*, 64 (1986) 1165.
17. P K Kuo, E D Sandler, L D Favro, R L Thomas, *Can. J. Phys.* 64 (1986) 1168.
18. C Preethy Menon, J Philip, *Meas. Sci. Technol.*, 11(2000) 1744.

19. M Bertolotti, R Li Voti, G Liakhou, C Sibilìa, *Rev. Sci. Instrum* 64(6) 1576 (1993).
20. X Quelin, B Perrin, G Louis, P Peretti, *Phys. Rev B.* 48 (6) (1993) 3677.
21. M Bertolotti, V Dorogan, G Liakhou, R Li Voti, S Paoloni, C Sibilìa, *Rev. Sci. Instrum* 68(3), (1997) 1521.
22. N V Bhat, N. V. Joshi. *Plasma (Chem.) Plasma Process.* 14, (1994) 151.
23. F F Shi. *Surf. Coat. Technol.* 82, (1996) 1.
24. I H Coopes, H J Griesser, *Journal of Applied Polymer Science*, 37 (1989) 3413.
25. N Inagaki, S Kondo, M Hirata, H Urushibata, *Journal of Applied Polymer Science*, 30 (1985) 3385.
26. H Yasuda, H C Marsh, M O Bumgarner, N Morosoff, *Journal of Applied Polymer Science*, 19 (1975) 2845.
27. M Chen, T S Yang, X Zhou, *J. Polym. Sci.* 34 (1996) 113.
28. Ennis T Ogawa, Chuan Hu, Paul S. Ho, *J. Appl. Phys.* 86 (11) (1999) 6018.

Chapter 4

Photoacoustic Investigations on Conducting Polymers

4.1 Introduction

Generation of acoustic waves resulting from nonradiative relaxation of a photo-excited material is called photoacoustic effect. The detection of pressure fluctuations in a medium adjacent to the photo-excited material forms the basis of different photoacoustic (PA) configurations. This technique is essentially a closed cavity detection scheme in which the sample is kept in a closed cell and illuminated with an intensity modulated light beam. Thermal waves generated in the material causes pressure fluctuations in the adjacent gaseous medium. The pressure variations can be sensed by keeping a pressure transducer inside the cavity. The theoretical platform for the photoacoustic effect was developed by Rosencwaig and Gersho in 1976 [1]. An outline of the same is given in chapter1.

Open photoacoustic cell (OPC) configuration is a simple and convenient variant of the photoacoustic technique [2 - 9]. In the OPC method the solid sample is directly mounted on a pressure transducer (microphone) leaving a small volume of air in between the sample and the microphone. Being a minimal volume detection scheme, the signal strength in this case will be much higher than that in a conventional photoacoustic configuration. In conventional methods the size of the sample is restricted by the physical

dimensions of the photoacoustic cell. The OPC technique eliminates this limitation, so that properties of large area samples can be analyzed.

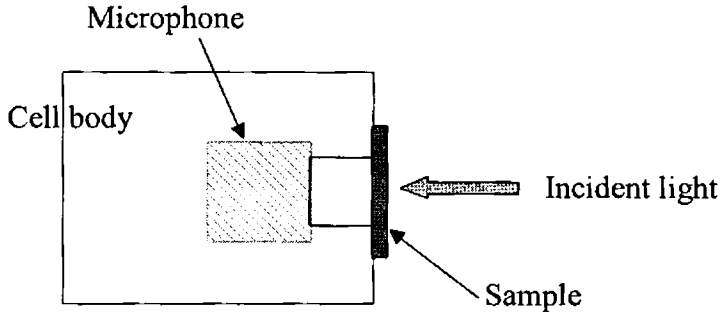


Figure 4.1: Basic OPC configuration

4.1.1 Theoretical outline

The expression for the PA signal from the 1-D heat flow model of Rosencwaig and Gersho is given by [1]

$$\delta P = \frac{\gamma P_0 I_0 (\alpha_g \alpha_s)^{1/2}}{2\pi l_g T_0 k_s f \sinh(l_s \sigma_s)} \exp\left[j\left(\omega t - \frac{\pi}{2}\right)\right] \quad 4.1$$

where γ is the specific heat ratio of air, P_0 and T_0 are the ambient pressure and temperature respectively, I_0 is the incident light intensity, f is the modulation frequency, and l_i , k_i and α_i are the respective length, thermal conductivity and thermal diffusivity of material i . Here the subscript i denotes the sample (s) and gas (g) and $\sigma_s = (1 + j)a_s$, with $a_s = (\pi f / \alpha_s)^{1/2}$ is the complex thermal diffusion coefficient of the sample.

If the sample is optically opaque and thermally thick,

$$\delta P = \frac{\gamma_0 P_0 I_0 (\alpha_g \alpha_s)^{1/2} \exp[-l_s (\pi f / \alpha_s)^{1/2}]}{\pi l_g T_0 k_s f} \exp\left[j\left(\omega t - \frac{\pi}{2} - l_s a_s\right)\right] \quad 4.2$$

where l_s and a_s are the thickness and thermal diffusion coefficient of the sample. According to equation (4.2), the phase of the PA signal varies with modulation frequency as $l_s (\pi f / \alpha_s)^{1/2}$. Thus thermal diffusivity can be obtained from the phase data. If there is thermo-elastic bending due to the temperature gradient generated within the sample across its thickness, then the phase will not vary linearly with square root of modulation frequency [10, 11]. In such a case,

$$\delta P = \frac{3\alpha_T R^4 \gamma P_0 I_0 \alpha_s}{4\pi R_c^2 l_s^2 l_g k_s f} \left[\left(1 - \frac{1}{x}\right)^2 + \frac{1}{x^2} \right]^{1/2} \exp\left[j\left(\omega t + \frac{\pi}{2} + \Phi\right)\right]; \quad 4.3$$

$$\text{where } x = l_s (\pi f / \alpha_s)^{1/2}, \quad 4.4$$

$$\Phi = \tan^{-1} \left[\frac{1}{x-1} \right] \quad 4.5$$

and α_T is the thermal expansion coefficient of the sample. R and R_c are the radii of the front hole of the microphone and OPC air chamber respectively. Now the thermal diffusivity can be obtained from the phase data by fitting the following equation,

$$\phi = \phi_0 + \tan^{-1} \left\{ \left[l_s (\pi f / \alpha_s)^{1/2} - 1 \right]^{-1} \right\} \quad 4.6$$

In the present study, thermal characterization of two typical conjugated polymers is performed using the OPC technique. The conducting polymers selected for this study are chemically prepared polyaniline (PANI) and polypyrrole (PPy). The effect of acid doping on heat diffusion in PANI is also

investigated. For this, PANI is doped with hydrochloric acid, sulphuric acid and camphor sulphonic acid and thermal diffusivity of the doped specimen in each case is determined.

4.2 Experimental setup

The PA setup consists of a suitable laser source to supply sufficient pump power, PA cell, chopper and lock-in amplifier.

4.2.1 Laser source

It provides the necessary pump power to the sample. In this study, a He-Ne laser (Melles Griot, 20 mW, 632.8 nm) with geometrical dimensions of length 50 cm and diameter 5 cm is used as the pump source. The $1/e^2$ beam diameter is 0.7 mm and the divergence is 1.2 milliradians.

4.2.2 Photoacoustic cell

An open photoacoustic cell is used for mounting the sample. An electret microphone (Knowles FG 3329) arranged in the OPC detects the acoustic waves. Necessary biasing (1.5 to 3V) is applied to the microphone according to its specifications. The electret microphone used has adequate sensitivity and flat response in the frequency range chosen for the experiment.

4.2.3 Mechanical chopper

Intensity modulation of the pump beam is achieved through the use of a mechanical chopper (Stanford - SR 540). The chopping frequency falls in the range of 4 Hz – 4 kHz. The whole frequency range operation requires two blades - a 6-slot blade for operation in the frequency range 4Hz - 400 Hz and 30-slot blade for 400 Hz to 4 kHz. A chopper control unit adjusts the frequency of the system.

4.2.4 Lock-in amplifier

Lock-in detection is generally employed for extracting the amplitude and phase of the photoacoustic signal from the microphone. This detection scheme enjoys all the advantages of phase sensitive detection. Noise immunity is very large in such detection schemes. For the present work, a Stanford Model SR830 lock-in amplifier is used. This instrument can measure voltages from 2 nV to 1 V with a fairly high degree of accuracy.

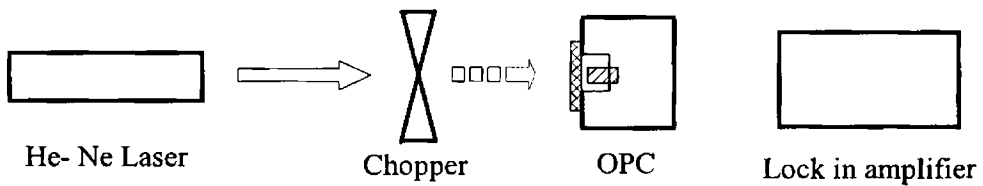


Figure 4.2 Block diagram of the PA setup.

A block diagram of the experimental arrangement is shown in figure 4.2. All the components of the experimental setup are arranged on a vibration-free table. Intensity modulated beam from the He-Ne laser is allowed to be incident on the sample fixed on the OPC. The laser beam is used without focusing to avoid lateral heat flow. The output of the microphone is fed to the lock-in amplifier. The photoacoustic signal is recorded by varying the modulation frequency. The thermal diffusivity of the conducting polymer samples is computed from the phase of the photoacoustic signal. The experimental setup is standardized using silicon wafer. The value ($9.2 \times 10^{-5} \text{ m}^2 \text{ s}^{-1}$) obtained is in agreement with the ones in literature [8, 12].

4.3 Preparation of polymer samples

Powder samples of Polypyrrole(PPy), polyaniline(PANI) and polyaniline doped with hydrochloric acid, sulphuric acid and camphor sulphonic acid are chemically prepared as described in section 2.3.1 of chapter 2. The polymer samples in the powder form are pelletised to form disks of diameter 1 cm and thickness less than 1mm for the PA measurements.

4.4 Thermal diffusivity measurements

The pelletised sample is fixed on the OPC in front of the microphone using a small amount of vacuum grease along the periphery of the pellet. The phase of the photoacoustic signal is measured using the lock-in amplifier for different frequencies. For each sample, measurements are carried out with two specimens of different thickness values. The frequency range for each sample is selected in such a way that it becomes thermally thick.

The phase of the photoacoustic signal is plotted against square root of frequency for each sample. From the resulting plots, the thermal diffusivity values are computed by fitting into the relation 4.6. The various plots are shown in figures 4.3 – 4.12.

4.5 Results and discussion

It is evident from the plots shown for the various samples that the variation of PA phase with square root of frequency is not linear. In such a case the effect of thermo elastic bending is to be taken into account. Hence analysis of the various plots obtained from PA measurements is performed based on equation 4.6 instead of equation 4.4.

The dependence of the phase of the PA signal on modulation frequency for undoped PANI is shown in figures 4.3 and 4.4. The values of thermal

diffusivity obtained from the plots are listed in table 4.1. The mean value of diffusivity in this case is much higher than that for plasma polymerized PANI film given in Table 3.2 of chapter 3. This observation can be justified by the fact that the properties of bulk and thin film forms of any material, in general, can differ. The structures of plasma polymerized films can be different from those of polymers synthesized by conventional chemical methods, due to a high degree of cross linking and branching reactions in plasma polymerization [13 – 19]. This inherent property of a plasma polymerized film results in a lower rate of heat diffusion. The structure is more ordered in the case of samples prepared through the chemical route. PANI belongs to the class of intrinsically conducting polymers where carriers like polarons contribute to the conductivity. But electrical conductivity is low in the undoped form. The conductivity, being too low to be applied to practical use, can be increased by protonation with common acids. While the increased concentration of carriers enhances the electrical conductivity, it can also assist heat transport in the polymer. Thus the increased thermal diffusivity of the chemically prepared PANI can be attributed to a significant contribution resulting from the nature of the conduction mechanisms existing in it and the presence of a local order in the chemical structure relative to the plasma polymerized counterpart.

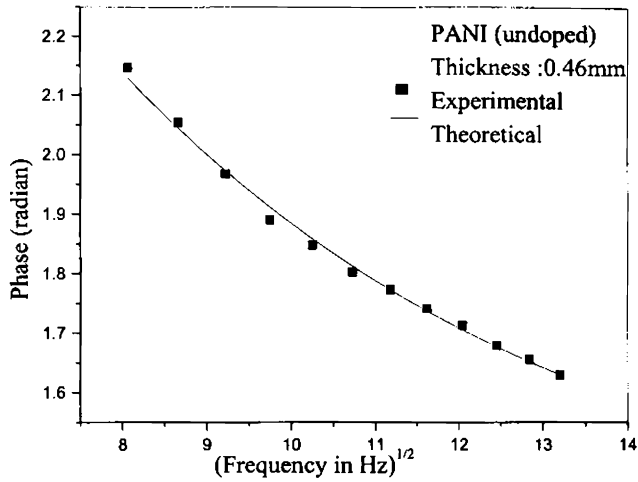


Figure 4.3 Variation of PA phase with frequency for undoped PANI of thickness 0.46mm

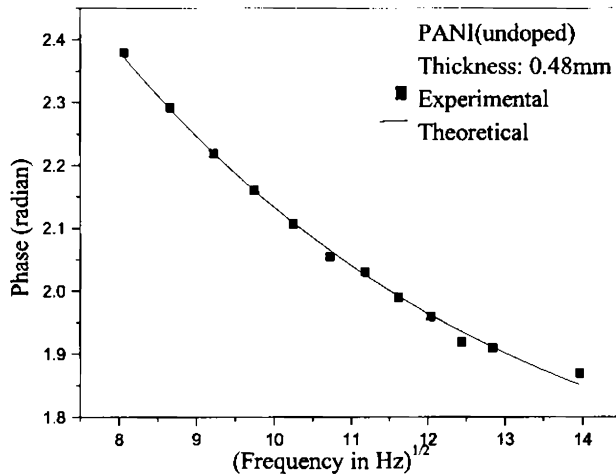


Figure 4.4 Variation of PA phase with frequency for undoped PANI of thickness 0.48mm

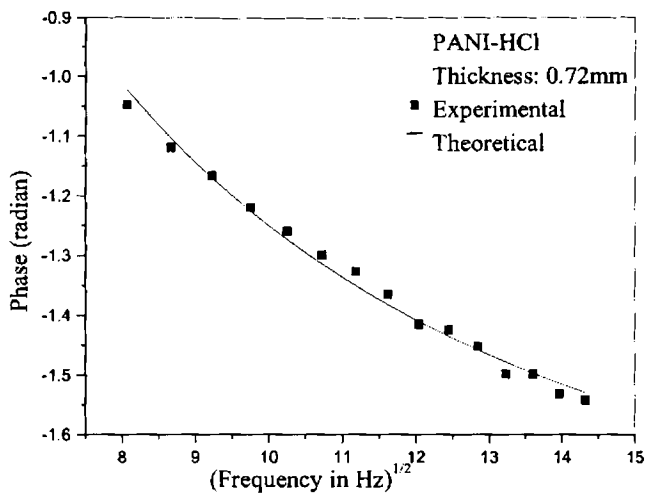


Figure 4.5 Variation of PA phase with frequency for PANI-HCl of thickness 0.72mm

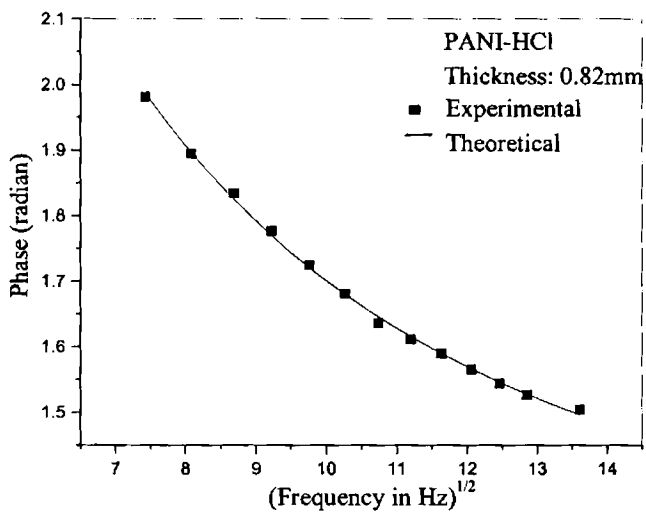


Figure 4.6 Variation of PA phase with frequency for PANI-HCl of thickness 0.82mm

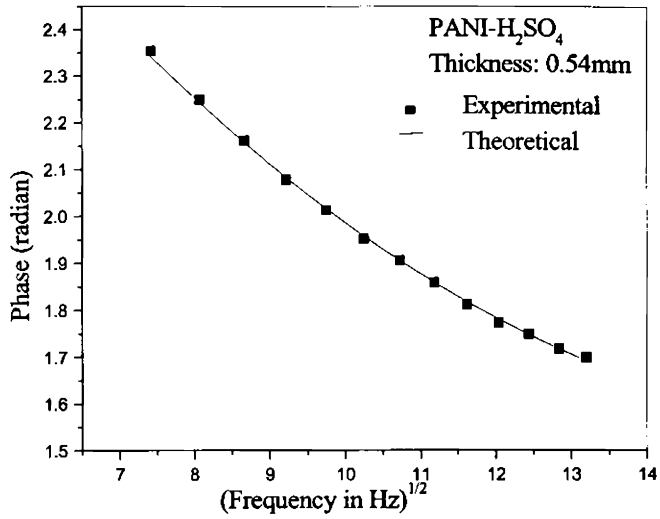


Figure 4.7 Variation of PA phase with frequency for PANI-H₂SO₄ of thickness 0.54mm

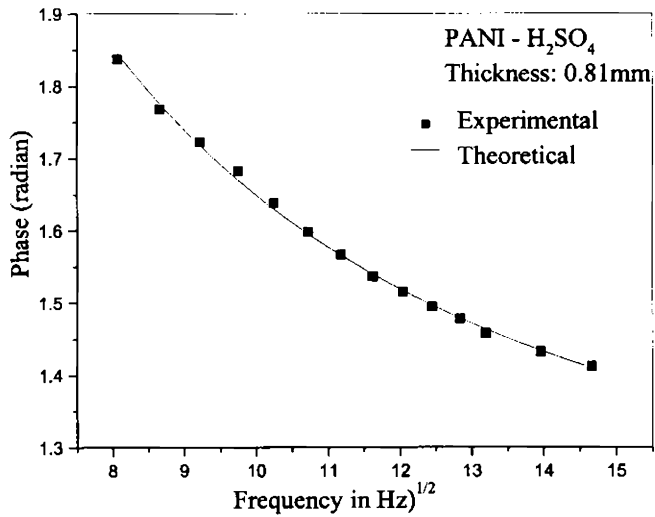


Figure 4.8 Variation of PA phase with frequency for PANI-H₂SO₄ of thickness 0.81mm

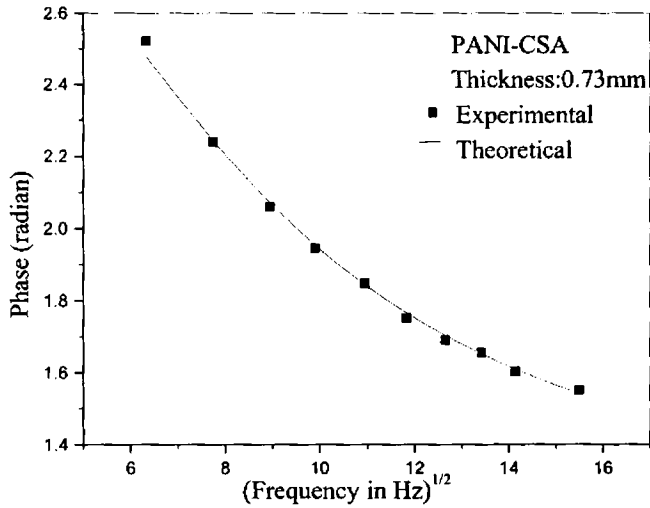


Figure 4.9 Variation of PA phase with frequency for PANI-CSA of thickness 0.73mm

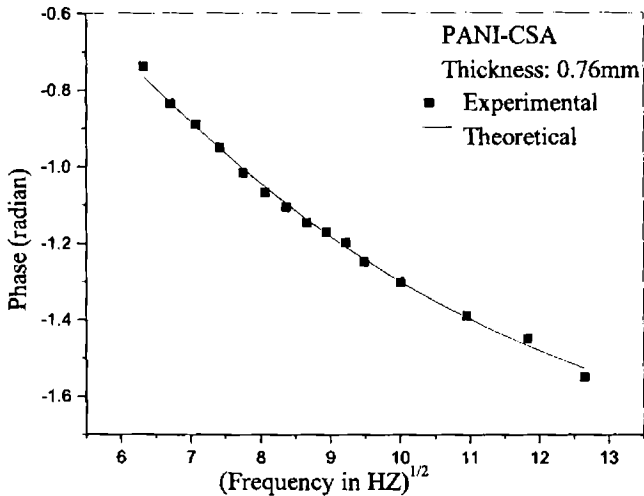


Figure 4.10 Variation of PA phase with frequency for PANI-CSA of thickness 0.76mm

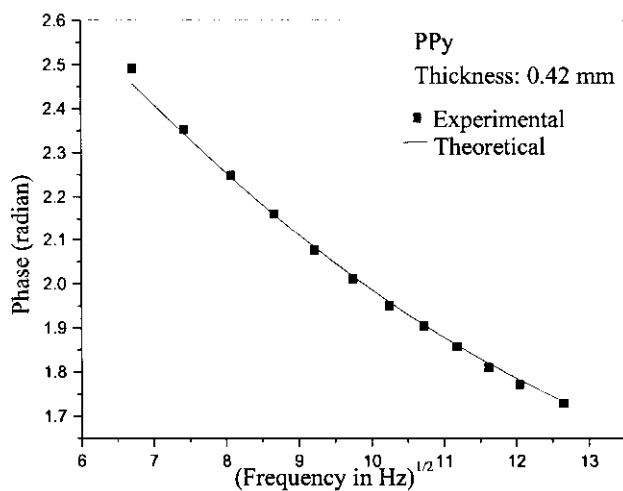


Figure 4.11 Variation of PA phase with frequency for as-prepared PPy of thickness 0.42mm

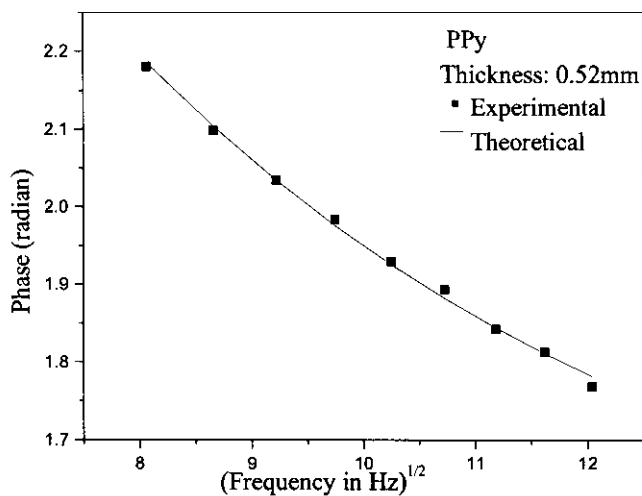


Figure 4.12 Variation of PA phase with frequency for as-prepared PPy of thickness 0.52mm

Figures 4.5 – 4.10 illustrate the dependence of PA phase on frequency for acid-doped PANI. PANI doped with hydrochloric acid and sulphuric acid

shows comparable thermal diffusivity values as given in table 4.1. But the samples doped with camphor sulphonic acid exhibits a relatively higher rate of heat diffusion.

Table 4.1: Effect of acid doping on heat diffusion in polyaniline

Polymer	Thickness (mm)	Thermal diffusivity ($\times 10^{-5} \text{ m}^2 \text{ s}^{-1}$)
PANI (undoped)	0.46	1.84 \pm .01
	0.48	1.88 \pm .01
PANI-HCl	0.72	3.69 \pm .03
	0.82	3.87 \pm .02
PANI-H ₂ SO ₄	0.54	3.49 \pm .01
	0.81	3.72 \pm .02
PANI-CSA	0.73	5.53 \pm .03
	0.76	5.35 \pm .02

The results obtained in the case of acid-doped PANI can be explained on the basis of the general principle of protonation of conjugated polymers with acids. Acid doping in polymers differs from conventional doping in semiconductors in the sense that the doping concentration is higher by several orders than that in semiconductors. In doped polymers the dopant ions are positioned interstitially between the chains, whereas in conventional semiconductors they are substituted directly into the host sites [20]. The carriers generated on doping increases the electrical conductivity by several orders. These carriers can effectively contribute to the heat transport in the system. This leads to an increase in thermal diffusivity. The value of thermal

diffusivity obtained for PANI-CSA is of comparable magnitude with the one reported earlier [21].

The dependence of PA phase on modulation frequency in the case of two as prepared samples of polypyrrole is shown in figures 4.11 and 4.12. The thermal diffusivity values computed from these plots are given in table 4.2. As in the case of PANI, the value of diffusivity is much higher than the value given in section 3.4.2 of chapter 3, for PPy film deposited by RF plasma polymerization. The obvious reason for this large mismatch in the values is the same as that given in the case of PANI. It is evident from these values that the rate of heat diffusion in as prepared polypyrrole is comparable with that in polyaniline.

Table 4.2: Thermal diffusivity of as-prepared polypyrrole

Polymer	Thickness (mm)	Thermal diffusivity ($\times 10^{-5} \text{ m}^2\text{s}^{-1}$)
PPy (as-prepared)	0.42	$2.08 \pm .01$
	0.52	$2.25 \pm .01$

Conclusion

Open photoacoustic cell method is employed to study heat diffusion in chemically prepared undoped and acid-doped forms of polyaniline and a similar conjugated structure – polypyrrole. The two polymers have comparable magnitudes for thermal diffusivity. Protonation by acids increases heat diffusion rate in polyaniline, which is accounted for by the polaron-assisted transport mechanisms existing in electrically conducting polymers.

References

1. A Rosencwaig, A Gersho, *J. Appl. Phys.* 47 (1976) 64.
2. L F Perondi, L C M Miranda, *J. Appl. Phys.* 62 (1987) 2955
3. A P Neto, H Vargas, N F Leite, L C M Miranda, *Phy. Rev. B*, 40 (1989) 3924.
4. A P Neto, H Vargas, N F Leite, L C M Miranda, *Phy. Rev. B*, 41 (1990) 9971.
5. M V Marquezini, N Cella, A M Mansanares, H Vargas, L C M Miranda, *Meas. Sci. Technol.* 2 (1991) 396.
6. S O Kanstad, P E Nordal, *Opt Comm.* 26, (1978) 367.
7. P M Nikolic, D M Todorovic, A J Bojicic, K T Radulovic, D Urosevic, J Elzar, V Blagojevic, P Mihajlovic, M Miletic, *J. Phys: Condens. Matter*, 8 (1996) 5673.
8. E Marin, H Vargas, P Diaz, I Reich, *Phys. Stat. Sol. (a)* 179 (2000) 387.
9. O D Vasallo, A C Valdes, E Marin, J A P Lima, M G Silva, M Sthel, H Vargas, S L Cardoso, *Meas. Sci. Technol.* 11, (2000) 412.
10. N F Leite, C Cella, H Vargas, L C M Miranda, *J. Appl. Phys* 61 (8) (1987) 3025.
11. G Rousset, F Lepoutre, L Bertrand, *J. Appl. Phys.* 54 (1983) 2383.
12. M Bertolotti, V Dorogan, G Liakhov, R Li Voti, S Paoloni, C Sibilina, *Rev. Sci. Instrum* 68(3) (1997) 1521.
13. Jinggong Wang, K G Neoh, E T Kang, *Thin Solid Films*, 446 (2004) 205.
14. G J Cruz, J Morales, R Olayo, *Thin Solid Films*, 342 (1999) 119.
15. G J Cruz, J Morales, M M Catello-Ortega, R Olayo, *Synth. Met.* 88 (1997) 213.
16. N V Bhat, D S Wavhal, *J. Appl. Polym. Sci.* 70 (1998) 203.

17. L M H Groenewoud, G H M Engbers, R White, J Feijen, Synth. Met. 125 (2002) 429.
18. H E Boeing, in: H F Mark, J I Kroschwitz (Eds.), Encyclopedia of Polymer Science and Engineering, John Wiley and Sons, New York, Vol. 11 (1986) p.248.
19. H Yasuda, Plasma Polymerization, Academic Press, Orlando, 1985.
20. N F Mott, E Davis, Electronic processes in Non-crystalline Materials, Carendon, Oxford, 1979.
21. Sajan D. George, S. Saravanan, M. R. Anantharaman, S. Venkatachalam, P. Radhakrishnan, V. P. N. Nampoore, C. P. G. Vallabhan, Phys. Rev. B, 69 (2004) 235201.

Chapter 5

Heat Diffusion in Conducting Polymer Composites

5.1 Introduction

The past few decades witnessed tremendous progress in the synthesis and characterization of conducting polymers. The possibility of synthesizing materials capable of simultaneously presenting the properties of organic polymers and of semiconductors has attracted much interest from both academic and industrial researchers. Of all known conducting polymers, polyaniline, polypyrrole, polythiophene and their substituted forms are the most frequently used in commercial applications. These polymers enjoy long term stability of their conductivity and form composites with optimal mechanical properties. The list of the wide variety of applications of conductive polymers include energy storage devices, sensors, EMI shielding materials, antistatic coatings, displays and radar absorbing materials [1 – 8]. Traditionally these polymers are synthesized by chemical or electrochemical polymerization.

5.1.1 Tailoring processability of polymers

In order to make a polymer technologically viable, the processability and thermal stability of polymers must be improved. The simplest approach to achieve this is copolymerization. The physical properties of conductive

polymers can be tailored by incorporating it into a host polymer so as to form blends, composites or interpenetrated networks. This is a widely used technique to combine the electrical properties of a conductive polymer with the desirable physical properties [9, 10]. Polyaniline and polypyrrole are considered to be the most promising candidates for the fabrication of conductive blends or composites with industrially important polymers [11].

Interpenetrating network conductive composite can be synthesized through in-situ polymerization of monomers of conducting polymers inside the matrices of the conventional linear polymers like polymethyl methacrylate (PMMA), polyvinyl chloride (PVC), etc. Co-processing of conductive polymers with other industrially important polymers can be effected through chemical or electrochemical means. The electrochemical method uses an electrode coated with conventional polymers [12, 13]. Oxidizing agents such as ferric chloride or cupric chloride is introduced into the polymer in chemical polymerization [14 - 16]. The polymer is then exposed to monomer vapour, or to a solution of monomer in appropriate liquid.

Conductive polymer composites and blends have many applications in the field of microwave engineering. They are used as coating in reflector antenna, coating on the frequency selective surface of electronic equipments, electromagnetic shielding material, etc. It is used as a radar absorbing material (RAM) to reduce the radar cross section (RCS) of military aircrafts, so that the vulnerability of the aircraft can be minimized [17]. The microwave absorbing properties of conducting polymers and composites can be tailored by controlling the inter-chain distance and the localization length [18]. The inter-chain distance can be modified by ring substituted monomers or counter anions with different sizes [19, 20]. The localization length can be controlled by changing the defect rates in the polymer [21].

5.1.2 Open Photoacoustic Cell configuration

Photoacoustic (PA) techniques are widely used in material characterization. This non-contact non-destructive technique can be applied to the thermal characterization of a wide variety of conducting polymers. Open photoacoustic cell (OPC) configuration described in chapter 4 is a simple and elegant technique to study thermal properties of materials. The theoretical background of the conventional photoacoustic technique was developed by Rosencwaig and Gersho [22]. The open cell photoacoustic theory was developed by Helander et. al. and was later modified by McQueen et. al. [23 - 27]. In the OPC technique the sample is directly mounted on an electret microphone arranged inside the PA cell, leaving a small volume of air in between the sample and the microphone. Compared to conventional PA methods, large area samples can be analyzed using OPC configuration. The sensitivity and noise immunity is relatively high in this technique.

An outline of the theory of OPC is already given in section 4.1.1 of chapter 4.

5.2 Preparation of Polymer Composites

In this work, the conducting polymers selected for the preparation of polymer composites are polyaniline (PANI) and polypyrrole (PPy). Polyvinyl chloride is selected as the polymer host matrix. Synthesis is carried out so as to form composites of PANI/PVC and PPy/PVC.

5.2.1 Preparation of PANI/PVC

Chemical oxidative polymerization of aniline is carried out using ammonium persulphate as initiator in the presence of 1M HCl and emulsion

grade polyvinyl chloride. The polymerization is carried out for about four hours at room temperature. It is then filtered, washed and dried at room temperature in vacuum for forty eight hours. Different compositions of PANI:PVC composite (3:1, 2:1 and 1:1) are prepared using the above procedure.

5.2.2 Preparation of PPy/PVC

PPy/PVC composite is prepared by polymerization of pyrrole with ferric chloride. The reaction is carried out for twenty minutes at 0 to 5° C. It is then filtered, washed and dried under vacuum for sixteen hours at room temperature. Different compositions (3:1, 2: 1 and 1: 1) of PPy-PVC composite are prepared as described above.

5.3 Thermal diffusivity measurements

Thermal diffusivity measurements in PANI/PVC and PPy/PVC composites are carried out using OPC technique. The experimental setup of the OPC configuration used in thermal diffusivity measurements is shown in figure 4.2 of chapter 4.

PAN/PVC and PPy/PVC in the powder form are pressed into pellets of diameter 1cm and thickness less than 1mm. Each pellet is mounted on the inlet of the OPC cell using vacuum grease. Intensity modulated radiation (20mW, 632.8nm) from a He-Ne laser (Melles Griot) with beam diameter 0.7mm and divergence 1.2 milliradians is allowed to fall on the sample. A mechanical chopper (Stanford Research Systems SR 540) with a chopping frequency range of 4 Hz to 4 kHz is used for intensity modulation. An electret microphone (Knowlès FG 3329) arranged inside the PA cell detects the acoustic waves produced by the PA effect. The microphone output is fed to a lock-in amplifier

(Stanford Research Systems Inc. SR830) for phase sensitive detection of the signal.

The phase of the photoacoustic signal is measured at different values of the modulation frequency. The thermal diffusivity of each sample is computed from the plot of phase versus square root of frequency, taking into account the effect of thermo elastic bending, as already described in section 4.4 of chapter 4.

5.4 Electrical conductivity measurements

In order to study the relation between electrical conductivity and heat transport of the different composites, conductivity measurements are carried out on the composites. For this, polymer samples in the powder form are pelletised to form pellets of about 1cm diameter. Silver paste is coated on either side so as to serve as terminals for applying a DC voltage. V-I measurements are carried out using Keithley Model: 236 Source Measure Unit, keeping the pellets in a conductivity cell. The room temperature electrical conductivity of all the samples are determined from V-I measurements.

5.5 Results and discussion

The dependence of PA phase on frequency for pure PANI is given in figure 5.1. The corresponding plots for the three different compositions of PANI/PVC composite are shown in figures 5.2 - 5.4. The plots for pure PPy and PPy/PVC composites are shown in plots 5.5 – 5.8. The thermal diffusivity values of all the samples computed by curve fitting are listed in table 5.1. As is evident from the table, there is a marked reduction in the rate of heat diffusion for both the composites with increase in the content of PVC.

The values of electrical conductivity computed from V-I measurements for all samples are listed in table 5.2. It is observed that there is a reduction in

electrical conductivity for both PANI/PVC and PPy/PVC composites with increasing content of PVC. Electrical conduction in PANI and PPy takes place through the polarons and bipolarons. The different conduction mechanisms in these polymers are affected by the presence of the host matrix, which is an insulator. As concentration of PVC in the composite increases, conductivity is found to decrease drastically. There is a corresponding reduction in the rate of heat diffusion also. This implies a carrier assisted heat transport mechanism in conducting polymers. Figure 5.9 and 5.10 shows the nature of variations of thermal diffusivity and electrical conductivity with the concentration of PVC in the two composites.

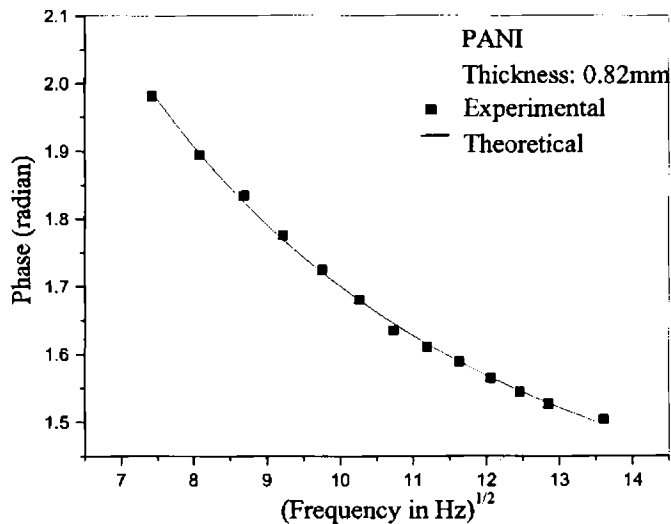


Figure 5.1 Variation of PA phase with frequency for PANI

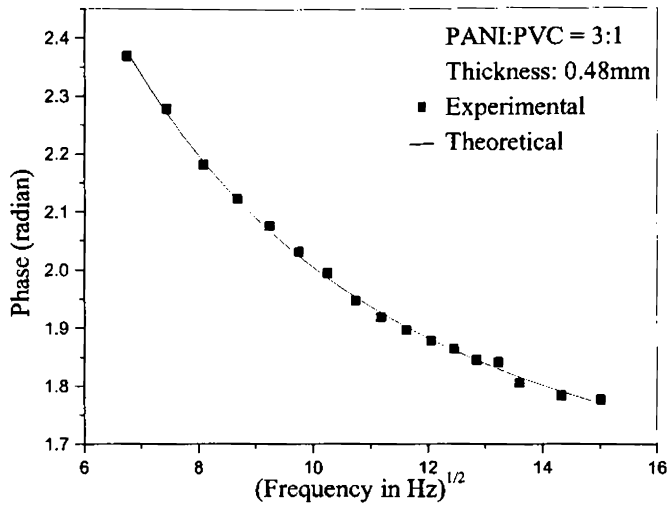


Figure 5.2 Variation of PA phase with frequency for PANI:PVC=3:1

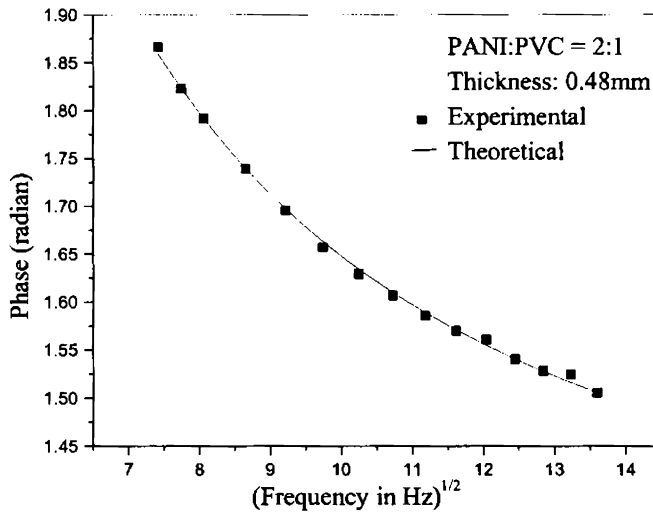


Figure 5.3 Variation of PA phase with frequency for PANI:PVC=2:1

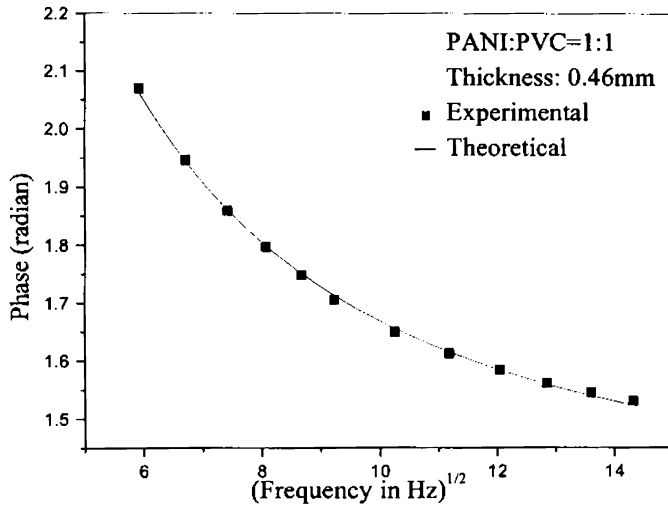


Figure 5.4 Variation of PA phase with frequency for PANI:PVC=1:1)

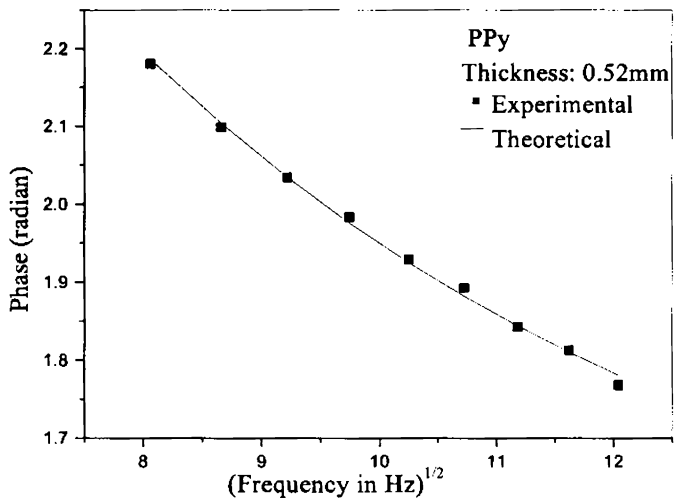


Figure 5.5 Variation of PA phase with frequency for PPy

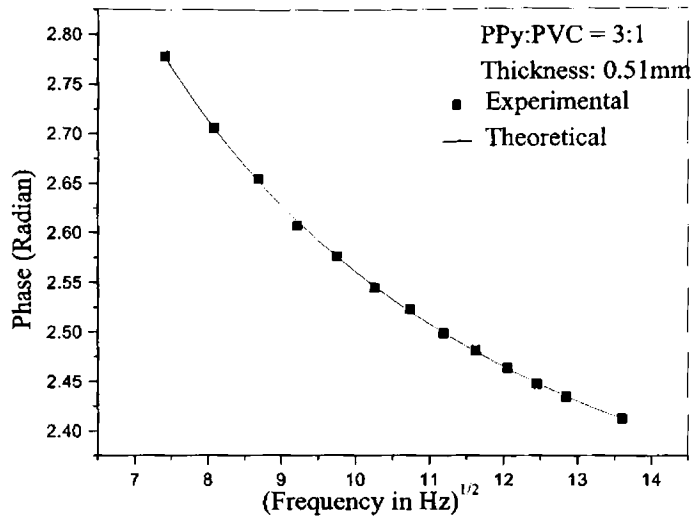


Figure 5.6 Variation of PA phase with frequency for PPy:PVC=3:1

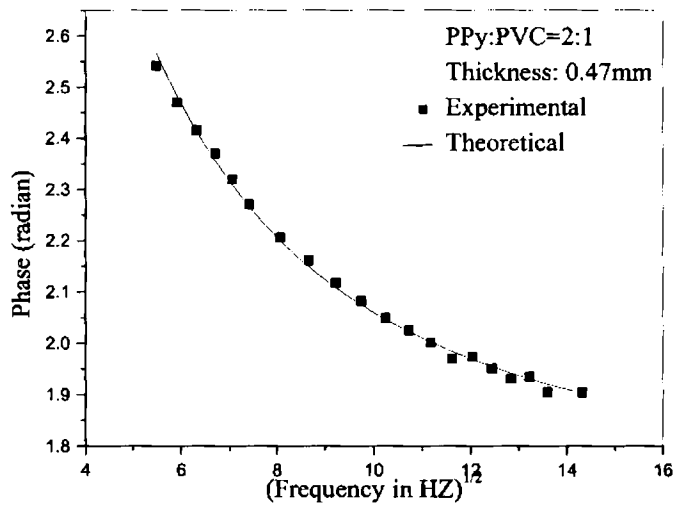


Figure 5.7 Variation of PA phase with frequency for PPy:PVC 2:1

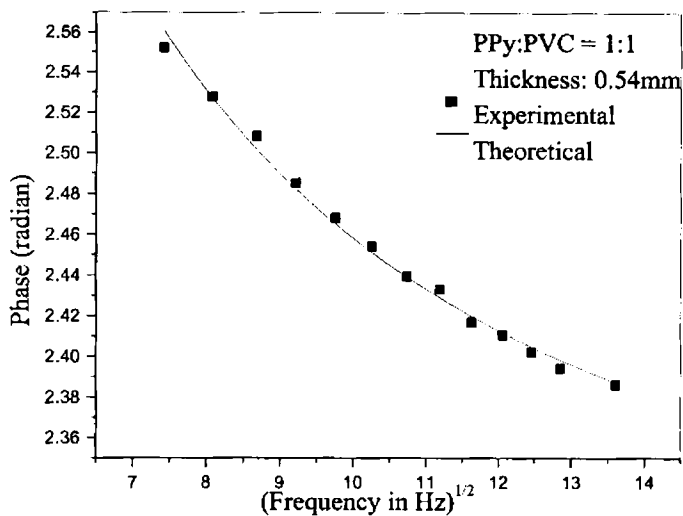


Figure 5.8 Variation of PA phase with frequency for PPy:PVC 1:1

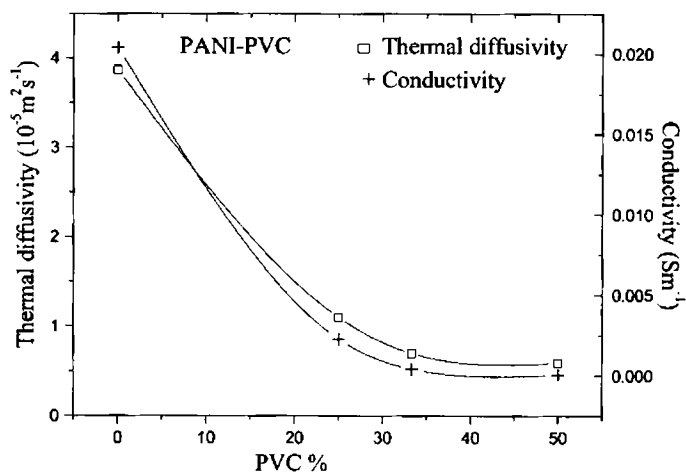


Figure 5.9 Variation of thermal diffusivity / conductivity with PVC % in PANI-PVC)

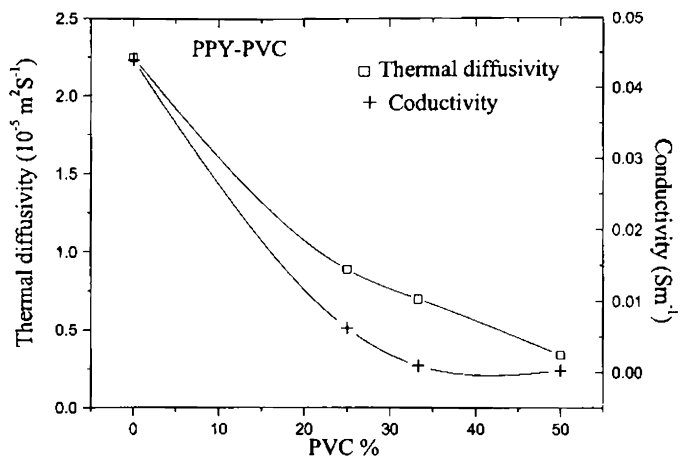


Figure 5.10 Variation of thermal diffusivity / conductivity with PVC % in PPy-PVC

Table 5.1: Effect of composition on thermal diffusivity of PANI/PVC and PPy/PVC.

Polymer	Composition	Thermal diffusivity ($\text{m}^2 \text{ s}^{-1}$)
PANI/PVC	Pure	$(3.87 \pm .02)10^{-5}$
	3:1	$(1.10 \pm 0.01)10^{-5}$
	2:1	$(7.53 \pm 0.02)10^{-6}$
	1:1	$(5.95 \pm 0.03)10^{-6}$
PPy/PVC	Pure	$(2.25 \pm .01)10^{-5}$
	3:1	$(8.83 \pm .03)10^{-6}$
	2:1	$(6.94 \pm .02)10^{-6}$
	1:1	$(3.38 \pm .03)10^{-6}$

Table 5.2: Effect of composition on electrical conductivity of PANI/PVC and PPy/PVC.

Polymer	Composition	Electrical conductivity (Sm^{-1})
PANI/PVC	Pure	2.04×10^{-2}
	3:1	2.26×10^{-3}
	2:1	4.19×10^{-4}
	1:1	7.69×10^{-5}
PPy/PVC	Pure	4.41×10^{-2}
	3:1	6.20×10^{-3}
	2:1	9.43×10^{-4}
	1:1	2.41×10^{-4}

Conclusion

Thermal diffusivity measurements of two composites (PANI/PVC and PPy/PVC) synthesized in three different compositions are carried out using the open photoacoustic cell technique. With increasing content of the insulating polymer (PVC) in the conducting polymers (PANI and PPy), the heat diffusion is found to be hindered. Electrical conductivity measurements show a similar reduction in electrical conductivity with increasing content of insulating polymer. Thus it can be concluded that the reduction in thermal diffusivity occurs due to a decrease in the contribution from polaron assisted mechanisms with increasing concentration of the insulating polymer.

References

1. D MacInnes Jr., M A Druvy, P J Nigrey, D P Nairns, A G Mac Diarmid, A J Heeger, J. Chem. Soc. Chem. Comm. (1981) 317.

2. T F Otero, J Rodriguez, H Grande, J. Braz. Chem. Soc. 5 (1994) 179.
3. T F Otero, H Grande, J Rodriguez, J. Electroanal. Chem. 394 (1995) 211.
4. E K Sichel, Carbon Black –Polymer Composites, Marcel Decker, New York, 1982.
5. J H Bourroughes, D D C Bradley, A R Brown, R N Marks, K Mac Kay, R H Friend, P L Burn, A B Holmes, Nature (London) 347 (1990) 539.
6. G Grem, G Leditsky, B Ulrich, G Leising, Adv. Mater. 4 (1992) 36.
7. S Becker, C Ego, A C Grimsdale, E J W List, D Marsitzky, A Pogantsch, S Setayesh, G Leising, K Mullen, Synth. Met. 125(1) (2001) 73.
8. V Saxena, V Shirodkar, J. Appl. Polym. Sci. 77 (2001) 1050.
9. Andreatta, A J Heeger, P Smith, Polym. Commun. 31 (1990) 275.
10. S S Im, S W Byun, J. Appl. Polym. Sci. 51, (1994) 1221.
11. H S O Chan, H Hopok, E Khor, M M Tan, Synth. Met. 31 (1995) 95.
12. M A De Paoli, R J Waltman, A F Diaz, J Bargon, J. Chem. Soc. Chem. Commun. (1984) 1015.
13. J H Han, T Matobe, Y E Wang, S Miyata, Synth. Met. 45 (1991) 261.
14. B Tieke, W Gabriel, Polymer, 31 (1990) 20.
15. M Makhlouki, M Morsli, A Bonnet, A Conan, A Pron, S Lefrant, J. Appl. Polym. Sci., 44 (1992) 443.
16. T K Mandal, B M Mandal, Synth. Met. 80 (1996) 83.
17. E F Knott, J F Schaeffer, M T Tuley, Radar Cross Section, 2nd Edn., Artech House, (1993).
18. A K Jonscher, Dielectric Relaxation in Solids, Chelsea Dielectric (1983).
19. Z H Wang, et. al., Phys. Rev. B, Condens. Matter, 43 (1991) 5373.
20. A Kobayashi, Z Xu, H I Shirakawa, J. Appl. Phys. 72 (1992) 5702.
21. H W Helborg, Phys. Stat. Sol., 81 (1) (1984) 381.
22. A Rosencwaig, A Gersho, J. Appl. Phys. 47 (1976) 64.

23. P Helander, J. Photoacoust., 1 (1982) 251.
24. J Helander, J. Appl. Phys. 59 (1986) 3339.
25. D H Mc Queen, J. Phys. E. 16 (1983) 738.
26. N F Leite, C Cella, H Vargas, L C M Miranda, J. Appl. Phys. 61 (8) (1987) 3025.
27. G Rousset, F Lepoutre, L Bertrand, J. Appl. Phys. 54 (1983) 2383.

Chapter 6

Summary and Conclusions

The emergence of thermal wave physics paved the way to several technological advances in material characterization. Photothermal methods, in general, are based on the detection of thermal waves generated in a material when exposed to intensity modulated light. From the role of a versatile spectroscopic tool, it emerged as a powerful technique for material characterization. The non-destructive nature of photothermal methods makes it particularly suited for investigating different material parameters of delicate samples. Since the methods are dependent on the thermal waves generated in a material on excitation by an intensity modulated beam, the thermal and transport properties of the material can be analyzed by these methods. Choice of a particular method for material characterization depends on the nature of the material under investigation. In this thesis, an account of the use of two popular photothermal techniques – transverse probe beam deflection and open photoacoustic cell - in the evaluation of heat diffusion in conducting polymers is presented.

Transverse probe beam deflection technique is a special case of probe beam deflection technique, where the two light beams (pump and probe) are perpendicular to each other with one beam grazing the sample surface. When the probe beam traverses the region having a refractive index gradient caused by the pump beam, it undergoes periodic deflection. The transverse component of this signal is measure of the temperature distribution parallel to the sample surface. The temperature distribution along the sample surface is a function the

thermal diffusivity of the sample. This method is particularly suited for the thermal diffusivity measurements in thin films.

Open photoacoustic cell configuration, on the other hand is a simple and convenient form of the general photoacoustic method. It enjoys several advantages compared to conventional photoacoustic setup. The design is simple and convenient to use. By the very nature of design, it provides large signal strength resulting in better noise immunity compared to conventional methods. In this method an intensity modulated beam incident on a sample generates thermal waves in the material. This, in turn, produces corresponding pressure variations in a small cavity. The pressure variations called the photoacoustic signal, is sensed by a pressure transducer, which is usually a sensitive microphone.

Conducting polymers form a class of materials which enjoys prime significance in a variety of technological applications. The polymers selected for this study have wide ranging applications in diverse fields. The intrinsic conductivity of this class of polymers is low. The conductivity can be tailored to suit specific applications by a process usually referred to as doping. The process of doping conducting polymers is significantly different from the one used in the case of semiconductors. As in the case of semiconductors both p-type and n-type doping can be employed to increase the conductivity. p-type doping results in oxidation of the polymer whereas n-type causes reduction. The conductivity of electrically conducting polymers arises due to conduction mechanisms involving solitons, polarons and bipolarons. The effective band gaps get reduced with the presence of dopants.

Usually conducting polymers are synthesized by chemical or electrochemical methods. Glow discharge polymerization is a technique used for the deposition of thin polymer films. Pin hole-free and flawless films with

good adhesion to substrate can be prepared by radio frequency plasma polymerization technique. In the present study, four monomers – aniline, pyrrole, N-methyl pyrrole and thiophene – are polymerized under radio frequency plasma conditions to yield the respective thin films. In-situ iodine doping is carried out in all the films so as to enhance the conductivity. The structure and properties of plasma polymers are known to be dependent on various deposition parameters. In order to study the effect of pressure in the reaction chamber on heat diffusion in thin films, one of the polymers (polyaniline) is prepared under different values of chamber pressure. To study the effect, if any, of thickness on heat transport in films, polythiophene films of different thickness are prepared in this study.

Two of the selected polymers – polyaniline and polypyrrole are also prepared by chemical oxidative polymerization. To increase the conductivity and to study the effect of acid doping on heat diffusion, polyaniline is doped with hydrochloric acid, sulphuric acid and camphor sulphonic acid.

Optical absorption in the uv-vis-NIR region is analyzed in the case of all the plasma deposited films. Direct and indirect transition energy gaps are computed from the absorbance data. It is observed that the direct band gaps of all the polymer films are of comparable magnitudes and fall in the range of 2 – 3 eV. The value of indirect transition energy gap of all these films is observed to be : 2eV. The band gap values in all the plasma polymerized samples suggest that the intrinsic conductivity is low so that the polymers behave as insulators or semiconductors. The observed DC electrical conductivity of these polymers is : 10^{-14}S.cm^{-1} . This very low conductivity value prohibits the use of these polymer films in applications where reasonable conductivity is a desirable feature. It is observed that the conductivity of these films increased by about two orders upon iodine doping. The temperature dependence of

conductivity in chemically prepared samples of polyaniline and polypyrrole points a variable range hopping mechanism in these polymers. The variation of conductivity with temperature is such that the plot between natural logarithm of conductivity versus $T^{-1/4}$, where T is the absolute temperature, is linear. This sort of variation is characteristic of the 3D variable range hopping conduction.

Knowledge of the rate of heat diffusion in conducting polymers becomes relevant when performance of devices fabricated from such polymers is influenced by the heat generated in the device or in its surroundings. In other words, a proper thermal design is of prime concern for the proper functioning of delicate elements made of conducting polymers. Thermal diffusivity is an important thermo-physical parameter which measures the rate at which heat diffusion occurs in a material. In the present study, the thermal diffusivity values of conducting polymers in the pure and doped forms are determined by photothermal methods.

Transverse probe beam deflection technique is employed for thermal diffusivity measurements in plasma polymerized films. Thermal characterization of pure and iodine-doped forms of polymer films is carried out. It is observed that the phase of the transverse component of the photothermal signal follows a linear relation with the pump-probe offset. The thermal diffusivity values of the polymer films (polyaniline, polypyrrole, poly N-methyl pyrrole and polythiophene) in the pure and doped forms are determined from the values of the slopes of the respective plots of phase versus pump-probe offset. The values of the thermal diffusivity for all these polymers are of comparable magnitudes. In agreement with the theoretical predictions, the natural logarithm of amplitude of the photothermal signal is found to be proportional to the pump-probe offset. The values of thermal

diffusivity computed from $\ln(\text{amplitude})$ versus offset plots agree well with the corresponding values obtained by phase method. It is evident from the observed values of thermal diffusivity of the samples under study that the rate of heat diffusion in these films is very small, which is characteristic of most of the insulating materials. It is reported in several studies that the structure of plasma polymerized films differ substantially from that of the chemically prepared counterpart. A characteristic feature of all plasma polymer films is the high degree of cross linking in its structure. This reduces rate of heat diffusion in such films. On doping with iodine, the thermal diffusivity is found to show a decline. This can be related to the increased phonon scattering at the iodine sites. This is to be distinguished from the corresponding electrical behaviour, where the conductivity increases with iodine doping.

An analysis of the dependence of pressure inside the reactor on heat diffusion in polyaniline film shows that there is reduction in the rate of heat diffusion at lower values of pressure. This can be related to the higher degree of fragmentation and cross linking occurring at reduced pressure conditions.

In the determination of thermal diffusivity by probe beam deflection technique, the accuracy of the results depends on the relative magnitudes of the values of thermal diffusivity of the sample and the coupling fluid. In this study, the thermal diffusivity of the coupling fluid (carbon tetra chloride) is less by one order than that of the polymer films. Thus contribution from the coupling fluid to the photothermal signal can be neglected. If the substrate on which the film is coated is absorbing at the pump wavelength there can be contribution to the photothermal signal from the substrate. In such a situation the substrate-film combination has to be considered as a layered structure. In the present case, the substrate contribution to the photothermal signal can reasonably be

neglected since glass is used as the substrate, which is transparent in the pump wavelength region.

An open photoacoustic cell is fabricated and thermal diffusivity of bulk conducting polymer samples is determined by this method. Heat transport in polyaniline and its acid-doped variants, and polypyrrole are analyzed using this powerful technique. All the polymer samples used in this photoacoustic study exhibit thermo-elastic bending, which arises due to the temperature gradient generated in the bulk sample resulting from intensity modulated excitation. The observed values of thermal diffusivity show an increase by about two orders of magnitude compared to that of thin films. This enhanced rate of heat diffusion in bulk samples shows the basic difference between the two forms of polymer with regard to heat transport. The bulk forms of conducting polymers show semiconductor behaviour and the observed values of thermal diffusivity fall in the range of semiconductors. The absence of cross linking in these conjugated structures presents a better local order which can lead to a higher diffusivity. Acid doping increases the electrical conductivity. The electrical conduction in doped polymers is effected through the polarons and bipolarons that are generated, depending on the level of doping. The present study shows that acid doped samples exhibit a higher rate of heat diffusion, which can be related to polaron and bipolaron assisted conduction in these polymers.

The processability of conducting polymers can be tailored to suit specific applications by forming composites with other common polymers. In the formation of composites the electrical, mechanical and thermal properties of conducting polymers get modified. The electrical conductivity with desirable mechanical and thermal properties makes the composites ideal candidates for several dedicated applications. Heat diffusion in two polymer composites, namely, polyaniline–poly vinyl chloride and polypyrrole –

polyvinyl chloride are analyzed by open photoacoustic cell method. The values of thermal diffusivity for different compositions are determined in the two cases. It is observed that there is a progressive reduction of the rate of heat diffusion in these composites with increasing content of poly vinyl chloride. A similar behaviour is observed in the case of electrical conductivity of these two composites. The present result seems to point to the polaron assisted heat transport mechanism in these composites.

In short, this thesis mainly describes the use of two versatile photothermal techniques in the thermal characterization of a special class of polymers which has extensive technological applications.

